Electric Field Modulation of Cells: From Signaling Pathway to Physiological Behaviors

by

Minxi Hu

A Dissertation Presented in Partial Fulfillment
of the Requirements for the Degree
Doctor of Philosophy

Approved March 2023 by the
Graduate Supervisory Committee:

Quan Qing, Chair
Stuart Lindsay
Jia Guo

ARIZONA STATE UNIVERSITY

May 2023

ABSTRACT

The response of living cells to electric field (EF) has been observed for more than a hundred years, but the mechanism of how cells interact with EF is not entirely ascertained. Although many efforts have been devoted to the application of EF stimulation in tissue engineering and regeneration, the fundamental scientific principle of such practice remains unveiled and keeps drawing attention during the pursuit of consistent outcomes. In this regard, my research focuses on the underlying mechanism by which EF stimulation evokes cellular responses and the EF modulation of cell signaling pathways to physiological behaviors.

The first part of my research focuses on developing the platform for controlled EF stimulation and real-time imaging/analysis. High-k dielectric passivated microelectrodes are fabricated to send capacitively coupled alternating current electric field (AC EF) stimulation to cells. I have developed two generations of EF stimulation devices with environmental control chambers: the first one is used to study cell signaling pathway dynamics; the second one is upgraded with long-term culture capability to study cell physiological behaviors.

The second part of my research focuses on the quantification and mechanistic study of AC EF perturbation of the extracellular signal-related kinase (ERK) signaling pathway. I demonstrate that AC EF stimulation can induce both inhibition and activation of the ERK pathway, with different AC EF amplitude thresholds and time and magnitude scales. The mechanistic study shows that the ERK activation is initiated by AC EF-induced epidermal growth factor receptor (EGFR) phosphorylation, and the ERK inhibition is related to AC EF-induced change of Ras activities. In addition, these ERK

responses show high sensitivity to AC EF waveform and timing, indicating electrostatic coupling mechanism and providing new parameter spaces for further investigation on the modulation of the ERK signaling pathway via AC EF stimulation.

The last part of my research steers to cell physiological behaviors under prolonged AC EF stimulation. I report that AC EF stimulation can clearly inhibit cell proliferation and migration, and the inhibition in cell proliferation is sensitive to AC EF amplitude, stimulation pattern, and pulse rising time. These findings can benefit the AC EF application in medical treatment.

ACKNOWLEDGMENTS

I would like to express my sincere gratitude to my advisor, Dr. Quan Qing, for his enduring support and encouragement throughout my Ph.D. study. His enthusiasm and devotion to research deeply affect me and every other student in his group. He has taught me not only how to conduct research, but also how to think as a scientist. I could not have taken this journey without his invaluable guidance. I also would like to express my appreciation to my committee members, Dr. Stuart Lindsay and Dr. Jia Guo, for their generous help and insightful comments. Thanks should also go to the School of Molecular Sciences and the Department of Physics at ASU for the resources and tutoring they provided during my Ph.D. study. In addition, I would like to extend my thanks to the Air Force Office of Scientific Research for the funding support.

I am also grateful to my friends and classmates, especially my colleagues Dr. Houpu Li, Ching-Wei Tsao, Sanjana Mukherjee, Dr. Xiangbing Jiao, Dr. Yuan Wang and Dr. Joshua Sadar. My whole Ph.D. study became more joyful with their support and accompanying. I wish them the best for their future endeavors.

Finally, I am deeply indebted to my parents for their unconditional love. Their absolute belief in me has given me the courage and strength to face any challenges during my Ph.D. career. I wish them good health and happiness.

TABLE OF CONTENTS

Page

LIST OF TABLES

LIST OF FIGURES

Figure Page

CHAPTER 1

INTRODUCTION

Electric field (EF) plays an essential role in many biological processes, including wound healing, embryonic development, tissue repair and regeneration and tumor growth (Levin, 2005; McCaig, Rajnicek, Song, & Zhao, 2005; Thrivikraman, Boda, & Basu, 2018; M. Zhao, 2009). The physiological or pathological EFs generated during embryogenesis and wound healing have been paid considerable attention to for decades. For example, Hotary et al. (1992) proved that shunting electric current out of the chick embryo could lead to much higher chance of developmental defects. In the early stage of *Xenopus* embryo development, HCN4 (hyperpolarization-activated cyclic nucleotide-gated channel 4) is very important in assigning anatomical left-right organ situs, pharmacologically blocking HCN4 can give rise to abnormalities in organ situs (Pai et al., 2017). Zhao et al. (2009) reported endogenous EF generated at skin wound not only directs cell migration in healing process, but also overrides other co-existing guidance cues like population pressure, gradients of chemoattractant etc.

EF stimulation has been found to evoke many cellular responses such as cell proliferation, migration, differentiation, and apoptosis. Among them, EF-induced cell migration, also known as electrotaxis or galvanotaxis, is the most well-studied phenomenon. Moreover, several related studies have been developed into lab techniques (e.g., cell fusion and transfection), or applications in tissue engineering and clinical treatment. However, some EF stimulation applications are still in lack of consistent effectiveness in different subjects or conditions, reflecting the need for a better understanding of underlying mechanisms of cellular responses elicited by EF stimulation.

Indeed, detailed mechanisms of how cells interact with EF stimuli would help design rational protocols and standardize therapeutic treatments.

There have been many studies on the relationship between applied EF stimulation and cellular responses, and several potential mechanisms have been proposed and validated with experimental results. In this chapter, I present an overview of recent studies as well as current understanding of the mechanisms. I want to share our perspective that cells, even non-electrogenic ones, can be considered as excitable systems, and it is worthwhile to emphasize high spatiotemporal resolution in cellular response characterization in order to capture meaningful transient information that may be overlooked or rarely investigated in previous studies.

Physiological EFs

Physiological EFs are generated from the transport of ions and charged particles across cell membrane and through tissues. The first observation of physiological EF could date back to 1791 when Luigi Galvani reported that electricity was able to trigger muscle twitching in dissected frogs. Now we can explain this phenomenon by the resting-potential/action-potential model (Figure 1A). Cells rest at a polarized state with a negative membrane potential maintained by ion pumps, when an internal or external stimulus occurs, the membrane potential raises above the threshold, leading to the activation of voltage-gated Na^+ channels and subsequent Na^+ influx. The entry of Na^+ increases the membrane potential and results in the positive feedback loop of depolarization. Once voltage-gated K^+ channels are triggered to open by the positive potential inside the cell, they pump out K^+, polarizing and restoring cells to their resting

state. The physiological EF at wound was first discovered in 1860 when DuBois-Reymond noticed that human finger with epidermal wound could generate current in saline. Later more advanced measurement tools and techniques enabled researchers to study this current with much more details: in normal skin tissue, there is a trans-epithelial potential difference up to 100 mV produced by ion transportation in polarized epithelia; when skin wound appears, the apical side and basal side are shorted and pulled to the negative potential, therefore an endogenous EF is build up due to the potential difference between wound edge and surrounding epidermis (Figure 1B).

Unlike electrogenic cells such as muscle cells and neurons, most non-electrogenic cells lack voltage-gated channels necessary for the action potential process, but they still exhibit various cellular responses upon EF stimulation. Over the years some potential mechanisms based on chemical cues or physical interactions have been proposed, yet the primary mechanism of how these kinds of cells sense and interpret electrical stimuli into biological signals still remains unclear.

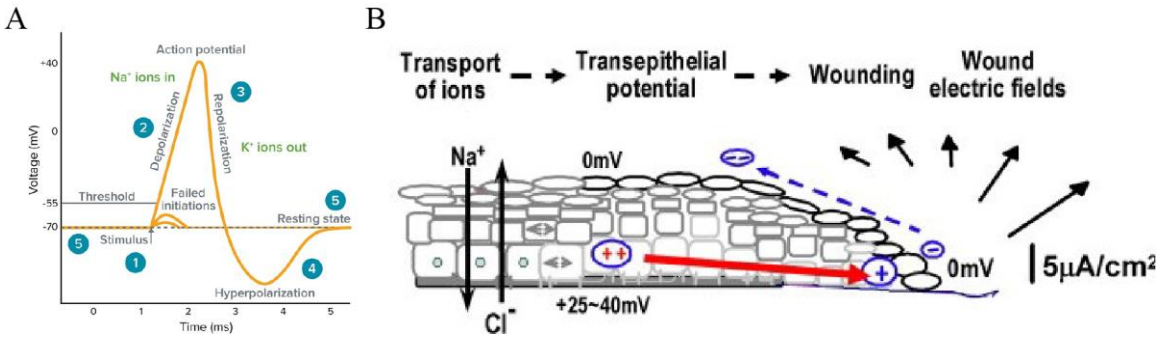

Figure 1. Examples of physiological EFs. (A) Action potential process (Junge, 1992). (B) The generation of electric current at wound (M. Zhao, 2009).

Since people have become more and more aware of the profound influence of physiological EFs in wound healing, embryonic development, and tissue repair, application of exogenous EF both in vitro and in vivo as a biomimicry tool for eliciting favorable biological responses has drawn a lot of attention. In bone tissue engineering, it has been reported in many studies that EF stimulation at the in vitro development stage can enhance cell attachment to the scaffold and promote cell growth (Bodhak, Bose, Kinsel, & Bandyopadhyay, 2012; Griffin, Iqbal, Sebastian, Colthurst, & Bayat, 2011; S. Sun, Titushkin, & Cho, 2006). For example, Bodhak et al. (2012) demonstrated that application of 25 μA direct current stimulation through Ti substrate could significantly benefit human fetal osteoblast cell (hFOB) attachment and proliferation. EF stimulation has also been proved as a useful therapeutic tool in neuromuscular system problems, both direct current EF and high duty-cycle alternating current EF have been reported to induce neuronal growth in vitro (Graves, Hassell, Beier, Albors, & Irazoqui, 2011; Zhu et al., 2019), Borgens et al. (1999) even demonstrated that oscillating EF treatment in naturally injured, neurologically complete paraplegic dogs could improve functional neurological recovery. Furthermore, deep brain stimulation has emerged as a viable surgical procedure in treating Parkinson's disease, seizure and other neurological movement disorders (Martinez-Ramirez, Hu, Bona, Okun, & Shukla, 2015), Kuncel er al. (2004) analyzed different selections of EF stimulation parameters for deep brain stimulation and found the typical EF parameters for Parkinson's disease treatment target subthalamic nucleus and globus pallidus are 1-3.5 V and in the frequency range of 130-185 Hz .

Tumor treating fields (TTFields) is a non-invasive anticancer treatment modality that employs low intensity (1-3 V/cm) and intermediate frequency (100-300 kHz)

alternating current EF to disrupt cell mitosis (Davies, Weinberg, & Palti, 2013; Kirson et al., 2004). So far it has been approved by FDA to treat human glioblastoma multiforme, malignant pleural mesothelioma (in combination with chemotherapy), and unresectable or metastatic liver cancer (Stupp et al., 2017; Wenger et al., 2018). As for the mechanism of TTFields, Kirson et al. (2007) proposed that the EF could interrupt tubulin subunits from forming microtubule spindle during mitosis and dielectrophoretic forces (DEP) could separate the newly formed daughter cells . However, Li et al. (2021) calculated the DEP effect in the TTFields range and found it not strong enough to drive macromolecules and cell organelles. So instead, they suggested that it was the alteration of cell membrane potential induced by TTFields that inhibited cell growth.

Parameters of EF Stimulations

Cellular response to EF stimulation is highly dependent on the applied electrical parameters, i.e., frequency, pulse shape, and intervals. For certain electric stimulus, different cell types could exhibit different responses due to various cell membrane compositions and ion environments. Based on frequency and EF strength, most EF stimulation used in biological experiments can be divided into 3 types: direct current electric field (DC EF), alternating current electric field (AC EF), and high strength pulse.

Direct current electric field (DC EF). DC EF is the most basic type of EF stimulation, usually established by 2 parallel planes or bars in experiments. The EF strength between electrodes is constant and can be calculated easily. DC EF has fixed direction from the high end to the low end, which can also cause directional flow of ions and electrochemically generated species in the medium. In most tests, DC EF can

generate highly reproducible physiological responses. However, the outcomes from DC EF stimulation may be attributed to a mixture of different mechanisms.

Alternating current electric field (AC EF). AC EF induces no direction flow and typically faradaic reaction on the electrode can be avoided. Different waveforms, such as sine wave, square wave, and triangle wave, can be integrated into AC EF. DC EF cannot pass through cell membrane as it is insulating, and only high frequency AC EF can couple with cytoplasmic components through capacitive coupling (Tadej Kotnik & Miklavčič, 2000).

High strength pulse. A pulse is a rapid, transient change in voltage from a baseline value (usually 0 V) to a higher or lower value, followed by a rapid return to the baseline value. A typical voltage pulse contains a short high voltage phase and a longer resting phase, so it also can be considered as a combination of transient AC EF wave and DC EF. Application of intense pulse on cells is able to penetrate cell membrane and affect intracellular structures like organelles and microtubules (Tadej Kotnik, Miklavčič, & Slivnik, 1998). In addition, high strength pulse can cause electroporation on the cell membrane, making it possible to introduce drugs (electrochemotherapy), and nucleic acid (electromediated gene transfer) into cells (T. Kotnik, Pucihar, Reberšek, Miklavčič, & Mir, 2003; J. C. Weaver, 2003; Xie & Tsong, 1990).

Cellular Responses to EF Stimulations

EF stimulation has been shown to evoke various cellular responses, for instance, proliferation, differentiation, migration, deformation etc. (Figure 2), all of which depend

on the cell type, EF parameter, and culture condition. The following parts are intended to further exemplify typical EF-induced cellular responses.

Cell proliferation. Numerous studies from literature have validated that EF stimulation can exert influence on cell proliferation, both positive and negative influences have been reported (Fitzsimmons, Strong, Mohan, & Baylink, 1992; Kirson et al., 2007). Hartig et al. (2000) once exposed osteoblast-like primary cells to 16 Hz AC EF stimulation and found a significant increase of cell proliferation. In another study, Hernández-Bule et al. (2014) reported that intermittent application of 448 kHz electrical stimuli could enhance the proliferation of adipose-derived stem cells without compromising stem cell multipotentiality. On the other hand, as mentioned before, TTFields can arrest proliferation in fast growing cancerous cells and the treatment efficacy has been confirmed in animal tumor models and clinical trials (Kirson et al., 2007; Stupp et al., 2015).

Cell differentiation. EF stimulation has been used to guide cell differentiation in a number of studies, especially with neural stem cells and osteogenic cells (Ross et al., 2015; Ryan, Doulgkeroglou, & Zeugolis, 2021; H. Zhao, Steiger, Nohner, & Ye, 2015). Chang et al. (2016) investigated the morphological and phenotypic changes of mouse neural stem and progenitor cells (mNPCs) after 48 h, 300 mV/mm pulsed EF stimulation and found that mNPCs differentiated into neurons, astrocytes, and oligodendrocytes simultaneously. PC12 cell, derived from rat pheochromocytoma, can be induced to both proliferation and differentiation depending on extracellular growth factor treatment (Hyunryul Ryu et al., 2015). Jing et al. (2019) discovered that EF stimulation in the range of 30-80 mV/mm could enhance the neuronal differentiation of PC12 cell mediated by

EF triggered intracellular reactive oxygen species (ROS) generation . Researches of using EF stimulation to promote osteogenic differentiation have been motivated heavily by the discovery of piezoelectric effect of bones (Fukada & Yasuda, 1957). Pulsed electromagnetic fields (PEMFs) have been reported to boost both osteogenic and chondrogenic differentiation of human mesenchymal stem cells (hMSCs), facilitating beneficial cellular response in bone tissue regeneration (Pettersen, Anderson, & Ortiz-Catalan, 2022; Varani et al., 2021).

Cell migration. The directional migration of cells under EF stimulation, also known as electrotaxis or galvanotaxis, has been studied comprehensively with various types of cells (Djamgoz, Mycielska, Madeja, Fraser, & Korohoda, 2001; J. Zhang et al., 2011; M. Zhao, 2009; M. Zhao, Agius-Fernandez, Forrester, & McCaig, 1996). Some cells can be guided to migrate toward the cathode while some toward the anode. For example, Banks et al. (2015) observed cathodally directed migration in hMSCs under EF stimulation. In another study, Guo et al. (2010) found that human dermal fibroblasts, unlike keratinocytes, migrated slowly toward the anode when applied with DC EF stimulation. EF stimulation condition also plays a part in electrotaxis, the Schwann cell only shows increased migration speed without directional preference with low EF intensity, however, when EF is increased to 200 mV/mm, this cell orientates and migrates toward the anode (Forciniti, Ybarra III, Zaman, & Schmidt, 2014; L. Yao, Li, Knapp, & Smith, 2015). Electrotaxis is an attractive feature as it enables manipulation of cell migration both in vitro and in vivo, thus it is frequently applied in tissue engineering and regenerative medicine (L. Li & Jiang, 2011; L. Yao, Pandit, Yao, & McCaig, 2011).

Cell alignment. Cell alignment is a common phenomenon observed after EF stimulation (Luther, Peng, & Lin, 1983). Early in 1981, Hinkle et al. (1981) studied Xenopus neurons and myoblasts at low amplitude DC EF stimulation and found that neurites grew and turned to the cathode of applied DC EF and spherical myoblasts elongated with a direction perpendicular to the EF direction. Some other types of cells, like cardiac adipose tissue-derived progenitor cells (Llucià-Valldeperas et al., 2015) and adipose-derived stromal cells (Hammerick, Longaker, & Prinz, 2010), also align perpendicularly to the EF direction to mitigate EF gradient along the cell body. Yet some cells exhibit alignment parallel to the EF vector due to EF-induced redistribution of cytoskeletal elements, such as PC12 cells (Chen et al., 2019) and rat ventricular myocytes (Radisic et al., 2004).

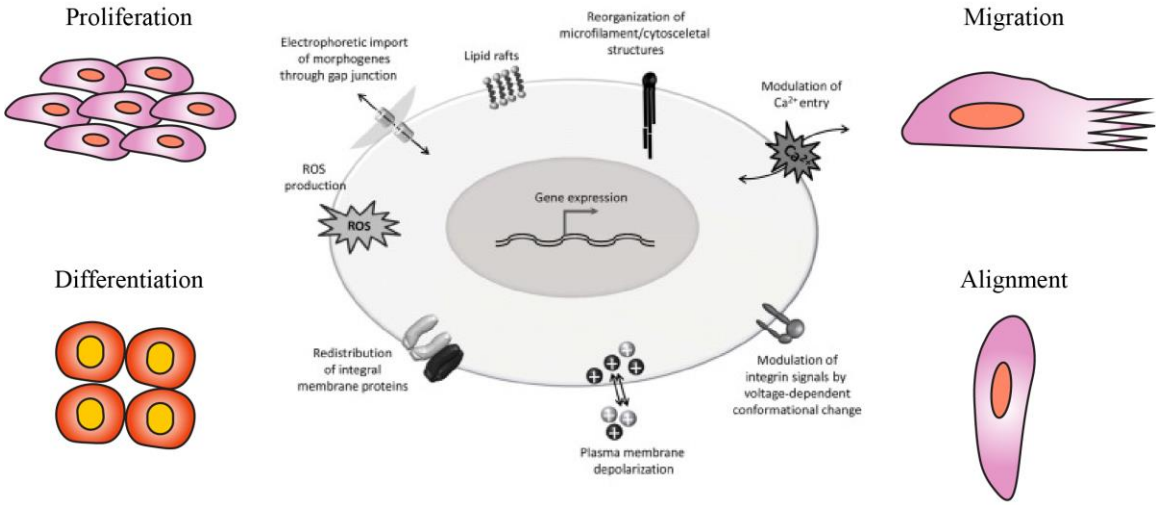

Figure 2. Cellular responses to EF stimulations and proposed mechanisms (Leppik, Oliveira, Bhavsar, & Barker, 2020).

Mechanisms of EF-induced Cellular Responses

Due to the complexity of biological processes, a cellular response can be the result from more than one signaling pathways regulated by many feedback loops, so it has always been very difficult to pinpoint the initial molecular mechanisms by which cells couple to EF. When a cell is exposed in EF, the bilayer structure of cell membrane isolates the conductive cytoplasm from extracellular DC EF in most conditions (Tian Y Tsong & Gross, 2012), but the AC component of EF stimulation would distribute unevenly at different parts of the cell. When frequency is not very high (<1 GHz), most of the EF energy would be focused on the cell membrane. Therefore, one possible mechanism implicates the alteration/redistribution of cell membrane receptors and proteins due to EF stimulation, which can initiate the activation of downstream signal transduction pathway (Tian Yow Tsong, 1989; Xie & Tsong, 1990). Another possible mechanism is related to the transmembrane voltage potential. When this potential is modulated by the extracellular EF, some voltage-gated ion channels can be activated, leading to intracellular ion concentrations changes (Taghian, Narmoneva, & Kogan, 2015). Furthermore, when the applied EF exceeds a certain level (high frequency or high amplitude), extracellular EF can also penetrate cell membrane and generate power dissipation in the cytoplasm or cause electroporation on the cell membrane (Tadej Kotnik & Miklavčič, 2000; J. C. Weaver, 2003). These and other potential mechanisms (Figure 2) are further summarized in the following sections.

Cell signal transduction pathways. Cell signal transduction pathways are comprised of signaling proteins that communicate through complex molecular mechanisms (Arkun & Yasemi, 2018). They can transform the information of

extracellular signals to the DNA in the cell nucleus which converts the information into cellular functions, therefore they play a pivotal role in EF-induced cellular responses. Highly conserved Mitogen-activated protein kinase (MAPK) cascades are key signaling pathways involved in the regulation of normal cell proliferation, survival, and differentiation. Currently there are four MAPK cascades identified in eukaryotic cells: the extracellular signal-related kinases (ERK1/2), the c-Jun N-terminal kinases (JNK1/2/3), the p38-MAPK and the ERK5 (Safa, Abak, Shoorei, Taheri, & Ghafouri-Fard, 2020). Sheikh et al. (2013) once found that 7.5GHz EF stimulation applied to endothelial cells via cavity resonator could increase MEK and ERK phosphorylation in cells, leading to enhanced angiogenic responses. However, JNK or p38 activation was not detected after this EF stimulation. In another study, 60 Hz electromagnetic field was demonstrated to induce differentiation of human leukemia cell HL-60, later the same group proved that ERK was activated in HL-60 cells, verifying their hypothesis that the EF-induced differentiation was mediated by MAPK/ERK pathway (Nie & Henderson, 2003; Tao & Henderson, 1999).

PTEN/PI3K/AKT pathway, an essential regulator of many biological processes like cell proliferation, survival, motility, metabolism etc. (Carracedo & Pandolfi, 2008), is also closely involved in many EF-induced cellular responses. When PI3K is activated, it phosphorylates PIP2, which thereby generates PIP3. AKT is activated in the downstream of PIP3, regulating various downstream targets. PTEN negatively regulates PI3K/AKT pathway by dephosphorylating PIP3 to PIP2 (Carnero & Paramio, 2014). Zhao et al. (2006) identified that PI3K and PTEN mediated directional cell migration in response to electrical signal during wound healing process. In a DC EF stimulation study,

human lung cancer cell line CL1-5 shows clear directional migration and orientation toward anode and gene expression measurement reveals that PTEN is down-regulated due to DC EF stimulation (Huang et al., 2011).

Ca^{2+} fluctuation. Ca^{2+} is reported as a multi-role intracellular signal molecule, and it works as a secondary messenger and is involved in numbers of signaling pathways. It is also well-established that Ca^{2+} is necessary in many cellular responses to EF stimulation (Karabakhtsian et al., 1994; Onuma & Hui, 1988). When a cell is exposed to EF stimulation, depending on its cell type and EF parameters, intracellular Ca^{2+} concentration can be changed via two fundamental ways: the first is through the activation of voltage-gated Ca^{2+} channels (VGCCs) or stretch-activated cation channels (SACCs) on the cell membrane, resulting in Ca^{2+} influx from extracellular medium; the second one is through the activation of intracellular plasma receptors or specialized channels , releasing Ca^{2+} from endoplasmic reticulum (Michael R. Cho, Thatte, Silvia, & Golan, 1999). Ca^{2+} influx plays an important role in EF-induced cell migration, Funk et al (2009) once observed Ca^{2+} concentration increase in fibroblasts after DC EF stimulation and the initial spot of Ca^{2+} elevation seemed to be dependent on the directional migration of cells in the DC EF. Ca^{2+} is also essential in determining stem cell fate as it is deeply implicated in signaling pathways through cell differentiation stage (Tonelli et al., 2012). Notably, Sun et al. (2007) found a correlation between intracellular Ca^{2+} oscillation and extracellular osteo-inductive factors in hMSCs, moreover, EF stimulation can alter the Ca^{2+} dynamics in hMSCs and therefore facilitate osteo-differentiation.

Reorganization of cytoskeletal structures. It is a common sensory transduction process that cells can convert mechanical stimuli into electrical or biochemical signals (Martinac, 2004). In reverse, electrical stimuli can also be transformed into mechanical forces, leading to reorganization of cytoskeletal structures. Both DC EF and low frequency AC EF stimulation have been reported to induce redistribution of microfilament structure in cells, causing either directed migration or changes from aligned cable structures to discontinuous globular patches (Michael R Cho, Thatte, Lee, & Golan, 1996; Xuefeng Li & Kolega, 2002). Microtubule, comprised of polymerized α, β-tubulin subunits, is a major component of cell cytoskeleton. Chafai et al. (2019; 2020) first demonstrated artificial modulation of tubulin assembly by pulsed EFs in solution, later this group verified this cytoskeleton remodeling capability in cells, providing a new method to manipulate microtubule structure.

Surface receptor redistribution. Many cellular processes are initiated and modulated by ligands binding to their corresponding receptors on the cell membrane. Due to the high electrical resistance from cell membrane, DC EF and most low frequency AC EF stimulation could not penetrate inside the cell, leaving induced potential and power dissipation on the cell membrane. Consequently, a lot of EF-induced signal transductions can be traced back to the redistribution of charged surface receptors. In most cases, the receptor distribution is driven by EF-induced electrophoretic and electroosmotic forces, but sometimes cytoskeletal structure reorganization could also bring about this effect (S. Zhao, Mehta, & Zhao, 2020). In an EF-induced cathodally directed cell motility study, Zhao et al. (1999; 2002) discovered that EF could not only up-regulate epidermal growth factor receptor (EGFR), but also cause asymmetric EGFR redistribution on the cathodal

side, directing cell's leading edge to the cathode. Besides EGFR, extracellular matrix receptor α2β1 integrin is found polarized and redistributed in anterior cruciate ligament cells under EF stimulation, which proves to be essential in directed cell migration (Tsai, Lin, & Chao, 2013).

ATP synthesis. ATP synthesis is of vital importance in biological processes as it provides and regulates energy supply needed in all biochemical reactions. Both DC EF and AC EF stimulations have been reported to enhance membrane-bound ATP synthesis (Cheng et al., 1982; Teissie, Knox, Tsong, & Wehrle, 1981). Mechanistically, for DC EF and low frequency AC EF stimulations, it is believed that EF stimulation can guild protons migrating towards the mitochondrial membrane-bound H1-ATP, producing more ATP (Cheng et al., 1982; Zrimec, Jerman, & Lahajnar, 2002); for higher frequency AC EF stimulation, Tsong et al. (1989) proposed a mechanism called 'electroconformational coupling', membrane-bound ATPase could absorb electrical energy with certain frequency and amplitude and then transform it into chemical energy, subsequently the energy could enforce the conformational change of this enzyme, enabling the catalytic action of ATP synthesis . Once the ATP synthesis is boosted by the applied EF stimulation, all cellular biochemical reactions limited by energy are augmented as well. As the EF effect may vary from different cell types, Titushkin et al. (2009) found depleted intracellular ATP in hMSCs after the exposure to DC EF stimulation. Since ATP depletion is documented to closely correlated with the net conversion of monomeric G-actin to polymeric F-actin (Atkinson, Hosford, & Molitoris, 2004), this EF caused ATP reduction in cells leads to the membrane separation from the cytoskeleton.

Lipid rafts. As mentioned above, charged proteins and receptors on the cell membrane can sense applied EF stimuli and trigger downstream activations and regulations. However, they are not the only candidates for EF sensors, lipid rafts, nanodomains of dynamic assemblies of proteins and lipids in the cell membrane, are also proposed as a primary response element in EF perception. Since 50 Hz symmetric AC EF stimulation can still provide directed migration guidance in cells, ruling out the involvement of electrophoretic and electroosmotic effects (Tsai et al., 2013), Lin et al. (2017) continued to dig for the underlying mechanism and then confirmed that lipid raft was the primary sensing mechanism to the EF stimulation. The EF-induced lipid raft redistribution results in the clustering and activation of caveolin and integrin, promoting directed cell migration. In addition, lipid raft also plays a major role in cellular response to nanosecond pulsed electric field (nsPEF), depletion of membrane cholesterol can increase the permeability of cells after nsPEF treatment (Cantu, Tarango, Beier, & Ibey, 2016).

Reactive oxygen species (ROS). ROS is also a crucial mechanism in the EF-induced cellular responses. There are basically two ways of ROS generation from EF stimulation. One is inside cells via nicotinamide adenine dinucleotide phosphate (NADPH) oxidase. Díaz-Vegas et al. (2015) demonstrated that EF stimulation could increase ROS in skeletal muscle cells through released extracellular ATP and activation of $P2Y_1$-PKC-NOX2 pathway. In another study about directed migration of glioma cells under DC EF stimulation, Li et al. (2013) pointed out that the DC EF could increase the production of ROS in cells and therefore cause cytoskeleton polarization and activation of ERK1/2 and AKT, facilitating directed migration. The other way of ROS generation is

on the electrode surface via faradaic reactions. Extracellular ROS had been considered as stress to cells until physiologically relevant level of ROS was found to be implicated in several important signaling pathways. For example, Wolf-Goldberg et al. (2013) proposed that ROS generated in the anodal area could be the mechanism of unevenly distributed EGFR activation in cells after EF stimulation .

Heat shock proteins (HSPs). HSPs are a family of intracellular proteins expressed in response to a variety of stressors including heat, cold, and UV light. In some cases, exposure to electromagnetic fields is also considered as stressor to cells as it has been shown to prompt HSPs expression. For instance, in a study of osteoblastic differentiation from hMSCs after AC EF stimulation, Hronik-Tupaj et al. (2011) detected an upregulation of HSP 27 and it was correlated with the cellular response, suggesting its participation in the EF-induced differentiation. Interestingly, 70 bp sequence from the HSP 70 promoter is found to be necessary in the promotion of HSP 70 expression during EF stimulation, removal of this sequence could disable its response to EF stimulation but does not impair its response to heat shock (H. Lin, Blank, Rossol‐Haseroth, & Goodman, 2001).

All these mechanisms mentioned above may be solely or collectively involved in the complex and precisely regulated cellular responses. With the emergence of advanced technology and increasing demand from clinical applications, it is believed that all the cloudy and intertwined mechanisms will be elucidated in the near future.

A Closer Look into the Dynamics and Kinetics of EF-induced Signaling Pathway Activities

In all the aforementioned potential mechanisms, cell signaling pathway activities seem to play a major part in cellular responses to EF stimulation, so here I want to take a closer look into the dynamics and kinetics of the cell signaling pathway activities during those processes. As suggested in recent literatures (Devreotes et al., 2017; Pal, Li, Banerjee, Miao, & Devreotes, 2019), we would like to consider cells as excitable systems, including non-electrogenic cells without voltage-gated ion channels. Specifically, the EF can couple with both the signal sensors as well as signal transducers/amplifiers, possibly mainly at the cell membrane, which will cause the original dynamic characteristics of existing signaling pathways to shift, leading to new thresholds for the feedback loops and new patterns in time and/or space in terms of distribution of species and concentration fluctuations. This kind of information will be integrated and processed through the cell system to regulate cell behaviors as well as bring changes to cell fates. Hence, using an external EF to modulate cells is more like perturbing the whole cell system, rather than a single input signal to a specific receptor. From this prospect, the impact of EF should not be evaluated simply by the rising and falling of a specific downstream signaling protein, but rather, detailed investigation should be conducted on the dynamic spatial and temporal changes of key components in the signaling pathway.

The spatiotemporal resolution of cellular responses. While most studies into EF effects on cells focus on which signal molecule is activated due to EF, it is also crucial to find out when and for how long it is activated. As most biological processes

need some time in a certain state to take effect, if the characterization result can show the onset time of the target molecule, it might reveal critical information on the detailed procedures of signal transduction. Although from current research literature, the temporal resolution of cellular responses is limited due to timed cell harvesting and target molecule detection method, they can still provide a glimpse into the timing of each step involved in the signal transduction process.

As summarized in Figure 3 and Table 1, we have compared the different temporal information from cellular response and noticed some patterns. The first one is that different cellular responses have very distinctive timeframes as they work through different mechanisms. For example, the ion flux in electrogenic cells, such as Ca^{2+} influx (Bagalkot, Leblanc, & Craviso, 2019) and H^{+} bubble (Perike et al., 2014), is always faster than the pathway process in non-electrogenic cells to take place.

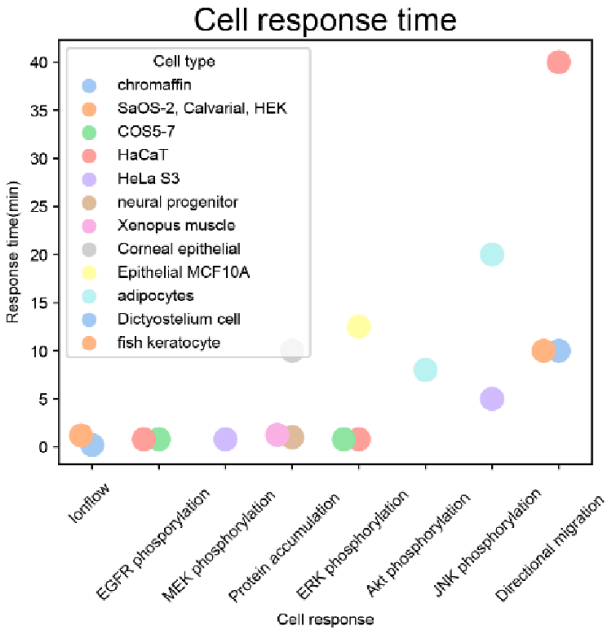

Figure 3. Cell response time categorized by response type and cell line. Response type is illustrated in different x-axis positions and different cell lines are indicated in different colors. Data and references are summarized in Table 1.

Table 1

Summary of the Response Time of EF-induced Cellular Responses

Cell type	**Stimuli**	**Pathway**	**Response**	**Response time**
Chromaffin cells (Bagalkot et al., 2019)	Pulse	Ca^{2+}	Ca^{2+} influx	Several seconds
SaOS-2, Calvarial, HEK cells (Perike et al., 2014)	DC	NHE3	H^{+} bubble	1.2 min
Neural progenitor cells (Meng et al., 2011)	DC	-	EGFR accumulate towards cathode	1 min
Xenopus muscle cells (H. L. Zhang & Peng, 2011)	DC	-	AchR accumulation towards cathode	0.5-2 h
Corneal epithelial cells (M. Zhao et al., 2002)	DC		EGFR accumulate towards cathode	10 min
COS5-7 cells (Wolf-Goldberg et al*.,* 2013)	Pulse	EGFR-ERK	EGFR phosphorylation	<1 min
HaCaT cells (Wolf-Goldberg et al., 2013)	Pulse	EGFR-ERK	ERK phosphorylation	<1 min
HaCaT cells (Y. Cho, Son, Jeong, & Shin, 2018)	DC	-	Directional migration	30-50 min
HeLa S3 cells (Morotomi-Yano, Akiyama, & Yano, 2011)	Pulse	EGFR-ERK	MEK phosphorylation	1 min
HeLa S3 cells (Morotomi-Yano, Uemura, Katsuki, Akiyama, & Yano, 2011)	Pulse	JNK	JNK phosphorylation	5 min
Adipocytes (Ito et al., 2011)	Insulin (no EF)	Akt	Akt phosphorylation	<10 min
Adipocytes (Ito et al., 2011)	Insulin (no EF)	JNK	JNK phosphorylation	10-30 min
Epithelial MCF10A cells (L. Guo et al., 2019)	AC	EGFR-ERK	ERK phosphorylation	10-15 min
Dictyostelium discoideum (Jeon et al., 2019)	DC	RasG, Gβ	Directional migration	10 min
Fish keratocytes (Y. H. Sun et al., 2018)	DC	-	Directional migration	10 min

The next pattern we have found is that in the same cell, different responses take different time to happen. Take HaCaT cell (colored in orange in Figure 3) as an example, EGFR phosphorylation, ERK phosphorylation and directed migration happen in different timeframes. As for Hela S3 cell (colored in purple in Figure 3), the MEK phosphorylation (take place within 1 min) is quicker than the JNK phosphorylation. These differences may indicate that faster cellular response locates in the upstream of the signaling pathway or in a different shorter signaling pathway. Cell migration is a complicated process which needs several pathways to coordinate, therefore it usually takes longer time (30-50 min) for cells to show different migrational behavior. In some experiments, cells under EF stimulation need hours to reach maximum speed (Y. Cho et al., 2018; Jeon et al., 2019; Y. H. Sun et al., 2018).

The last pattern is that even for the same cellular response, different cell types need different time to progress. For instance, EGRF accumulation in neural progenitor cells only takes less than 1 min (Meng et al., 2011), yet it takes about 10 min in corneal epithelial cells (M. Zhao et al., 2002). This discrepancy indicates that the upstream interactions may be different in these two types of cells, or possibilities are that plasma membrane features are better developed in neural cells rather than epithelial cells to coordinate this response. With regard to directed cell migration under EF stimulation, fast-moving cells like *Dictyostelium discoideum* can reach a maximum speed of 4 μm/min within 10 min and reverse direction within 10 min when EF polarity changes (Jeon et al., 2019); while slow-moving epithelial HaCat cells need around 30 min to show noticeable migrational change and 50 min to reach maximum speed (Y. Cho et al., 2018).

The spatial distribution of cellular response is also worth investigating. In some reports, one cell can show different responses on its anode side and cathode side when applied with unform EF stimulation, suggesting non-uniform distribution of signal molecules inside the cell. When cells are exposed to nanosecond pulsed electric field (nsPEF), the EF can penetrate cell membrane and exert effect on cytoplasmic structures like mitochondria (Beebe, Chen, Sain, Schoenbach, & Xiao, 2012), microtubules (Chafai et al., 2020), etc. In these circumstances, high spatial resolution is necessary to locate which organelle is affected by nsPEF.

Furthermore, most current studies only report averaged results from large population of cells. However, cells applied with electrical stimuli can have heterogeneous responses which have already been observed in some chemical stimulation experiments (Sparta et al., 2015). Therefore, single-cell behavior characterization is also needed to examine the diverse responses among a group of cells. Recently, there are some newly developed FRET reporters (Fosbrink, Aye-Han, Cheong, Levchenko, & Zhang, 2010) and translocation reporters (Regot, Jacob, Bryce, Carrasco, & Markus, 2014) available for kinase activity detection. Based on phosphorylation switch, these reporters can provide real-time kinase response in single-cell resolution. So instead of discrete data point from conventional biological analysis method, it is now possible to get continuous reading of individual cell behavior, providing a huge advance in the study into EF influence on cells.

The regulations by feedback loops in cellular responses. While we consider EF as an extracellular signal that can be transmitted through signaling pathways and result in proper cellular responses, it is certainly not a one-way process since signaling pathways

are always regulated by both positive and negative feedback loops in cells. Through different kinds of regulatory feedback loops, the extracellular signal can be converted into certain activation pattern that corresponds to particular cellular outcome. Take ERK signaling pathway for example, there are three positive and one negative internal feedback loops, as well as two external feedback loops in which TACE is positive and ARGOS is negative (Arkun & Yasemi, 2018). Together they shape the dynamics of ERK activation (frequency, amplitude, duration etc.) and then cells can generate proper responses from proliferation, differentiation or apoptosis (Shin et al., 2009). When comparing the ERK activation triggered by epidermal growth factor (EGF) and EF pulses, Wolf-Goldberg et al. (2013) found that although EGFR phosphorylation caused by EGF was much stronger than EF pulses, but the final ERK phosphorylation levels are similar, indicating the involvement of regulatory feedback loops in the signal transduction process. Given the above, when studying how EF interacts with cells, the regulation effect form different feedback loops should also be taken into consideration.

The Motivation of My Research

Considering the current understanding of how EF influences cells, we think the impact of intermediate frequency AC EF has been overlooked. As hypothesized by Kotnik and Miklavcic (2000), when cells are exposed to external EF, the simulated power dissipations in the cytoplasm (P_i), the cell membrane (P_m) and the surrounding medium (P_e) are plotted in Figure 4A. According to their simulation results, from DC to medium frequency, the power dissipation generated in the membrane is higher than that in the medium, and the power dissipation in the cytoplasm is negligible. Only when the

frequency is above 100 kHz, the power dissipation in the cytoplasm starts to increase. Weaver and Astumian's (1990) theoretical study implies that cell membrane macromolecules can directly respond to EF at magnitude of 10^{-3} V/cm, leading to conformational changes. In addition, this kind of 'electroconformational' coupling is frequency dependent, typical optimal coupling rate is in the intermediate frequency of 10^2 to 10^6 Hz (Figure 4B). From what has been discussed above, in our further exploration of how EF affects cellular functions, we have decided to employ 50 kHz AC EF as EF stimuli. First, AC EF cannot cause directional forces or ionic flows to cells, ruling out some interferences from EF effect; second, 50 kHz EF stimulation is able to induce high voltage and power dissipation in the cell membrane, making it more possible to introduce conformational change. In order to compare cell responses from the same group/condition, we need to make the EF stimulation highly localized. To this end, we design and fabricate microelectrodes to deliver electrical stimuli. Besides, we also utilize a real-time fluorescent biosensor to probe cell signaling pathway activity with single-cell and high spatiotemporal resolution.

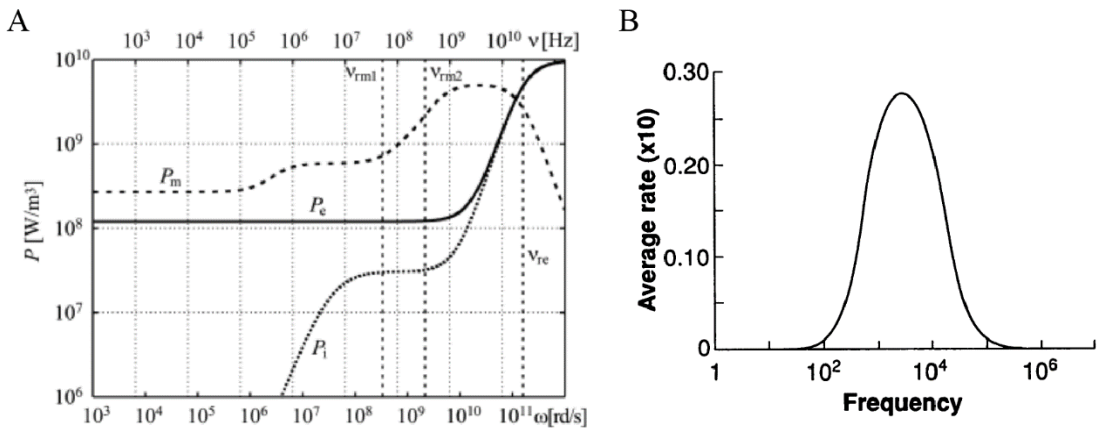

Figure 4. The relationship between EF effect and frequency. (A) Simulation results of power dissipation in the cytoplasm (P_i), membrane (P_m), and the surrounding medium (P_e) at $\sqrt{2}$ ×100V/cm as functions of frequency (Tadej Kotnik & Miklavčič, 2000). (B) The frequency dependence of the average rate of conversion of substrate S into product P by the periodic field (James C Weaver & Astumian, 1990).

In this dissertation, Chapter 2 focuses on the development of the two generations of EF stimulation devices and environmental chambers to study cell signaling pathway activities under EF stimulation, as well as cell proliferation and migration. Chapter 3 is dedicated to the study of how AC EF affects cell signaling pathway: AC EF regulation of ERK signaling pathway. We have found that intermediate frequency AC EF can trigger ERK activation and inhibition in different conditions and these ERK responses show dependence on AC EF parameters. Last, how AC EF affects cell physiological behavior is investigated in Chapter 4, focusing on cell proliferation and migration. We have proved that prolonged AC EF stimulation can inhibit cell proliferation and migration and the inhibition effect on cell proliferation depends on AC EF amplitude, stimulation pattern

and pulse rising time. Finally, a summary of conclusions and future directions are pointed out in Chapter 5.

CHAPTER 2

ELECTRIC FIELD STIMULATION DEVICES

Introduction

Since last century, several EF stimulation devices and set ups have been developed for both in vitro and in vivo applications. Nowadays with significant advances in material science and electronic devices, EF stimulation devices are under the trend of miniaturization and compatibility. According to EF coupling method, EF stimulation devices can be basically divided into three kinds: direct coupling, capacitive coupling, and inductive coupling.

Direct coupling is the most straightforward method to apply EF stimulation to cells as it just consists of two electrodes immersed into the medium (Figure 5A). The EF effect from direct coupling is often very robust and reproducible, so it is also the most used one in research. However, as the electrode is in direct contact with medium, faradaic reactions can happen on the electrode surface, producing some cytotoxic byproducts such as hydrogen peroxide and free radical intermediates. To overcome this drawback, a common practice is to set up two salt bridges on anode and cathode respectively (Figure 5B). As a result, chemicals produced on the electrode surface can be separated from the medium reservoir.

Inductive coupling is a non-invasive EF stimulation method in which EF is produced across cell culture medium in an oscillating magnetic field (Figure 5C). As electrodes are not in contact with medium, there is no risk from faradaic reaction byproducts. This technique has been used in a variety of subjects covering body, tissue, cell and protein samples in lab research (Pilla, 2007). Still, there are some disadvantages

in using inductive coupling method: first is the requirement of a complicated instrument system; second is that the inductive EF is always in combination with magnetic field, making it more difficult to explain the underlying mechanism.

Capacitive coupling happens when there are dielectric layers between electrodes and the cell medium (Figure 5D), so it is also a non-invasive EF stimulation method. The dielectric layer can be made of insulating polymers, inorganic materials, air, or other dielectric materials. When a voltage is established between two electrodes, all components in the cell culture medium would be polarized by the EF. Due to the high impedance from dielectric layers, capacitive coupling devices usually need high voltage power sources.

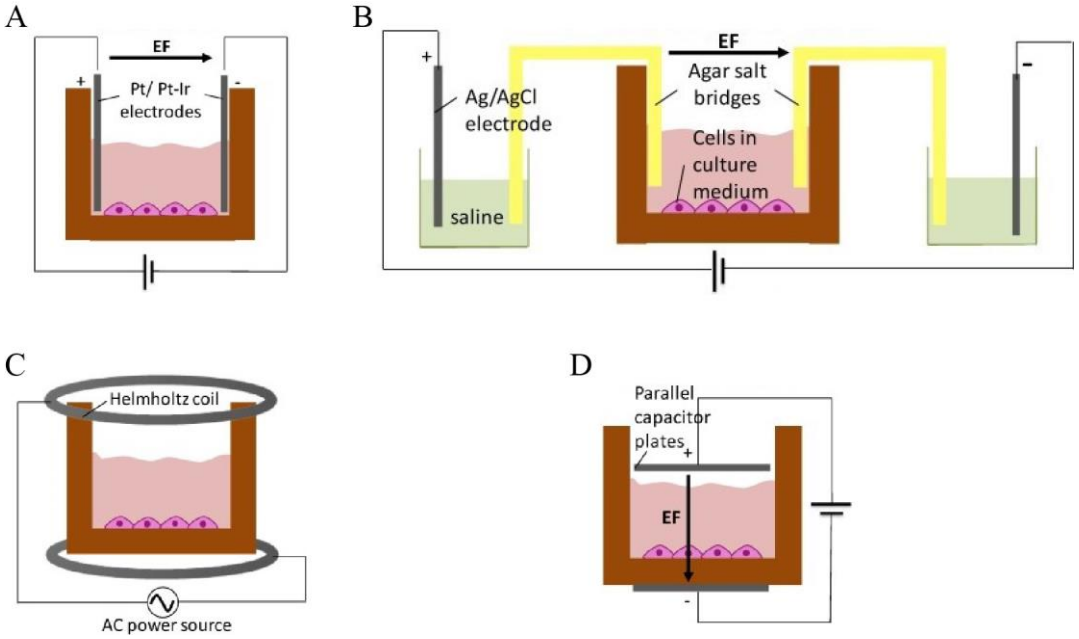

Figure 5. Methods to apply EF stimulation to cells. (A) Direct coupling. (B) Direct coupling with salt bridges. (C) Inductive coupling. (D) Capacitive coupling (Thrivikraman et al., 2018).

Microelectrodes to Deliver Localized AC EF

In our research, we adopt capacitive coupling method to deliver AC EF to cells. As stated in the motivation, we want to make the EF stimulation highly localized, so instead of using conventional metal wires or bars as electrodes, we design and fabricate thin-film microelectrodes via photolithography. The microelectrode design and structure are illustrated in Figure 6A-B.

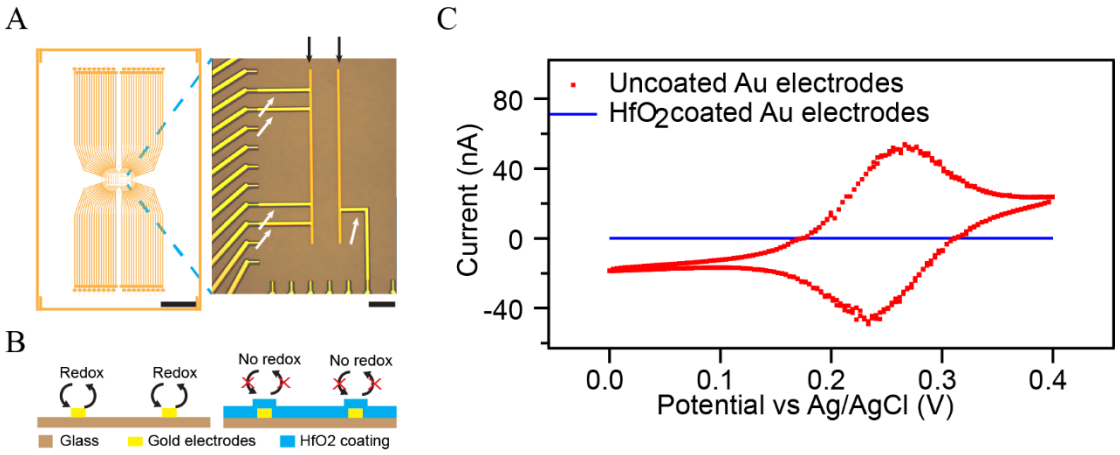

Figure 6. Microelectrodes with HfO_2 coating. (A) Left: design of microelectrode array on the glass coverslip. Scale bar: 5mm. Right: image of a pair of microelectrodes from the center area. Scale bar: 200 µm. The white arrows indicate metal connections that are insulated by SU-8 polymer. The black arrows mark the exposed electrodes used to interface with cells. (B) Left: redox reactions can happen on bare gold electrodes. Right: redox reactions can be suppressed by the high-k HfO_2 coating. (C) Cyclic voltammetry scan in 5 mM $[Fe(CN)_6]^{4-}/[Fe(CN)_6]^{3-}$ solution of bare gold microelectrodes (red dot) and HfO_2 coated microelectrodes (blue line) (L. Guo et al., 2019).

In the microelectrode design and fabrication process, there are several key considerations: (1) On the microelectrode chip, only pairs of microelectrodes are exposed to interface with cells, the other connection parts are passivated by insulating polymer SU-8. Therefore, the EF delivered by microelectrodes is highly localized: very strong near microelectrodes and rapidly decayed outside the vicinity. (2) Microelectrodes are fabricated on a 170 μm thick, 40 mm × 24 mm glass coverslip. This transparent substrate enables direct cell observation on a microscope during EF stimulation. Moreover, by carful pattern design, multiple microelectrode pairs can be placed on the coverslip and operated independently, increasing test efficiency significantly. (3) To achieve capacitive coupling and exclude any faradaic reactions on the microelectrodes, we deposit a layer of high-k HfO_2 on top microelectrodes via atomic layer deposition (ALD). Our test results show that a layer of 10 nm HfO_2 can fulfil the task of passivation without considerably increasing the impedance. The cyclic voltammetry test results of uncoated and HfO_2 coated microelectrodes are depicted in Figure 6C, redox reactions are completely suppressed by HfO_2 layer.

First-generation EF Stimulation Device

To maintain the cell culture environment during EF stimulation experiment, the glass coverslip patterned with microelectrode arrays is assembled into an on-stage incubation chamber where cells can be plated on top of microelectrodes. After assembly and connection, the chamber can be mounted on an inverted microscope for cell imaging. Cell culture condition (37 °C, 5% CO_2, and humidity) is maintained by customized sensors and control modules.

The schematics of the first-generation EF stimulation device and cell experiment setup are shown in Figure 7. Specifically, there are two major components. First one is the cell culture chamber with microelectrodes: microelectrode chip is connected to a printed circuit board (PCB) using wire bonding, and a petri dish with a 13-mm hole is sealed on top of the chip serving as cell culture medium reservoir. The other component is the on-stage incubator: a CNC machined aluminum box is designed to fit on the stage of an inverted microscope and equipped with environmental sensors as well as heating, CO_2 flow and humifying modules. In the cell experiment, the incubator can keep cells healthy for several hours. We employ this device to study how AC EF influence cell signaling pathway dynamics.

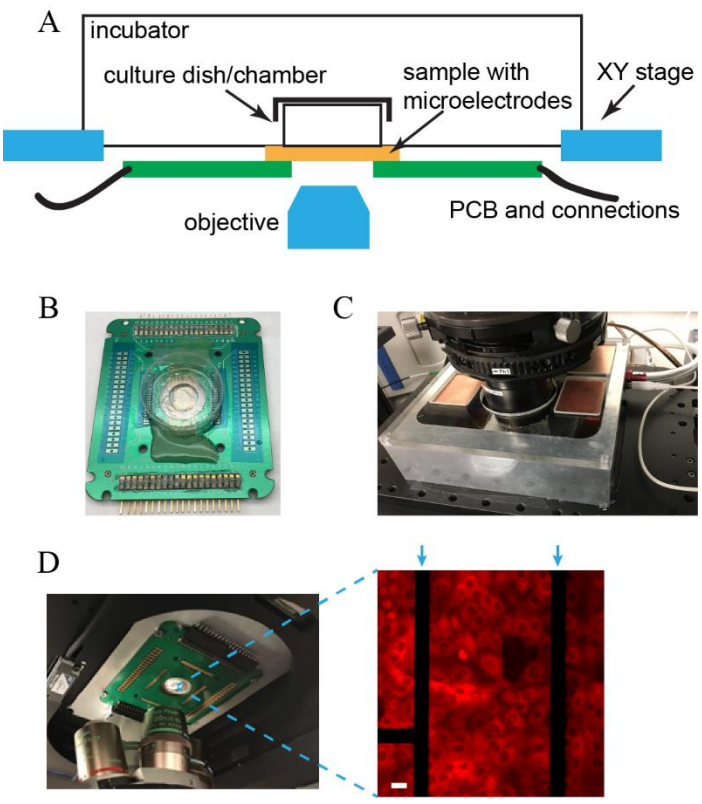

Figure 7. Schematics and experiment setup of the first-generation EF stimulation device. (A) Schematics of the first-generation EF stimulation device. (B) Image of the cell culture chamber with microelectrodes. (C)) Image of the device mounted on an inverted microscope. (D) Left: image from the bottom part of the device when mounted on the microscope. Right: a typical fluorescent image of cells during EF stimulation test. The blue arrows indicate the positions of exposed microelectrodes. Scale bar: 10 μm.

Based on the design of the first-generation EF stimulation device, here we report the fabrication and assembly process. The fabrication of microelectrodes was based on a #1, 24 × 40 mm microscope coverslip (Thermo Scientific). First the glass coverslip was treated with piranha solution, a mixture of sulfuric acid (Sigma-Aldrich) and hydrogen peroxide (GFS Chemicals), to clean organic residues and hydroxylate the surface. Then a

layer of 740 nm silicon oxide was deposited on the glass surface using a plasma enhanced chemical vapor deposition (PECVD) system (Oxford PLASMALAB 100 PECVD) to increase the surface uniformity and smoothness. Photolithography (OAI Model 808 MBA Mask Aligner) and thermal evaporation (Cressington 308R Thermal Evaporator system.) were used to define the Cr/Au (1/25 nm) microelectrodes on the glass surface. For bare gold microelectrodes, an insulating layer of 500 nm SU-8 (MicroChem Inc., SU-8 2000.5) was patterned to cover all the connection parts. For HfO_2 coated microelectrodes, after a layer of 1 nm Chromium oxide (Lesker PVD75 sputter coater) for better adhesion, a uniform HfO_2 coating was deposited with an ALD system (Cambridge Savannah ALD system), in the end the 500 nm SU-8 insulating layer was constructed.

The PCB manufactured by Sunstone Circuits was used as an interface to connect microelectrode arrays to AC EF signals. First, the microelectrode chip was glued on a PCB with polymethyl methacrylate (PMMA, MicroChem), then connection pads on the chip were linked to the PCB via wire bonding (7KE convertible manual wire bonder, West-Bond, Inc.). Afterwards, a 35 × 10 mm petri dish with a 13-mm hole on the bottom was glued on the chip using Kwik-Sil silicone elastomer (World Precision Instruments) to serve as a reservoir for cell culture medium (Figure 7B).

The customized on-stage incubator was CNC machined by Xometry, and it was integrated with sensors for temperature, humidity, and CO_2, as well as polyimide heating pads (Digi-Key) and CO_2 supply tubing. The PCB based cell culture chamber was attached to the bottom of the incubator by 4 insulating screws. During the EF stimulation experiment, the incubator was connected to a control module which could switch on or off the heating and CO_2 injection in the incubator according to sensors' readings.

Second-generation EF Stimulation Device

The first-generation EF stimulation device is fairly reliable to maintain cell condition for several hours, which is long enough to conduct tests of cell signaling pathway activities. However, when our investigation ventured into cell physiological changes in response to EF stimulation, which could take several days to complete the observation, it became necessary to develop a new EF stimulation device with improved capability for maintaining cell culture environment.

The schematics of the second-generation EF stimulation device and experiment setup are illustrated in Figure 8, there are a few key considerations in this device upgrading. First, the exposed microelectrodes that are used to interface with cells are extended from 350 μm to 1500 μm (Figure 8B) so that more cells can be affected by EF, increasing sample size. Second, we use push button switches to connect microelectrodes to their corresponding pins on the PCB instead of wire bonding. When the microelectrode chip is sandwiched between PCB and the metal base plate with 4 screws, a stable contact is naturally formed between microelectrodes and the conductive bottom of the switches (Figure 8C). This design makes the connection more reliable and convenient. Third, a 3D printed chamber with a removable lid is glued on top of the PCB (Figure 8D), maintaining humidity and 5% CO_2 for the cells cultured in it. Last, a PureBox (Tokai Hit) is installed on the microscope as a clean enclosure to prevent cell contamination during experiments. Additionally, the PureBox supports laminar flow of filtered warm-air and forced-air circulation, keeping optimal temperature condition for long-term culture.

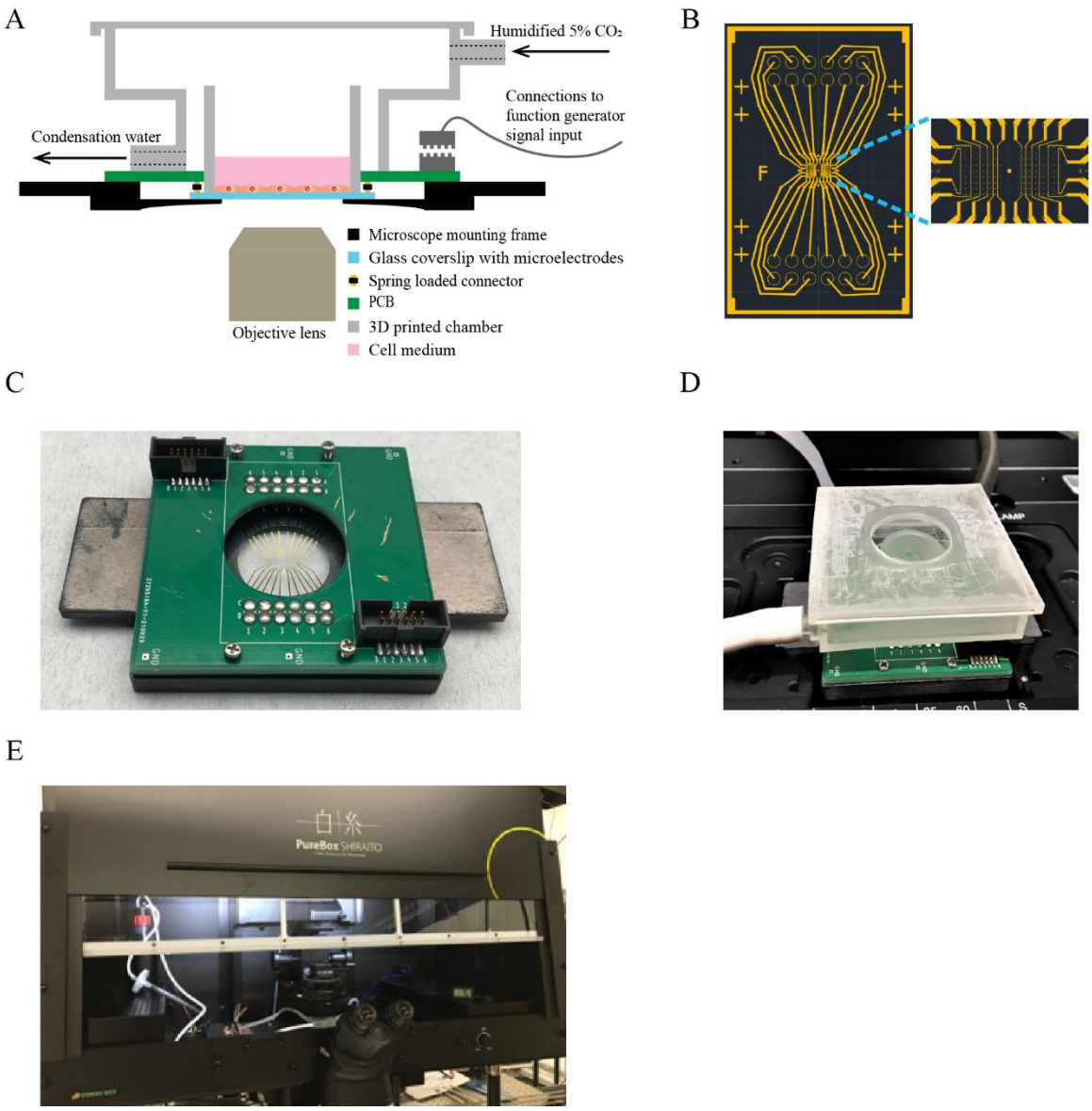

Figure 8. Schematics and experiment setup of the second-generation EF stimulation device. (A) Schematics of the second-generation EF stimulation device. (B) Left: the AutoCAD design of extended microelectrode arrays on the glass coverslip. Right: the zoomed in image of exposed microelectrodes from the center area. (C)) An image of connected PCB, microelectrode chip and base plate assembly. (D) An image of an assembled cell culture chamber mounted on a microscope. (E) An image of the PureBox installed on the microscope.

The fabrication process of the extended microelectrode chip is similar to the previous one, only the microelectrode pattern is completed in two photolithography steps. As we use push button switches to connect microelectrodes to PCB, the contact area at the microelectrode needs thicker Au layer to ensure connection. However, the exposed microelectrodes interfacing with cells must be thin enough to secure insulated HfO_2 coating. Hence, the Cr/Au (1/25 nm) inner electrodes were patterned on the glass coverslip first, then the Cr/Au (3/100 nm) outer electrodes were defined in alignment with inner electrodes. The last parts are the HfO_2 coating and SU-8 passivation steps.

In the cell culture chamber assembly, first push button switches (Digi-Key) were soldered on PCB, then PCB, microelectrode chip, and metal base plate were aligned together and fixed with 4 screws. Next, a cylindrical component, and a chamber with removable lid and tubing connectors were designed in AutoCAD and 3D printed with Form3 printer (Formlabs). Thereafter, the cylindrical component was glued on the microelectrode chip center to make a culture medium reservoir using Kwik-Sil silicone elastomer (World Precision Instruments), then the chamber was glued on top of the PCB. On the chamber lid, a glass coverslip was glued to cover the opening for the light path during cell imaging. In the cell experiment, the cell chamber was connected to humidified, 5% CO_2 air supply. Temperature control was supported by PureBox.

Summary

In summary, we have developed two generations of EF stimulation devices for different research purposes: the first-generation device is used to study cell signaling pathway activity under EF stimulation (short time), and the second-generation device is

used to investigate cell physiological changes when applied with EF stimulation (long time). In particular, we design and fabricate HfO_2 coated microelectrode arrays to deliver capacitively coupled EF to cells, making the EF simulation highly localized. Moreover, as there are multiple microelectrode pairs on one chip, different EF stimulation tests can be conducted on one chip with the same group of cells. In the actual test, cells are plated on top of microelectrodes and maintained at culture condition during the whole experiment. These EF stimulation devices have laid the groundwork for our research of cellular response to EF stimulation.

CHAPTER 3

ELECTRIC FIELD REGULATION OF ERK SIGNALING PATHWAY

Introduction

Many signaling pathways are involved in the EF regulation of cell functions. Among them, ERK signaling pathway, a member of the MAPK cascades, is of our most interest. First, as ERK signaling pathway plays a significant role in cell growth, proliferation, migration, and metabolism, dysregulation of this pathway is a major trigger for several types of cancers (Y. J. Guo et al., 2020; Lavoie, Gagnon, & Therrien, 2020). Therefore, ERK pathway has been a common therapeutic target in oncological research. Second, many EF elicited cellular response, such as directed cell migration (M. Zhao et al., 2002) and proliferation alteration (Xu et al., 2016), are correlated with ERK pathway, yet the mechanistic study so far has been unsatisfactory.

The canonical ERK signaling pathway has been well characterized. As shown in Figure 9A, the signaling pathway is initiated when some specific extracellular ligands, e.g., epidermal growth factor (EGF), bind to epidermal growth factor receptor (EGFR) at the cell membrane. This binding process prompts receptor dimerization and autophosphorylation on its cytoplasmic tyrosine kinase domains, which then act as recognition sites for adaptor proteins Shc and Grb2. Afterwards, Son of sevenless (SOS) is subsequently recruited from cytosol to the cell membrane through Shc and Grb2, leading to the formation of the Shc-Grb2-SOS complex. Next, this complex acts as the major guanine nucleotide exchange factor that catalyzes the conversion of the membrane-bound protein Ras, from inactive Ras-GDP to active Ras-GTP. The activated Ras- GTP then recruits Raf to the cell membrane for activation. Once Raf is activated, it is capable

of activating downstream MEK1/2, which eventually activates ERK1/2. These two activation steps are both achieved by double phosphorylation at their respective kinase domains. Finally, the phosphorylated ERK can translocate to the cell nucleus to activate a wide variety of transcription factors and other nuclear substrates, facilitating appropriate cellular functions (Barbosa, Acevedo, & Marmorstein, 2021; Lake, Corrêa, & Müller, 2016).

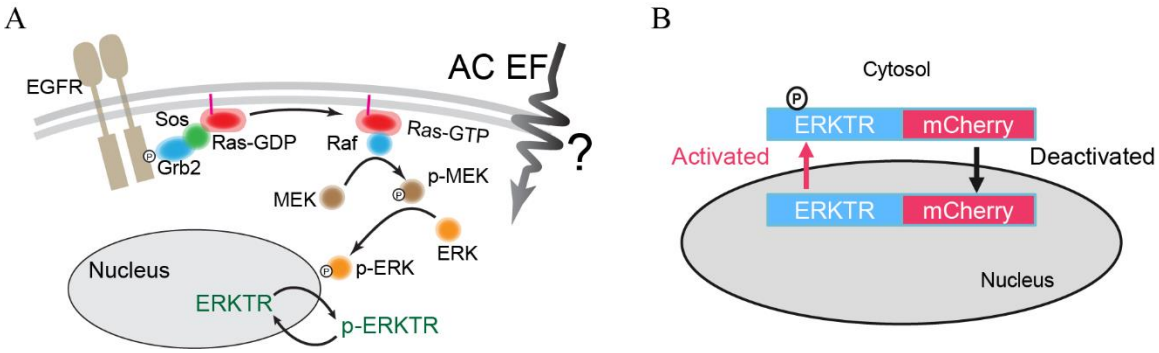

Figure 9. Schematics of ERK signaling pathway and ERKTR. (A) The signaling cascade of EGFR-Ras-ERK pathway. (B) The translocation mechanism of ERKTR based on kinase phosphorylation. When ERK is activated, the red fluorescent ERKTR stays in the cell cytosol; when ERK is deactivated, it stays in the cell nucleus.

To study ERK activities under EF stimulation, we need to find a tool to quantitatively measure ERK dynamics in live cells with high spatiotemporal resolution. In the light of recent advances in fluorescent live cell reporters for kinase activity detection, we choose an ERK translocation reporter (ERKTR) based on phosphorylation-stimulated nuclear/cytoplasmic translocation to quantify ERK dynamics. As depicted in Figure 9B, the ERKTR consists of an mCherry-tagged substrate targeting activated ERK,

a bipartite nuclear localization signal (bNLS) and a nuclear export signal (NES). The bNLS is negatively regulated by phosphorylation while the NES is positively regulated. Therefore, when ERK in the cell is not activated, bNLS is enhanced and this mCherry-labeled ERKTR stays in the cell nucleus; Once upon ERK activation, the reporter gets phosphorylated by activated ERK, thus NES is enhanced, making the reporter translocate from cell nucleus to the cytosol. This translocation of ERKTR can introduce a change in the fluorescent intensity ratio of cytosol (Fc) to nucleus (Fn), through which we can quantify ERK level in single-cell resolution. Unlike conventional biological analysis methods like western blot and immunofluorescence that are limited to results after cell fixation, this ERKTR enables us to get real-time ERK response reading during experiments, improving our test efficiency greatly.

In this project, we use 50 kHz AC EF to stimulate mammary epithelial cell MCF10A and discover that by variation of AC EF parameters and cell conditions, the dynamics of ERK activity in MCF10A cells can be modulated. Besides, this modulation of ERK signaling pathway by AC EF shows dependence on waveform and pulse timing. Furthermore, we propose our understanding of how AC EF stimulation perturbs ERK signaling pathway and causes opposite reactions of activation and inhibition.

Materials and Methods

Cell culture. MCF10A cell line in co-expression of EKAR3 and ERKTR was kindly provided by Zhao Lab (UC-Davis), and it was constructed using the method described in reference (Sparta et al., 2015). First co-transfection of pPBJ-EKAR3-nes and the pCMV-hyPBase transposase vector was used to make cells stably express EKAR3,

then MCF10A-EKAR3 cells were infected by retroviral particles carrying ERKTR-mCherry, resulting in MCF10A-EKAR3-ERKTR cells.

MCF10A in co-expression of Raf-RBD-GFP and CFP-Lyn-FRB was obtained from Devreotes Lab (JHU). Cell transfection method was mentioned in reference (Zhan et al., 2020). In brief, transient transfection was applied using Lipofectamine 3000 reagent (ThermoFisher Scientific). Stably transfected MCF10A cells were selected and/or maintained in culture medium with 2 μg/ml Puromycin (ThermoFisher Scientific) and 2 mg/ml Zeocin (ThermoFisher Scientific).

Both kinds of MCF10A cells were cultured in Dulbecco's modified Eagle's medium (DMEM)/F-12 (Gibco) supplemented with 5% horse serum (Gibco), 0.5 mg/ml hydrocortisone (Sigma-Aldrich), 10 mg/ml human insulin (Gibco), 20 ng/ml EGF (Life Technologies), 100 ng/ml cholera toxin (Sigma-Aldrich), 50 U/ml penicillin and 50 U/ml streptomycin (Gibco). Cells were incubated in a humidified atmosphere containing 5% CO_2 at 37 °C.

Live cell imaging. The first-generation EF stimulation device was used in this project. Time-lapse images were acquired from a Nikon Eclipse Ti-U microscope equipped with a pco.edge 4.2 sCMOS camera and a SOLA SE II 365 light engine. Cell images were taken using a 20X CFI S Plan Fluor Ph1 objective with 0.45 numerical aperture and recorded via NIS-Elements software. ET-mCherry and ET-EYFP (49008 and 49003, Chroma Technology Corp) filter sets were used in mCherry and YFP channels, respectively. As for the Ras activity test, a spinning disk module (BD CARVII) was used to capture confocal images of cells.

Before cell plating, the microelectrode chip assembled into EF stimulation device was treated with FNC coating mix (AthenaES) to increase cell attachment. MCF10A-EKAR3-ERKTR cells were dissociated into single cell suspension with 0.25% trypsin-EDTA (Gibco) and seeded in the cell chamber. After plating, cells were cultured in the incubator overnight for attachment. In order to minimize background fluorescence, DMEM/F12 without phenol red (Gibco) was used in all cell imaging experiments. In ERK inhibition experiments, to maintain cells at high ERK level, the medium without phenol red was supplemented with 5% horse serum, 0.5 mg/ml hydrocortisone, 10 mg/ml human insulin, 20 ng/ml EGF, 100 ng/ml cholera toxin, 50 U/ml penicillin and 50 U/ml streptomycin. In ERK activation experiments, lower ERK level was needed to enhance contrast, so the medium without phenol red was just supplemented with 0.5 mg/ml hydrocortisone, 100 ng/ml cholera toxin, 50 U/ml penicillin and 50 U/ml streptomycin. Additionally, Cells also needed to be starved in this medium for 4 hours prior to EF simulation test to deplete EGF inside cells. In the Ras activity test, MCF10A-FRB-RBD and MCF10A-EKAR3-ERKTR cell suspensions were first mixed with equal density and then plated on the microelectrode chip. After plating, mixed cells were also cultured in the incubator overnight to allow attachment. After all cell preparation, the stage top incubator with cells was mounted on the microscope and connected to the control module. The cell culture environment was maintained at 37°C in 5% CO_2 during the whole process of live cell imaging.

Electrochemical test. The cyclic voltammograms of both bare gold and HfO_2 coated microelectrodes were acquired with a Keithley 263B source meter in combination with custom Igor Pro (Wave Metrics) software interface. Two-electrode setup was used

in the scan: one microelectrode was used as working electrode and the other one as ground to mimic the application of AC EF stimuli in cell experiment. The scans were conducted in a electrolyte of 5 mM $[Fe(CN)_6]^{4-}$/$[Fe(CN)_6]^{3-}$ and 0.1 M KCl.

AC EF stimulation. The 50K Hz AC EF stimuli with different waveforms were designed and generated using an arbitrary function generator (AFG 31000 series, Tektronix). The function generator was first connected to an isolated amplifier to avoid potential differences. Next the electrically isolated signal was distributed to PCB pins using a relay circuit which was controlled by an Arduino board. Connection from PCB pins to microelectrodes were made by wire bonding as mentioned in the device assembly steps from Chapter 2.

Cell membrane electroporation, Ca^{2+} and ROS tests. MCF10A-EKAR3-ERKTR cells were plated in the first-generation EF stimulation devices, after starvation, cells in different devices were treated with 50 μM SYTOX orange (Invitrogen), 3 μM Ca^{2+} chelator BAPTA AM (Life Technologies) and 350 μM ROS quencher Trolox (Sigma-Aldrich), respectively. Then AC EF stimulations were applied to cells through microelectrodes. For electroporation test, fluorescent cell images were acquired with excitation filter of 525-535 nm and emission filter of 550-600 nm; for Ca^{2+} and ROS tests, cell ERK activity was recorded with ET-mCherry and ET- EYFP filter sets.

Local temperature measurement after AC EF stimulation. Patch clamp pipettes were constructed using Borosilicate capillary glass (GC150-10, Warner Instruments). The capillary pulling process was performed with a micropipette puller (P-1000, Sutter Instruments). Next, the pipette was filled with 0.1M KCl solution and connected to a patch clamp amplifier (EPC800 USB, HEKA). In the measurement, an

Ag/AgCl electrode was used as reference electrode, and 10 mV of bias was applied to the pipette. The current output was collected with an ITC-18 data acquisition system from HEKA with a sampling rate of 20 kHz. When the room temperature was stabled at 21.6±0.2 °C, the pipette tip was positioned between a pair of microelectrodes in a first-generation EF stimulation device. The cell chamber was filled with culture medium, and the pipette tip was placed about 10 μm above the glass chip surface using a micromanipulator (MP-225, Sutter Instrument). If the temperature increases after AC EF stimulation, then the ion mobility would rise as well, which leads to higher conductivity. Considering the patch clamp tip has a diameter of around 1 μm, the conductivity would be very sensitive to the local temperature variation at the opening. In the test, the first 10 min without AC EF stimulation was referred as a silence period, during which the current was recorded to correct any slow drifting. Then 60 sec of data immediately before and after AC EF stimulation were acquired to calculate the temperature change according to Arrhenius equation (J. Yao, Liu, & Qin, 2009):

$$T = \frac{1}{\frac{1}{T_0} - \frac{R}{E_a}\ln\left(\frac{I}{I_0}\right)}$$

Where T_0 is the initial room temperature (21.6 °C, 294.75 K), R is the gas constant, E_a is the nominal activation energy (16.07 KJ/mol), and I and I_0 are the pipette currents recorded at T and T_0, respectively.

Blocker tests. The blocker tests with AC EF stimulations were conducted in the first-generation EF stimulation device and in a 96-well plate with EGF, respectively. During starvation process, 0.5 μM MEK inhibitor trametinib (Selleck Biochemicals), 20 μM Raf inhibitor sorafenib (Biotang), 5 μM TKI afatinib (Selleck Biochemicals), 2 μM

TKI erlotinib (Selleckchem), 50 μM TKI gefitinib (Selleckchem), and 100 μg/ml EGFR antibody cetuximab (ERBITUX) were supplemented in cell medium. Cell response was recorded using fluorescent imaging when applied with AC EF stimulation and EGF stimulation (20 ng/ml).

Data processing. Cell image processing was performed using NIS.ai Module (Nikon). After training, the Segment.ai module was used to segment cell nuclei from YFP channel fluorescent images as reporter YFP-EKAR3 was confined to the nucleus by a nuclear localization sequence. Based on the nucleus boundary, an inner ring as nuclear region and an outer ring as cytosolic region were defined by erosion and dilation. The mCherry channel florescent images from mCherry-ERKTR were used to calculate mean fluorescence intensity of nuclear region and cytosolic region. Cell ERKTR ratio was defined as the ratio of cytosolic to nuclear fluorescent intensity. Data from NIS.ai module was then imported to Igor pro (WaveMetrics) for cell tracking: a customized Igor function was developed to identify same cells from time-lapse images according to their coordinates. After cell tracking and ratio calculation, each cell's ERKTR ratio could be traced. In the Ras activity analysis, MCF10A-FRB-RBD and MCF10A-EKAR3-ERKTR cells are cultured together. The ERKTR ratio was still calculated by the fluorescent intensity ratio of cytosolic area to nuclear area. Due to the fact that the Ras activity in MCF10A cells is easily affected by the cell membrane contact from neighboring cells, we just choose single cell or cells have partial free cell membrane without any contacting for Ras analysis.

Results

AC EF can induce localized ERK activation in cells. The first-generation EF stimulation device with MCF10A-EKAR3-ERKTR cells were employed in the following experiments. Before tests, cells were deprived of serum and EGF for 4 h to stay at a low ERK activation state, then starved cells were applied with continuous 50 kHz bipolar symmetrical square wave. According to the fluorescent time-lapse images, we found that in some cells, around 3-6 min after AC EF started, the fluorescent intensity in cell nuclei decreased and that in cell cytosol increased, indicating ERK was activated in these cells. Figure 10A shows an mCherry channel image taken at 9 min after the onset of AC EF stimulation. When we zoomed in the areas close to microelectrodes (Figure 10B) and 200 μm further away from microelectrodes (Figure 10C), we noticed the different responses that only cells close to microelectrodes showed clear ERK activation while the rest of cells remained silent during AC EF stimulation. We also calculated the ERKTR ratio (Fc/Fn) of individual cells from these two areas (Figure 10D-E), cells near microelectrodes showed synchronized initial ERK activation about 9 min after AC EF stimulation started, then developed into different amplitude and duration. After around 30 min, the ERK level of the majority of cells gradually declined to the baseline. In the meantime, cells away from microelectrodes showed no ERK activation under AC EF stimulation. Given these results, we can first conclude that the AC EF stimulation can trigger highly localized ERK activation with synchronized initial response in MCF10A cells.

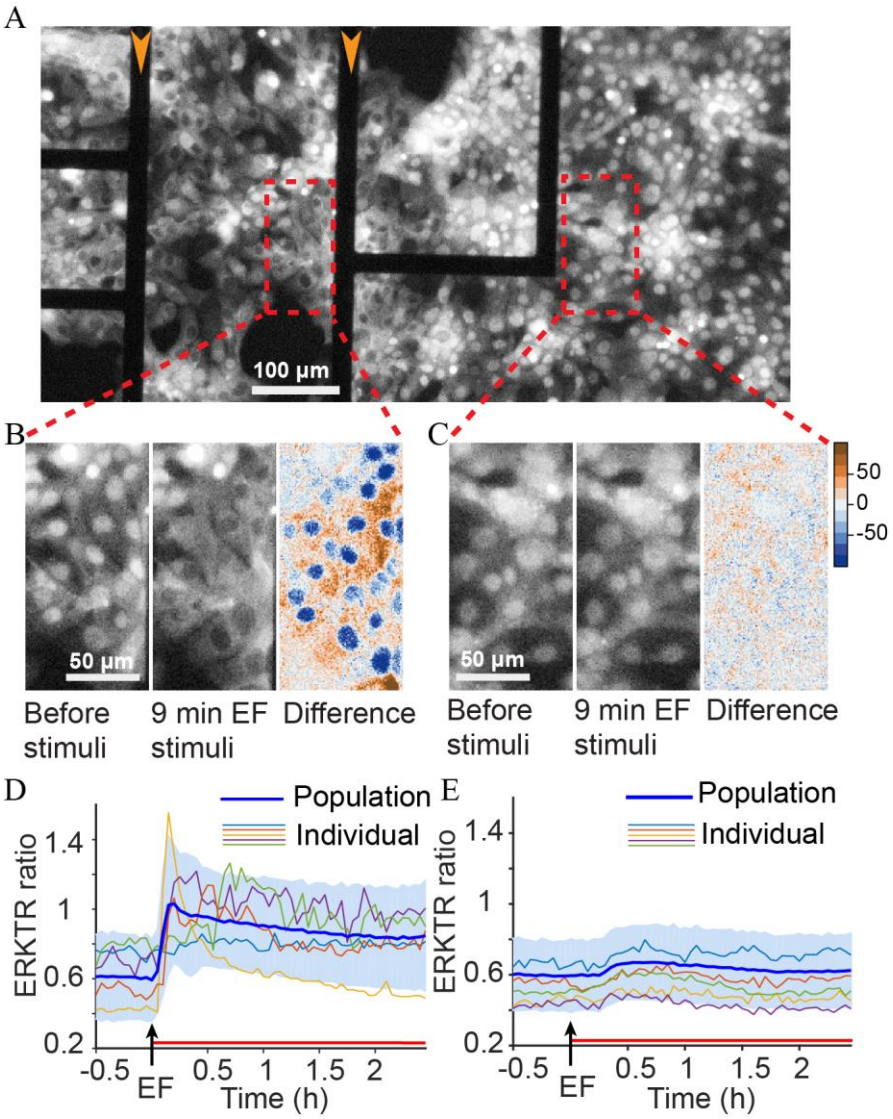

Figure 10. Localized ERK activation by AC EF. (A) Fluorescent cell image of ERK activation between microelectrodes delivering AC EF stimulation (the orange arrows indicate exposed microelectrodes). (B) Zoomed in image of cells between microelectrodes and (C) far away from microelectrodes. The image set from left to right: before AC EF, 9 min after AC EF started, and the fluorescent intensity difference of the two images (blue means intensity decrease and orange means increase). (D) Time traces of ERKTR ratio of cells near microelectrodes and (E) far away from microelectrodes.

The thick blue line and light shadow mark the mean and ±SD value of each timepoint. The black arrow denotes the time to apply AC EF stimulation and the beside red line indicates the sustained AC EF stimuli (L. Guo et al., 2019).

Frequency modulation of ERK activation by AC EF. Next, we have demonstrated that the frequency of ERK activation in selected cells can be modulated by the onset time of AC EF stimulation. In the previous test, we proved that highly localized and synchronized ERK activation could be achieved with AC EF stimulation, hence we figured the possibility to control the frequency of ERK activation just by cycling AC EF on and off with the right timing. In this test, starved MCF10A-EKAR3-ERKTR cells were applied with 3 min long bipolar square wave at 0 min, 48 min, and 93 min, AC EF was turned off during the rest of the time in the experiment. The cell images before and after AC EF stimulation at three timepoints are shown in Figure 11A. The same group of cells showed ERK activation after all three stimuli. We also plotted the time traces of ERKTR ratio from cells near microelectrodes (Figure 11B), we can clearly see 3 ERK activation peaks after each onset of AC EF stimulation, and the ERK level in cells decreased to a low state after around 10-20 min. In addition, as the cycle repeated, the activation peak from ERKTR ratio traces became higher each time, suggesting that the ERK activation in these cells were enhanced. According to the ERKTR time traces, we selected the ERK activation peak time and mapped them together (Figure 11C). From the peak time map, we learned that about half of the cells near microelectrodes showed ERK activation after all three short time AC EF stimulations, meanwhile about 30 % cells started to show response at the second time or the third time. These interesting findings

indicate that later AC EF stimulation can induce ERK activation in more cells, which is probably due to cell sensitization. To summarize, these results have verified that by careful time tuning, the frequency of ERK activation in MCF10A cells can be modulated by AC EF stimulation.

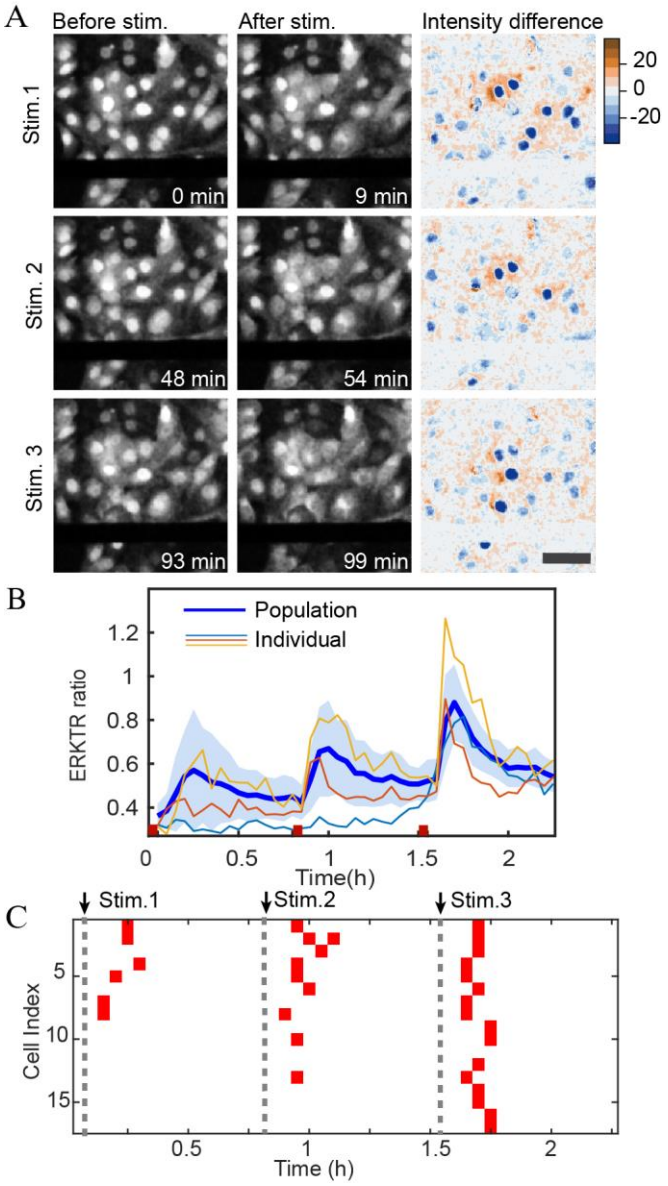

Figure 11. Frequency modulation of ERK activation by AC EF. (A) Fluorescent images of cells before (left column) and after (middle column) 3 min long AC EF stimulations at 0 min, 48 min and 93 min. The right column is the fluorescent intensity subtraction of the first two images, blue and orange indicate intensity decrease and increase respectively. Scale bar: 50 μm. (B) Time traces of ERKTR ratio of cells near microelectrodes. The thick blue line and light shadow mark the mean and ±SD value of each time point. The short red lines denote the time during which AC EF stimulation is applied to cells. (C) Map of ERK activation peak time picked from time traces in (B) (L. Guo et al., 2019).

Mechanism of AC EF-induced ERK activation. After studying the ERK signaling pathway activity caused by AC EF stimulation, we turned to the underlying mechanism of these phenomena. First, we needed to examine some common factors that could be introduced by EF stimulation, such as electrochemical reactions, ROS, Ca^{2+} influx, etc. As mentioned in Chapter 2, with the HfO_2 coating on microelectrodes, all faradaic processes were suppressed in the cyclic voltammetry test (Figure 6C), so we first ruled out the involvement of electrochemical reactions. Next, we continued to investigate if electroporation happened after AC EF stimulation. To check the integrity of cell membrane, SYTOX orange was added in the cell medium. This dye can only stain cell nucleus through compromised cell membrane, so if cells remain unstained after AC EF stimulation, then it means electroporation does not happen. According to cell images shown in Figure 12A-B, almost all the cells remained unstained after 1 hour of AC EF stimulation, only a few cells very close to microelectrodes showed fluorescence. This comparison has proved that cell membrane is intact after AC EF stimulation, excluding

electroporation as the mechanism of ERK activation. After that, we depleted Ca^{2+} and ROS in cells using Ca^{2+} chelator and ROS quencher respectively, and then applied AC EF stimulations. As shown in Figure 12C, in both cases cells still exhibited ERK activation after AC EF stimulations, confirming that neither Ca^{2+} nor ROS participates in the AC EF-induced ERK activation. At last, since temperature variation could cause biological response, we used a patch clamp pipet electrode to measure the local temperature near microelectrodes before and after AC EF stimulation. As the current passing through the patch clamp was sensitive to local temperature, we used the current from patch clamp to calculate temperature changes. Temperature measurements were conducted after 3 min and 10 min AC EF stimulations, respectively. As summarized in Figure 12D, the temperature variations on bare gold microelectrodes were 0.00 ± 0.05 °C and 0.01 ± 0.07 °C, meanwhile 0.03 ± 0.07 °C and 0.01 ± 0.05 °C on HfO_2 coated microelectrodes. Following that, we altered the cell culture temperature from 35 °C to 39°C. As displayed in Figure 12E, after 10 min incubation, only cells at 35 °C showed spontaneous ERK activation, the other sets of cells still stayed at low ERK level. Combined with the temperature measurements above, we can conclude that the temperature change after AC EF stimulation is not significant enough to cause ERK activation in MCF10 cells.

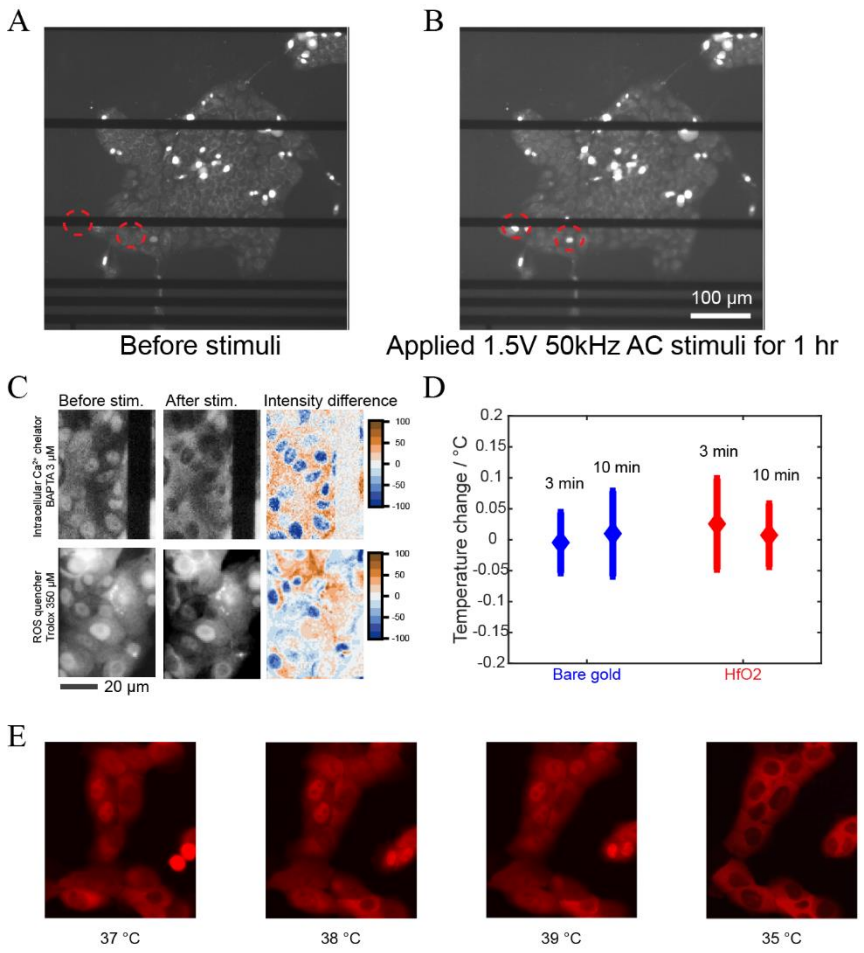

Figure 12. Verification tests of some possible mechanisms that may lead to ERK activation. (A) Fluorescent image of cells cultured with SYTOX orange before and (B) after AC EF stimulation. Circled regions mark the lit-up cells after AC EF stimulation, meaning electroporation happened on those cells. (C) Top: fluorescent images of cells cultured with Ca^{2+} chelator BAPTA AM, before and after AC EF stimulation as well as fluorescent intensity difference. Down: fluorescent images of cells cultured with ROS quencher Trolox, before and after AC EF stimulation as well as fluorescent intensity difference. (D) Local temperature variations after 3 min and 10 min AC EF stimulations. Blue indicates bare gold microelectrodes and red indicates HfO_2 coated microelectrodes.

(E) Fluorescent images of cells when exposed to different temperatures. From left to right: 37 °C, 38°C, 39°C, and 35°C.

Given the aforementioned test results, we have excluded the involvement of many EF related secondary effects in the AC EF-induced ERK activation, including faradaic process, electroporation, Ca^{2+}, ROS, and temperature fluctuation. We reckoned it was solely due to electrostatic effect, and consequently we turned our attention to the ERK signaling pathway itself and screened each signal molecule in the pathway for the AC EF coupling site that eventually leads to ERK activation. Specifically, we used chemicals to block each element along the ERGF-Ras-ERK pathway (Figure 13A), then treated cells with AC EF stimulation and EGF respectively, and compared ERK responses. We first inhibited MEK with trametinib, as shown in Figure 13C and H, ERK activation was inhibited in both AC EF and EGF stimulations. Similarly, when Raf was inhibited by sorafenib, cells remained at low ERK level state after both kinds of stimulations (Figure 13D and I). Next, we tested several small molecule tyrosine kinase inhibitors (TKIs) that could bind to the intracellular tyrosine kinase domain of EGFR. As displayed in Figure 13E and J, ERK activation was inhibited in all three cases. At last, we blocked the extracellular EGF binding site using EGFR antibody cetuximab but left the intracellular phosphorylation site unoccupied. Surprisingly, cells showed ERK activation after AC EF stimulation (Figure 13F), even though the fluorescent signal contrast was not as strong as the control group (Figure 13B). In the meantime, cells with EGF stimulation were still in silence (figure 13K), implying that the intracellular phosphorylation site was the target of AC EF to initiate ERK activation. The time traces of ERKTR ratio in all the above

blocker tests were summarized in Figure 13L. From these traces, apart from the control group without any blocker, only cells treated with EGFR antibody could still exhibit ERK activation when applied with AC EF stimulation. Besides, when compared with the control group, we also noted a slight delay of ERK activation in the EGFR antibody time trace. Based on this series of blocker tests results, we can conclude that the AC EF-induced ERK activation is initiated by EGF-independent kinase activity of EGFR resulting from AC EF coupling.

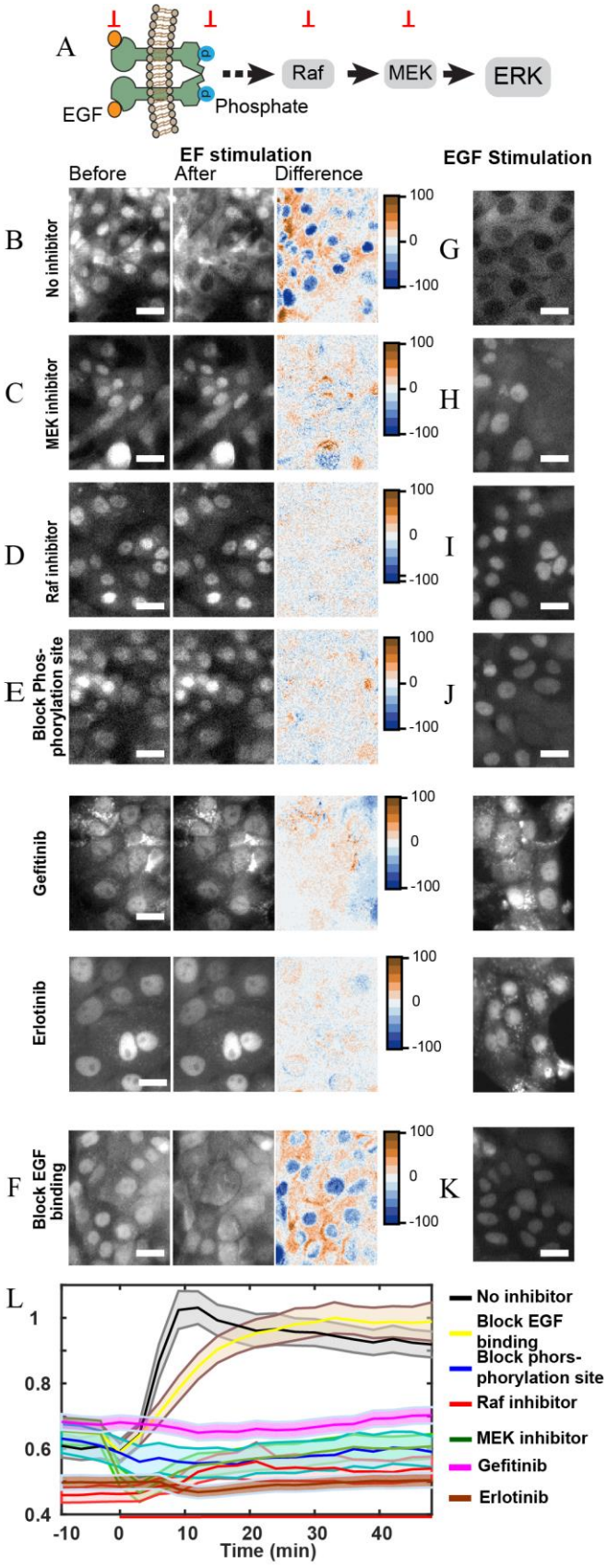
A
EGF
Phosphate
Raf
MEK
ERK
EF stimulation
Before
After
Difference
EGF Stimulation
B
No inhibitor
C
MEK inhibitor
D
Raf inhibitor
E
Block Phos-phorylation site
Gefitinib
Erlotinib
F
Block EGF binding
G
H
I
J
K
100
0
-100
L
1
0.8
0.6
0.4
-10
0
10
20
30
40
Time (min)
No inhibitor
Block EGF binding
Block phors-phorylation site
Raf inhibitor
MEK inhibitor
Gefitinib
Erlotinib

Figure 13. Blocker tests along the EGFR-Ras-ERK signaling pathway. (A) Schematics of the EGFR-Ras-ERK pathway as well as blocking sites. From left to right: EGFR extracellular EGF binding site, EGFR intracellular phosphorylation site, Ras, and MEK. (B-F) Fluorescent images of cells before and after AC EF stimulation, and the intensity difference. Cells were treated with no inhibitor (B), MEK inhibitor trametinib (C), Raf inhibitor sorafenib (D), TKIs afatinib, erlotinib and gefitinib (E), and EGFR antibody cetuximab (F), respectively. (G-K) Fluorescent images of cells stimulated with EGF, and the same blocker treatment was applied in each row. (L) Time traces of ERKTR ratio from cells applied with AC EF stimulations in all blocker tests. Mean and ±95% CI are marked as solid line and shadow region, respectively.

AC EF can induce both ERK inhibition and activation in cells with clear waveform-dependency. In the previous experiments of AC EF stimulation on cells, we focused on the activation response of ERK signaling pathway. However, in some cases, we did observe another type of ERK response. As shown in Figure 14A, when cells were applied with 3 min long, 50 kHz bipolar square pulse, a decrease in ERKTR ratio could first be observed, indicating the inhibition response of ERK, followed by a pronounced ERK activation peak after 15-20 min. We noticed that the later ERK activation had a consistent time and shape as in previous tests, but the earlier rapid ERK inhibition response was new and it appeared almost immediate after AC EF stimulation (within our time resolution of 30 sec per frame). We then fixed the amplitude, period, and duration of the AC EF stimulation to cells, and only changed the waveform from square wave to sine, triangular, and sawtooth waves, respectively. Between each trial of stimulation, the

cells were given a rest period of around 60 min, to ensure that the electrical signals from one stimulation were not affected by the previous one. At the end of these tests, the square wave was used again to confirm that reproducible response was received from this standard waveform and that there was no degradation of cell quality during the whole experiment process. Intriguingly, we observed clear waveform-dependency of the ERK response: the ERK activation peak disappeared when sine (Figure 14B) and triangular (Figure 14C) waveform AC EF stimulations were applied but could be recovered with sawtooth waveform AC EF stimulation (Figure 14D).

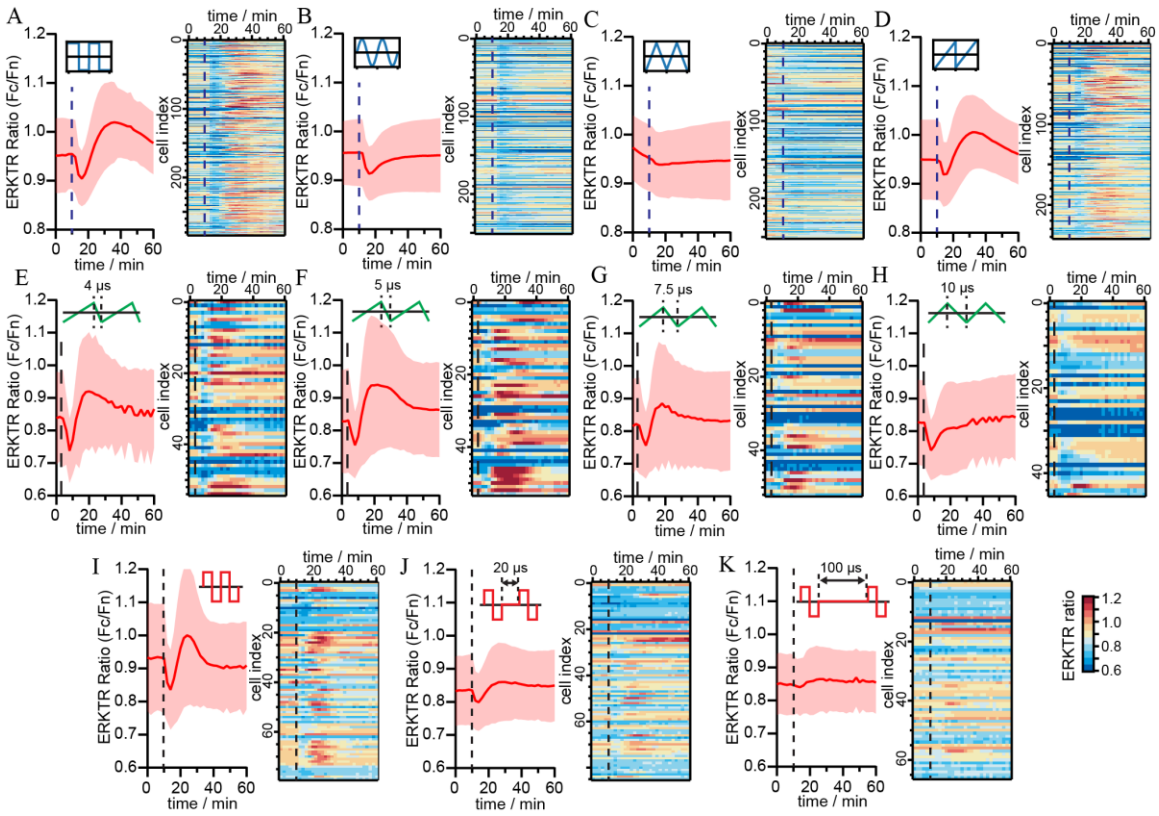

Figure 14. Waveform and timing dependency of AC EF-induced ERK inhibition and activation. (A-D) ERK activities when square, sine, triangle and sawtooth waveform AC EF stimulations of the same amplitude and period were applied to the same group of cells. (E-H) ERK activities when sawtooth waveforms of different duty cycles with ramping time from 4 µs to 10 µs were applied. (I-K) Responses of ERK when interval time between individual pulses changed from 0 to 100 µs. The dash lines mark the starting time of the AC EF stimulations.

Since all the stimulation parameters were the same except for the shapes of waveforms, the different responses suggested that the ERK activation was linked to the fast rising/dropping edges of the pulses sent to cells, as was only present in the square

and sawtooth waveform. Hence, we further examined the impact of the ramping speed of the AC EF on ERK responses. Specifically, we gradually programmed the duty cycle of the sawtooth waveform from 99% to 50% to bring the time of the dropping edge from 4 μs (bandwidth limited) to 10 μs for the same amplitude (Figure 14E-H). The ERK activation peak clearly became weaker and even disappeared when the ramping time was longer than 7.5 μs. Notably, the ERK inhibition response was persistent in all cases. In addition, we also tested different rest time between pulses. Namely, based on the 50 kHz bipolar square waveform, we inserted a rest time from 20 μs to 100 μs between the 20 μs pulses (Figure 14I-K). Both ERK activation and inhibition responses decreased with the prolonging of rest time between pulses. Overall, the inhibition response of ERK can be triggered by a broader range of waveform in comparison to the activation response.

The sensitivity of ERK responses to the shape of waveforms and the timing between pulses further proved that this kind of cellular response was not attributed to electrochemical processes or chemical species/cues produced during the application of AC EF stimulation in the culture medium. First, the range of the electrochemical potential sweep at the microelectrodes was all the same in these tests. Second, the high-k dielectric HfO_2 coating, which blocked all faradaic current, did not arrest the ERK responses. Last, since these bipolar stimulations did not have DC component passing through microelectrodes, there was no net current or ion flow that could impact cells either. Given all above, the observed coupling between AC EF and the ERK signaling pathway should be considered as the electrostatic modulation from the AC component.

AC EF-induced ERK inhibition shows lower threshold and different temporal characteristics than activation. As verified in previous experiment, the AC EF stimulation delivered by microelectrodes is highly localized, so only cells within 100 μm from the microelectrodes demonstrate ERK activation (Figure 10). On the other hand, we have found that ERK inhibition response caused by AC EF stimulation can be observed from cells more than 200 μm away from the microelectrodes (Figure 15A, left). For each AC EF stimulation test, considering variations in electrical impedance from chip to chip, the minimal amplitude of AC EF stimulation to trigger ERK activation, i.e., the threshold, was first determined using the 50 kHz bipolar square pulse as the standard waveform (Figure 15B). However, at a lower amplitude (about 75% of the threshold required for ERK activation), the AC EF stimulation could be tuned to just trigger ERK inhibition without activation for all adjacent cells (Figure 15A). Overall, the ERK inhibition demonstrates a lower threshold compared to the activation process. Given that the timing and duration of the ERK inhibition are also significantly different from those of ERK activation, we decided to further investigate the impact of AC EF stimulation on ERK inhibition. In all the above AC EF stimulation experiments, cells were starved in EGF-free medium so that the ERK level in cells started at a low baseline. To better characterize ERK inhibition response, we performed all the following experiments in normal culture medium with the presence of EGF, where the starting ERK level in cells was already high, such that we could capture the complete picture of AC EF-induced ERK dynamics under normal physiological conditions.

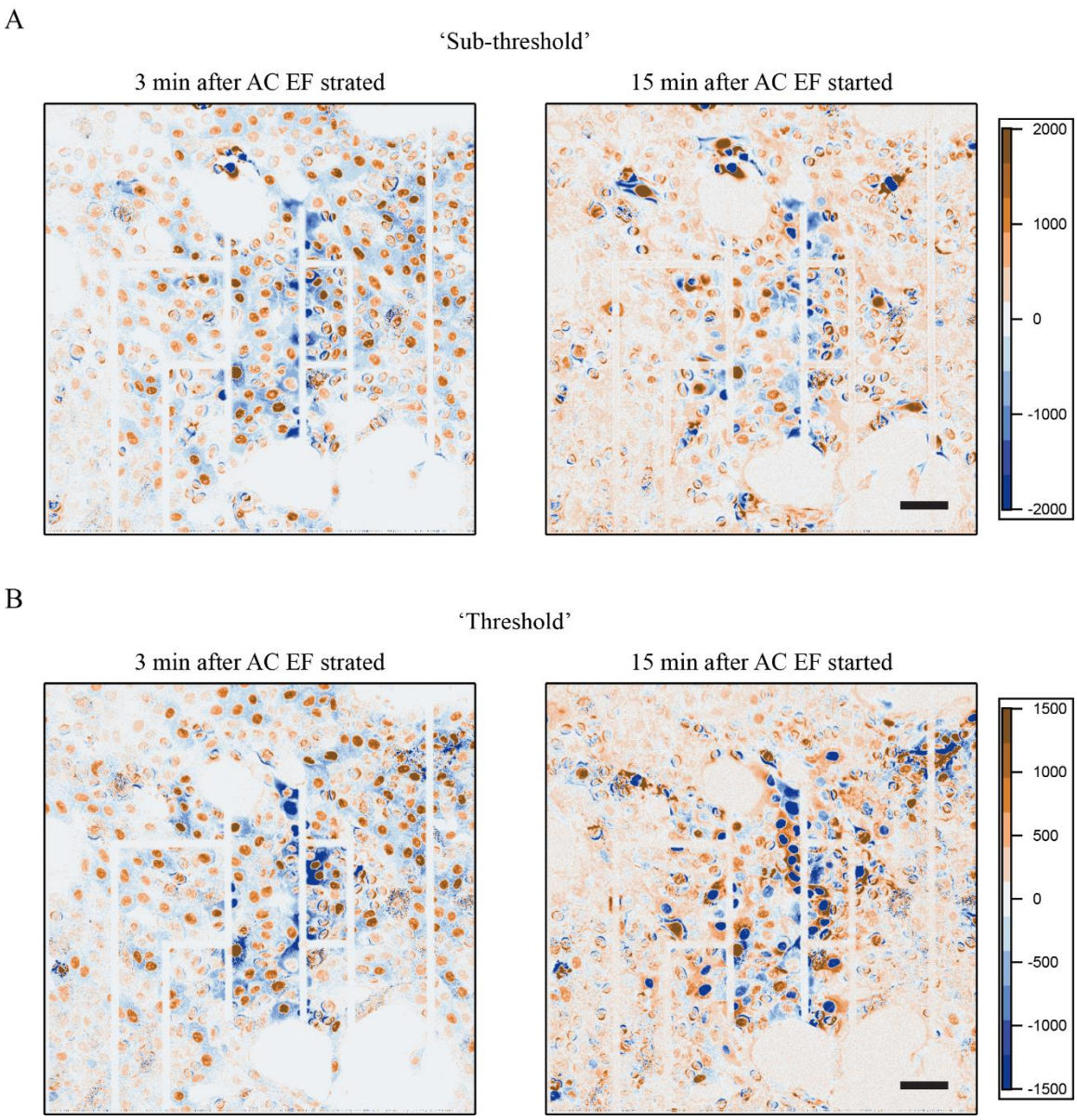

Figure 15. Different threshold and temporal characteristics of AC EF-induced ERK activation and inhibition. (A) Fluorescent intensity difference of cell images at 'sub-threshold' AC EF stimulation, ERK inhibition in cells could still be triggered by AC EF stimulation (left) while ERK activation could not be observed (right). (B) Fluorescent intensity difference of cell images at 'threshold' AC EF stimulation, both ERK inhibition

(left) and activation (right) could be observed at different time periods. Blue and orange indicate intensity decrease and increase respectively. Scale bar: 50 μm.

First, we tested 50 kHz AC EF stimulation with different waveforms in the normal culture medium to evaluate the exact amplitude threshold of ERK inhibition. In the test, 1 min long AC EF stimulations were applied to cells from low to high amplitude until ERK inhibition was observed, and this amplitude was the threshold of this particular waveform. Square, sine, and triangle waveform AC EF stimulations were tested in the same condition, and cells were rested for about 60 min after each test. The amplitude thresholds of different waveforms were summarized in Table 2, different waveforms exhibited different amplitude thresholds in triggering ERK inhibition. Square wave is the most effective waveform to induce ERK inhibition while triangle wave is the least effective.

Table 2

Summary of Amplitude Thresholds of Different Waveforms That Can Trigger ERK Inhibition

Waveform	**Amplitude threshold**
Square wave	0.7 V
Sine wave	0.8 V
Triangle wave	0.9 V

Second, we used ‘sub-threshold’ AC EF stimulation (at 75% threshold) to only induce ERK inhibition response from all cells, and gradually changed the duration of stimulation to compare the magnitude of the induced ERK inhibition and their ‘peak time’, which is the interval between the start of the AC EF stimulation and the time of the lowest ERKTR ratio. The cells were allowed to rest for around 60 min after each stimulation. The results (Figure 16A) showed that the ERK inhibition could be readily observed at a minimum AC EF stimulation of just 15 sec, reaching a consistent peak time of about 2 min as the AC EF duration increased. In addition, the inhibition magnitude saturated after around 3 min of AC EF stimulation (Figure 16B). These characteristics are clearly different from the ERK activation phase, where minimal AC EF stimulation duration required is about 3 min, and the peak time is 10-20 min.

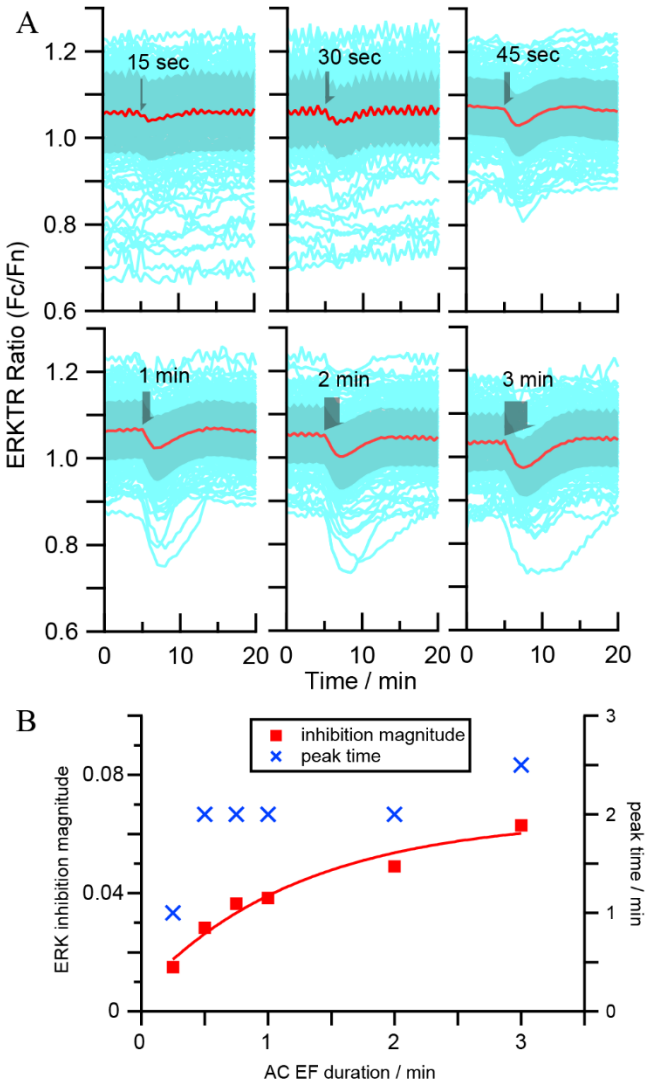

Figure 16. The magnitude and peak time of ERK inhibition depend on the duration of the AC EF stimulation. (A) Time traces of ERKTR ratio with different duration of AC EF stimulation from 15 sec to 3 min. The light blue traces are the raw ERKTR ratio from individual cells, the red trace and the shadow denote mean and ±SD value. (B) The ERK inhibition magnitude (red square) and peak time (blue crosses) vs duration of AC EF stimulation of the same magnitude from the same group of cells, as measured from the average traces (red) of (A).

Third, when two AC EF stimulations are placed too close to each other, the ERK inhibition magnitude would start to decrease. We cycled 1 min long AC EF stimulations using bipolar 50 kHz square pulses with interval time gradually decreased from 30 min to 5 min, and the ERK responses from the same group of cells are shown in Figure 17A-D. The magnitude of the inhibition extracted from the averaged ERKTR ratio time traces are summarized in Figure 17E. The AC EF-induced inhibition remained stable for intervals of 30, 20 and 10 min, but showed significant decay when stimulations were only 5 min apart, indicating a shorter refractory time for AC EF-induced ERK inhibition.

Last, we performed a sustained sub-threshold AC EF stimulation for an extended hour. After the rapid inhibitive ERK peak in the first 10 min, a slow fluctuation of ERK level that was overall below the baseline could be observed (Figure 17F). Comparing the two inhibition responses, the earlier rapid peaks were well aligned and consistent between cells as previous minutes long AC EF stimulations, while the later slow fluctuations were not as well synchronized and demonstrated larger variations in terms of magnitude and period from cell to cell. Besides, after the AC EF stimulation was stopped, the ERK level in cells gradually returned to the normal level in about 30 min, which proved that the lower ERK level was not due to photobleaching or cell quality degradation. The consecutive fast and slow fluctuations of ERK inhibition responses during the AC EF stimulation suggest that there may be several signaling feedback processes of different time scales involved in this dynamic behavior.

Previous mechanistic study of the AC EF-induced ERK activation reveals it is the AC EF-induced phosphorylation of EGFR that leads to the activation of ERK. Naturally, we wondered if these ERK inhibition responses were also initiated by AC EF-induced

changes in EGFR. To explore this, we compared the AC EF stimulation and chemical inhibition effect on cells. Specifically, we first treated cells with 1 μM of afatinib to inhibit the phosphorylation of EGFR, and recorded the time course of the ERK decrease as the control group (Figure 17G, red trace). Then, in another run, a 3-min, sub-threshold AC EF stimulation was applied right after adding the same amount of afatinib in the cell medium. The ERK level rapidly decreased to a deeper inhibition state during this period, but when the AC EF stimulation was stopped, it recovered briefly and returned to follow the same trend of slower decrease as in the control group (Figure 17G, green trace). At around 22 min when ERK level reached the same value as in the control group, another 3-min AC EF stimulation was applied, and we found again a deeper inhibition state, which recovered afterwards to the same plateau as in the control group. The different time characteristics of AC EF-induced ERK inhibition and its relative independence from the chemical EGFR inhibitor suggest that the EGFR may not be the only component impacted by AC EF at the cell membrane.

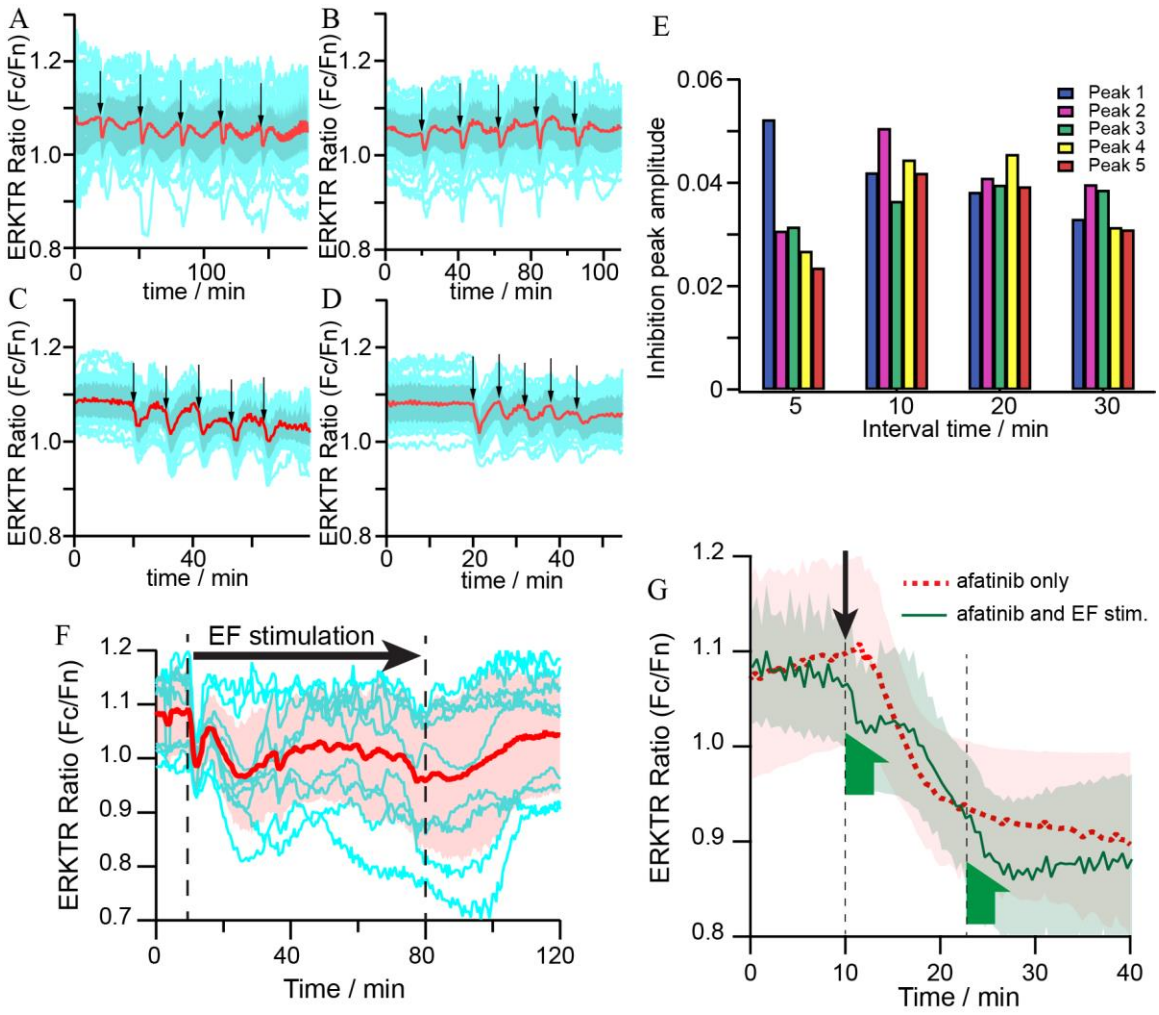

Figure 17. Time characteristics of AC EF-induced ERK inhibition and comparison with EGFR inhibitor afatinib. (A-D) Periodic modulation of ERK inhibition induced by short AC EF stimuli. Representative time traces of ERKTR ratio of individual cells when multiple cycles of 1 min AC EF stimuli are applied to the same group of cells with different time interval, thicker lines are population average, shadow region shows 25th and 75th percentile values. Interval time: (A) 30 min, (B) 20 min, (C) 10 min, (D) 5 min. (E) Comparison of ERK inhibition peak amplitude of different interval times in (A-D). (F) Fluctuation of ERKTR ratio with inhibitions when long sub-threshold 50 kHz square wave AC EF stimulation was applied. Dash lines mark the beginning (at 11 min) and the end (at

80 min) of the stimulation. (G) Red trace: ERKTR ratio showing ERK inhibition induced when 1 μM EGFR inhibitor afatinib was applied (marked by the black arrow). Green trace: ERKTR ratio showing inhibitive ERK responses as two separate 3-min AC EF stimulations (marked by the green half arrows) were applied after the application of afatinib (marked by the black arrow).

AC EF stimulation may perturb the activity of Ras at the cell membrane. Another possible candidate of AC EF coupling site on the cell membrane is the lipid-anchored Ras-GTP activated by the Grb2/SOS after EGFR phosphorylation, which serves as the amplifier to regulate downstream ERK signals. If the activity of the Ras-GTP complex is also influenced by the AC EF stimulation, it would likely cause more rapid change in the downstream signaling. To verify this possibility, we quantified the AC EF-induced changes in the Ras-GTP at the cell membrane. Specifically, we mixed equal amounts of MCF10A-FRB-RBD and MCF10A-EKAR3-ERKTR cells, and co-cultured them in the first-generation EF stimulation device. The MCF10A-EKAR3-ERKTR cells can give the ERK response in the mCherry channel as in previous experiments, and the MCF10A-FRB-RBD cells have been transfected with Lyn-FRB-CFP, which can track the activated Ras-GTP (Figure 18A).

During the experiment, we have found that the Ras activity near the cell membrane is very sensitive to neighboring cells, if two cells contact with each other, then the Ras-GTP near the contacting region would stay active. Therefore, to avoid interference from neighboring cells, we plated MCF10A-FRB-RBD and MCF10A-EKAR3-ERKTR cells at low density (around 0.15 M cells/cm^2) and only used single cell or cells with free cell

membrane edge for analysis. With confocal imaging, we captured the basal section of the MCF10A-FRB-RBD cells to obtain the average intensity of RBD-GFP at the cell membrane, which was compared to the ERKTR ratio calculated from the MCF10A-EKAR3-ERKTR cells in the same images (Figure 18B). At normal cell culture temperature (37 °C), a rapid decrease of the RBD-GFP intensity was observed right after the AC EF stimulation started, which synchronized with the initial inhibition phase of ERK. After about 10 min, the RBD-GFP intensity returned to the original level, and the ERK level also recovered during the same period. As a control, the temperature of the device was cooled down to room temperature at 20 °C, at which cell activities slowed down and the ERK level in cells all switched to a low state. Upon AC EF stimulation, the same decrease of RBD-GFP could still be observed, however, without recovery afterwards, and the ERK level stayed low with no response to AC EF at all.

To minimize the impact of photobleaching in the analysis, we further utilized the Lyn-FRB-CFP reporter as internal calibration to quantify the changes of RBD-GFP. Since no Rapamycin was introduced to cells to activate FRB, the intensity of the CFP signals could serve as the baseline to compare with other membrane-anchored molecules such as activated Ras. We calculated the intensity ratio of the GFP and CFP signals at the cell membrane from different cells, and discovered that the GFP/CFP ratio exhibited the same rapid decrease after AC EF stimulation, followed by a recovery process in around 10 min (Figure 18C). The consistent results in Figure 18B and C imply that there is an AC EF-induced change of Ras-GTP density at the cell membrane, and its temporal characteristics are aligned with the observed ERK inhibition and activation phases. The initial disruption of activated Ras seems to be a direct effect of the AC EF stimulation, and its later recovery

to high state is correlated to the signaling pathway activities associated with the ERK activation.

Last, we wanted to check whether the observed RBD-GFP change could be attributed to the electrochemical effect. In other words, is it possible that the AC EF stimulation suppresses RBD-GFP signal by destabilizing or pulling the Ras molecule away from the membrane. To answer this question, we lifted the focal plane to 4 μm above the chip surface to acquire the cross-section confocal images of cells. The intensity line profiles crossing the cell membrane at different positions were extracted from the GFP and CFP channels and then fitted with Gauss function. The offset between the peak positions of the GFP and CFP signals was used to evaluate how the GFP-labeled Ras shifted relative to the cell membrane. We are aware that the applied AC EF pulses are bipolar and has much shorter period (20 μs at 50 kHz) than the exposure time (500 ms). As a result, these images do not have enough time resolution to capture the real-time response of the GFP-labeled Ras to the fast-changing AC EF perturbations, and can only provide the average offset as a 'residue effect' between each exposure. Not surprisingly, we did find no significant offset variations between the GFP and CFP signals in most of the line profiles before, during and after AC EF stimulations, meaning that the RBD-GFP appeared to follow the cell membrane consistently on average. Nevertheless, in a small portion of the line profiles (10%), a large discrepancy between the GFP and CFP peak positions showed up only during the AC EF stimulation (Figure 18D), capturing the possible detaching event of Ras due to AC EF perturbation. We recognize that this is only a small subset of data, and more direct evidence and quantification with higher time resolution are needed to better track the response of membrane molecules to AC EF stimulation.

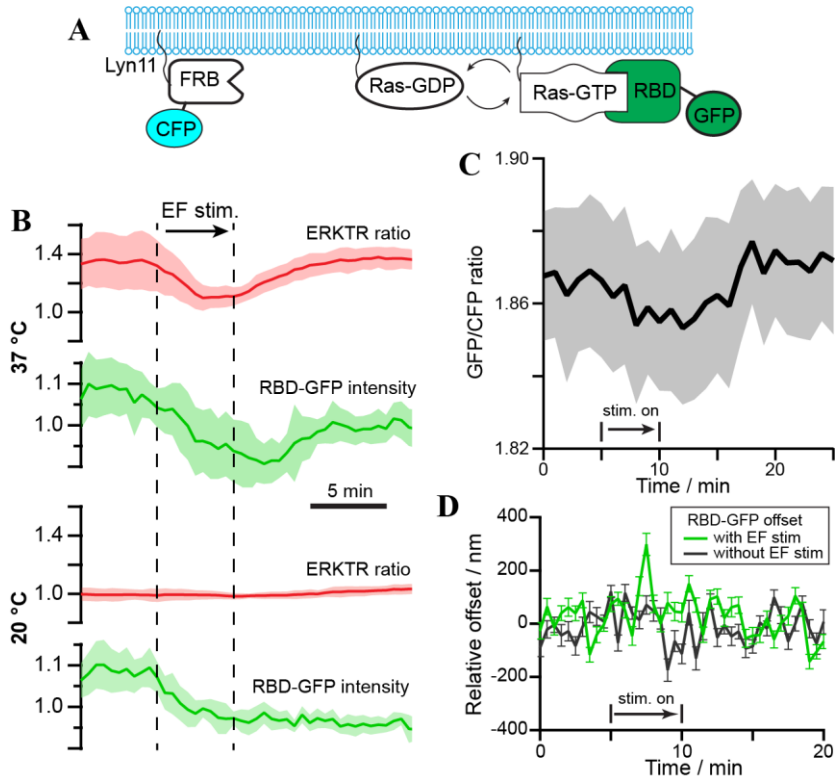

Figure 18. Ras-GTP changes during AC EF stimulation. (A) Schematics of the Lyn-FRB-CFP and RBD-GFP reporter expressed in the MCF10A cell line. (B) Comparison of ERK and Ras response at different temperatures with AC EF stimulation. Top group: at 37 °C, the ERK showed clear inhibition followed by recovery to activation upon AC EF stimulation, and the RBD-GFP intensity showed correlated decrease followed by recovery within the same period. Bottom group: at 20 °C, the ERK level of the same cells remained at low level during AC EF stimulation, and RBD-GRP intensity only showed immediate decrease during AC EF stimulation without recovery. The thick lines give the average results from cells (n=6) with standard deviation shown as the shadowed area. (C) The ratio of fluorescence intensity from RBD-GFP and Lyn-FRB-CFP showed clear decrease and recovery during and after AC EF stimulation. The thick line gives the average results from different cells (n=6) with standard deviation shown as the shadowed area. (D) The change

of offset between peak positions from RBD-GFP and Lyn-FRB-CFP signals upon AC EF stimulation demonstrated larger difference. Peak position calculated as a Gaussian fit in a line profile crossing the cell membrane in the fluorescence images. The chromatic offset between GFP and CFP has been subtracted from the data.

Conclusions

To sum up, in this project we have conducted a comprehensive study of how intermediate frequency AC EF stimulation influences the ERK signaling pathway. By the use of microelectrodes and real-time fluorescent reporter ERKTR, we can achieve localized AC EF stimulation and characterization of ERK status in cells with high spatiotemporal resolution. We have found that AC EF stimulation can cause activation and inhibition responses of the ERK signaling pathway with quite different threshold and temporal characteristics. With carful AC EF amplitude and time tuning, we have also demonstrated that the dynamics of ERK responses, including frequency, magnitude, and duration, can be modulated with AC EF stimulations. Another discovery that these ERK responses are sensitive to the waveform and timing of the AC EF stimulation strongly suggests an electrostatic nature of the AC EF coupling on the cell membrane. Further blocker tests along the ERK signaling pathway and cell membrane protein tracking analysis reveal that the AC EF-induced ERK activation and inhibition are associated with membrane proteins EGFR and Ras, respectively. The AC EF-induced EGFR phosphorylation is at the upstream of ERK pathway, therefore the activation process takes longer time to complete; while the AC EF perturbation on the Ras-GTP only affects the amplifier of the ERK pathway, leading to the rapid ERK inhibition response. To this

study, further investigations with faster imaging techniques and high-resolution analysis method are still needed to unveil the direct biophysical impact of AC EF stimulation on membrane proteins.

CHAPTER 4

PHYSIOLOGICAL EFFECT OF SPATIOTEMPORALLY PATTERNED PHYSICAL MODULATIONS: PROLIFERATION AND MIGRATION

Introduction

After the previous in-depth research on how AC EF perturbs the ERK signaling pathway in cells, we move forward to the long-term physiological effect of physical stimulation on cell behaviors such as cell proliferation and migration. Chemical and physical cues are often used to regulate cell behaviors, including cell proliferation, differentiation, and migration. In tissue engineering and regenerative medicine, the precise presentation of environmental cues directing cell behavior is of vital importance to a successful outcome (Ruprecht et al., 2016).

Chemical cues, including soluble chemicals in the medium and chemical properties of the substrate surface, are the most commonly used stimuli to modulate cell behaviors. Chemotaxis, a phenomenon by which the movement of cells is directed in response to an extracellular chemical gradient (Roussos, Condeelis, & Patsialou, 2011), is an important physiological process involved in the recruitment of inflammatory cells an stem cells in response to tissue damage for wound healing and tissue repair. Mishima et al. (2008) once systematically analyzed growth factors and cytokines for their ability to induce migration of human articular chondrocytes and hMSCs. According to their results, in human articular chondrocytes, only platelet-derived growth (PDGF) induced a significant increase in cell migration. However, hMSCs showed strong chemotaxis responses to a number of factors, including fetal bovine serum (FBS), PDGF, vascular endothelial growth (VEGF), insulin-like growth factor-1 (IGF-1), interleukin-8 (IL-8),

bone morphogenetic protein (BMP) -4, and 7. Furthermore, chemical cues can also affect the proliferation and differentiation behavior of the cells. For example, the adhesion of stem cells to their microenvironments is very important to their fate, studies have shown that changing the coupling strength of the receptor-binding domain (RBD) peptide on substrates could regulate the adhesion, diffusion, and differentiation of hMSCs (Choi et al., 2015). Phytochemicals have also become a kind of emergent chemicals that can be used to regulate cell behaviors (Xing et al., 2019). Icariin, extracted from the plant herb Epimedium brevicornum Maxim, has been found to be associated with the phosphorylation of ERK and p38, promoting the proliferation of rat bone mesenchymal stem cells (Qin, Zhou, Liu, Chen, & Wu, 2015).

Physical cues, such as mechanical forces exerted on cells, EF stimulation and surface topography, also play an essential role in the regulation of cell behaviors. Especially after many researches have revealed that geometrical microenvironment played a critical role in modulating cell behaviors, physical cues including mechanical properties, pore sizes, porosity, surface stiffness, 3D structures have drawn considerable attention. Electrospinning, a technique that cures nanofibers by high voltage electrostatic force, is a popular method for fabricating tissue engineering scaffolds with tunable microenvironments (Kanaan & Piedade, 2022). In tendon repairing, uniaxially stretched electrospun nanofibers have been reported to guide the arrangement of cells, improve the deposition of extracellular matrix, and promote the differentiation of stem cells to regenerate tendon (Kolluru et al., 2013). In recent years, interests in EF effects on cell behaviors have been boosted by the growing awareness of the profound influence of EF on biological systems. For instance, like chemotaxis, EF has also been documented to

induce directed cell migration, and this phenomenon is termed electrotaxis or galvanotaxis. cells undergoing electrotaxis exhibit a bi-phasic nature: migration towards cathode or anode both have been recognized. Interestingly, Tan et al. (2015) found that the directionality of EF-induced cell migration was even dependent on the passage number. In his experiment, the passage 1 bovine mesenchymal stem cells migrated primarily towards the anode; however, at passage 4, most cells reversed their direction and migrated towards the cathode. One possible explanation for this change might be that the mesenchymal stem cells were differentiating into chondrogenic phenotype while passaging and chondrocytes were found to migrate towards cathode when exposed to EF stimulation.

As we have shown in the previous chapters, well-tuned AC EF can be used to precisely modulate ERK signaling pathways with synchronized rhythms. The ERK activation dynamics has been known to rewire cell fate. For example, NGF induces long duration and osculation of ERK activation in PC-12 which results in neuronal differentiation, while EGF induces transient ERK activation that will not trigger cell differentiation but rather promote proliferation. Periodical addition and washout of EGF using microfluidics technique to induce duration and osculation of ERK activation indeed results in prolonged and oscillating ERK activity and subsequent differentiation (Bluthgen, 2015; H. Ryu et al., 2015). Our interest follows these observations and we wanted to explore how spatiotemporally patterned/programmed physical stimulations can be used to guide the spatiotemporal patterns of signaling pathways and what are the physiological effects of these modulations.

The first experiment of this part of is a collaborative effort with the groups at University of Maryland, College Park and Johns Hopkins University to study how spatial patterned nanotopography of just 100 nm in height can regulate the cytoskeletal excitable network (CEN) and signal-transduction excitable network (STEN) activities in cells to guide cell migration behaviors (Yang et al., 2022).

In this project, we fabricated parallel SU8 nanoridges on glass coverslips (width ~150 nm, height ~100 nm, spacing 5 μm, Figure 19B) via electron beam lithography, and employed fluorescent biosensors PHcrac-GFP and Lime-RFP in electrofused *Dictyostelium discoideum* to visualize PIP3 and F-actin, which represented STEN and CEN, respectively. After cell imaging and analysis, we found that the F-actin and PIP3 activities in electrofused *Dictyostelium discoideum* cells were correlated on both flat surfaces and nanoridges, but with different spatial organizations. On flat surfaces, PIP3 bands of around 2-3 μm in width spread on the basal membrane with a speed of 6-10 μm/min; in the meantime, F-actin appeared basically throughout the PIP3 bands (Figure 19A). On nanoridges, pronounced F-actin and PIP3 wave patterns were triggered by surface features (Figure 19C). Strong F-actin fluorescent signals were observed on ridges, but PIP3 fluorescent signals were not enhanced compared to those on flat surfaces. In some valleys between two nanoridges, F-actin and PIP3 formed travelling waves simultaneously. Even though the 100 nm high nanoridge was shorter than a typical actin wave (about 0.8 μm), this nanotopography still showed effective guidance to the migrational waves. Other markers and additional z-planes were also imaged (Figure 19D). F-actin fluorescent signals were observed at higher focal planes (1.6 μm) than PIP3 (0.8 μm). From the fluorescent images of cell membrane marker cAR1, we did not see

pronounced membrane deformation around the nanoridges (Figure 19E-F), suggesting that the enhanced F-actin fluorescent signal at nanoridges did not result from cell membrane folds.

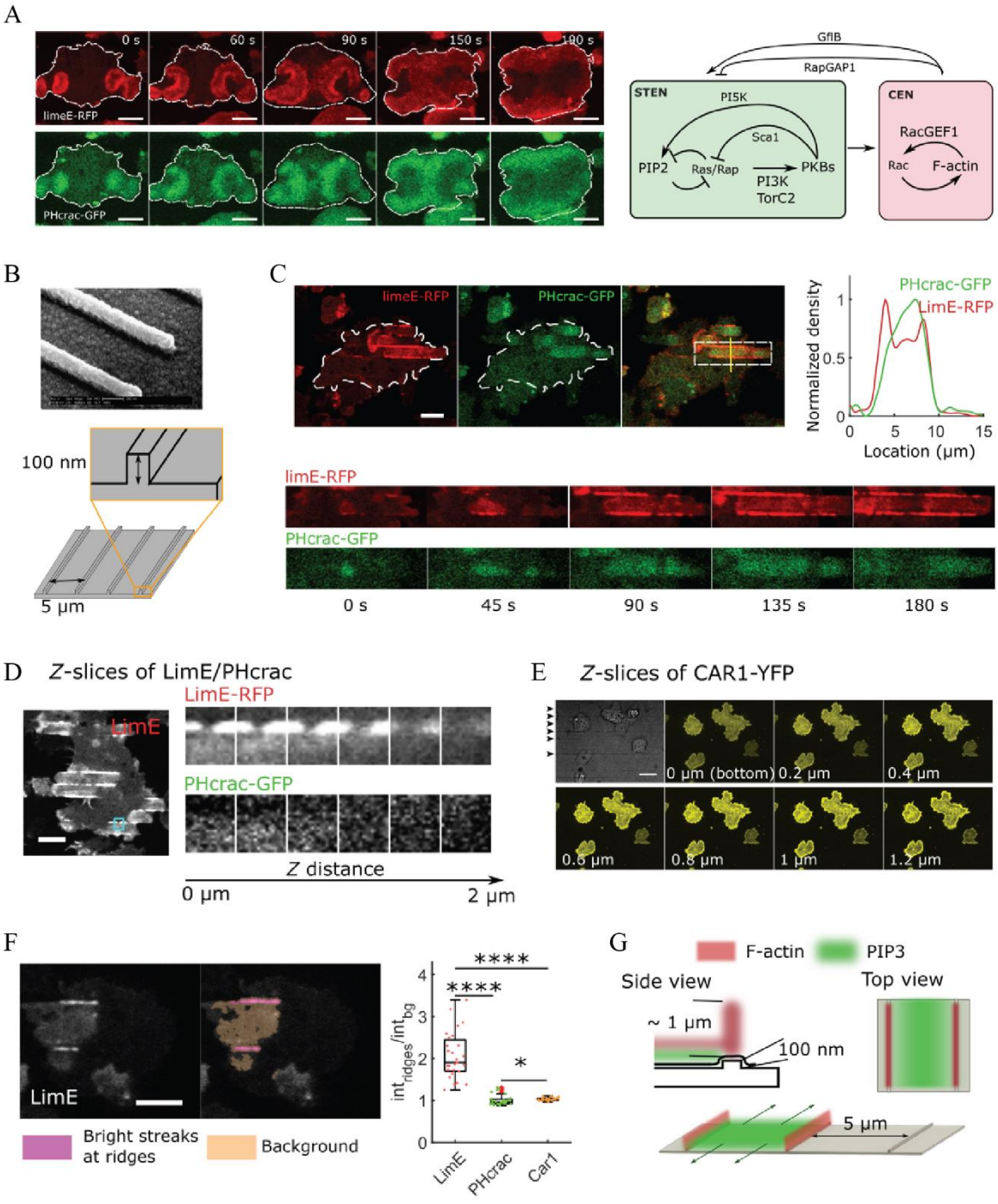

Figure 19. Coordinated F-actin and PIP3 activities on flat surfaces and nanoridges. (A) Time-lapse images of LimE-RFP (top row) and PHcrac-GFP (bottom row) from an electrofused giant cell on a flat resin surface. The right schematic shows the current understanding of the STEN and CEN network with key components. (B) Shape of the nanoridges. The height of each ridge is 100 nm, and the spacing between neighboring ridges is 5 μm. (C) Time series of LimE and PHcrac images from the giant cell set on nanoridges. The profile is from the vertical line in the combined image. The bottom rows show the temporal changes of the rectangular region highlighted in the combined image. (D) Z-stacks of LimE-RFP and PHcrac-GFP. (E) Z-stacks of CAR-YFP. (F) Fluorescence signals of LimE/PH/CAR1 biosensors near ridges (highlighted in pink) normalized to those in the surrounding regions (highlighted in orange). The left plot shows the ratios of ridge signals to background signals (N_{LimE} = 22, N_{PH} = 22, N_{CAR1} = 24, *N*: number of cells). ANOVA with Tukey's post hoc was applied to test the difference among LimE, PHcrac, and CAR1 signals. *P*-values: $P_{CAR1\text{-}PH} = 0.042$, $P_{CAR1\text{-}LimE} < 10^{-10}$, $P_{PH\text{-}LimE} < 10^{-10}$. The data reflects at least three different days of experiments. (G) Schematic illustration of the spatial coordination of F-actin and PIP3 waves on nanoridges. All the scale bars in this figure represent 10 μm (Yang et al., 2022).

Furthermore, we continued to study how temporally patterned AC EF stimulations can have a long-term effect on the cell proliferation and migration. Our hypothesis is that since the ERK signaling pathway can be impacted by AC EF stimulations, in the time scale of more than 24 hours (matching the proliferation time

cycle time for typical epithelial cells), the physiological impact of such modulation could be observed and controlled.

To characterize cell proliferation and migration under prolonged AC EF stimulation, we take advantage of the fluorescent reporter EKAR3 that is confined to the cell nucleus by a nuclear localization sequence. During the AC EF stimulation tests, fluorescent images of cell nuclei are recorded, then we employ an automated cell tracking pipeline to perform cell nucleus segmentation and cell migration tracking (Fazeli et al., 2020). As illustrated in Figure 20, this cell tracing pipeline is developed from the combination of StarDist, a deep learning network-based cell/nucleus detection method (Schmidt, Weigert, Broaddus, & Myers, 2018) and TrackMate, a popular particle tracking tool (Tinevez et al., 2017). Our trained StarDist model can differentiate fluorescent cell nuclei from background, obtaining cell quantity and cell mass center coordinates in each frame. Then TrackMate can link cells between frames according to preset tracking algorithm, generating cell trajectories. Due to cell division and moving out of frame during the experiment, cell trajectories are sorted and reorganized in a custom Igor function, afterwards all data is processed and summarized as cell proliferation and migration results.

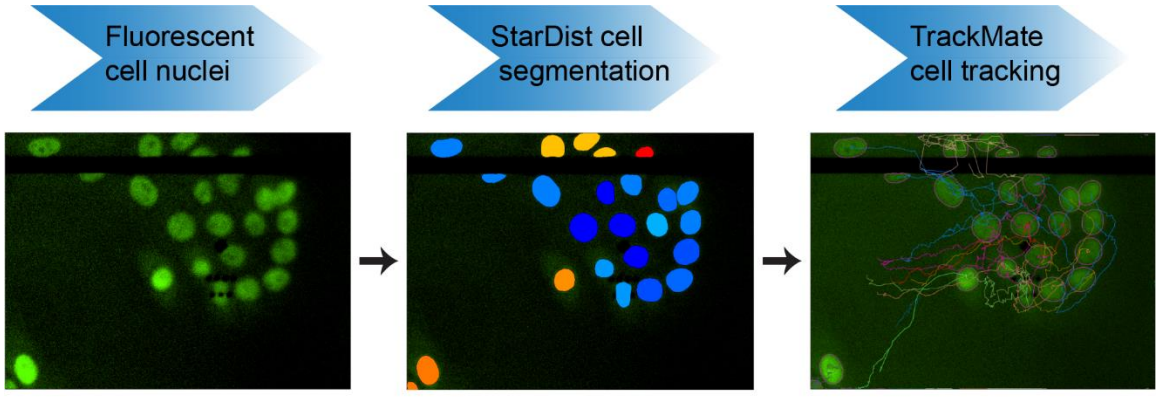

Figure 20. Schematics of cell proliferation and migration data analysis using StarDist and TrackMate. (A) Fluorescent image of cell nuclei. (B) Binary image of cell nuclei after segmentation by StarDist. (C) Cell trajectories generated by TrackMate based on cell nuclei positions.

In this project, we apply prolonged 50 kHz bipolar square waveform pulses (16 h) to mammary epithelial cell MCF10A and discover that this stimulation can produce inhibitory effect on both cell proliferation and migration. Moreover, the suppression effect on cell proliferation shows dependence on AC EF amplitude, stimulation pattern and pulse rising time. These results demonstrate the potential of AC EF as a versatile mean to regulate cell behavior with precise dosimetry adjustments.

Materials and methods

Cell culture. MCF10A cell line in co-expression of EKAR3 and ERKTR was kindly provided by Zhao Lab (UC-Davis), and it was constructed using the method described in reference (Sparta et al., 2015). First co-transfection of pPBJ-EKAR3-nes and the pCMV-hyPBase transposase vector was used to make cells stably express EKAR3, then MCF10A-EKAR3 cells were infected by retroviral particles carrying ERKTR-mCherry, resulting in MCF10A-EKAR3-ERKTR cells.

MCF10A cells were cultured in Dulbecco's modified Eagle's medium (DMEM)/F-12 (Gibco) supplemented with 5% horse serum (Gibco), 0.5 mg/ml hydrocortisone (Sigma-Aldrich), 10 mg/ml human insulin (Gibco), 20 ng/ml EGF (Life Technologies), 100 ng/ml cholera toxin (Sigma-Aldrich), 50 U/ml penicillin and 50 U/ml

streptomycin (Gibco). Cells were incubated in a humidified atmosphere containing 5% CO_2 at 37 °C.

Live cell imaging. The second-generation EF stimulation device (Figure 7) was used in this project. Time-lapse images were acquired from a Nikon Eclipse Ti2-E microscope equipped with a pco.edge 4.2 sCMOS camera and a SOLA SE II 365 light engine. Cell images were taken using a 20X CFI S Plan Fluor Ph1 objective with 0.45 numerical aperture and recorded via NIS-Elements software. ET-mCherry and ET-EYFP (49008 and 49003, Chroma Technology Corp) filter sets were used in mCherry and YFP channels, respectively. In the cell image acquisition process, the large-image option was enabled to capture all cells residing near the exposed microelectrodes. Three areas were scanned and stitched together with 15 % overlap, and the final image size is 1690.87 × 624.98 μm.

Before cell plating, the microelectrode chip assembled into the second-generation EF stimulation device was treated with FNC coating mix (AthenaES) to promote cell attachment. MCF10A-EKAR3-ERKTR cells were dissociated into single cell suspension with 0.25% trypsin-EDTA (Gibco) and seeded in the cell chamber. In order to minimize background fluorescence, DMEM/F12 without phenol red (Gibco) was used in all cell imaging experiments. In the prolonged AC EF stimulation test, cells were cultured in growth medium, so the no phenol red medium was also supplemented with 5% horse serum, 0.5 mg/ml hydrocortisone, 10 mg/ml human insulin, 20 ng/ml EGF, 100 ng/ml cholera toxin, 50 U/ml penicillin and 50 U/ml streptomycin. After cell adhesion, the cell culture chamber was mounted on the microscope and connected to CO_2 supply. The cell culture environment was maintained at 37°C in 5% CO_2 during the cell imaging. Since

the cell imaging process could take several days to complete, cell culture medium in the chamber was refreshed every 24 hours to keep nutrient concentration.

AC EF stimulation. The 50 kHz AC stimuli used in this project were generated by two instruments: a compactRIO controller (NI cRIO 9030 platform, National Instruments) equipped with an NI9269 4-channel voltage output module (National Instruments), and an arbitrary function generator (AFG 31000 series, Tektronix). In the cell experiments, these 2 instruments were connected to a multiplexer PCB, by which AC EF stimuli were distributed to PCB pins on the cell culture chamber. Connection from PCB pins to microelectrodes were made by the direct contact between microelectrodes and push button switches as mentioned in the device assembly steps in Chapter 2. The AC EF parameters were programmed with a customized LabVIEW software.

Data processing. Cell nucleus images were processed with an automatic cell tracking pipeline adapted from reference (Fazeli et al., 2020). Cell nuclei were segmented by StarDist, which required deep learning training to obtain a suitable model for our images. In the training process, 12 typical cell nucleus images were first segmented by StarDist pre-trained model '2D_versatile_fluo', then manually checked and annotated in Fiji. Next, these cell nucleus images and their segmented mask images were uploaded to the ZeroCostDL4Mic platform (Von Chamier et al., 2021) for model training. After 400 epochs, a trained model with satisfactory yield was obtained. In the new version of TrackMate, StarDist is integrated as a new detector module (Ershov et al., 2021), so cell nuclei segmentation and tracking can be completed in the same plugin in Fiji with our trained StarDist model. Cell tracks from TrackMate was imported to Igor pro (WaveMetrics) for sorting and reorganization: divided cells were separated from parent

cells and cells moving out of the frame were removed. At last, a customized Igor function was used to calculate cell numbers in each frame and summarize cell migration data.

Results

Prolonged AC EF stimulation can inhibit cell proliferation and migration.

MCF10A-EKAR3-ERKTR cells were plated in the second-generation EF stimulation device and maintained in a clean cell culture environment during experiments. In the test, symmetrical microelectrode pairs were chosen as control group and AC EF stimulation group. In the last chapter, we have demonstrated that minutes of AC EF stimulation is able to electrostatically perturb cell signaling pathway, but when AC EF stops, most cells can recover to original state very soon. Consequently, it can be postulated that minutes of AC EF stimulation is not enough to generate noticeable effect on cell physiological behaviors. Therefore, we extended the AC EF stimulation time to hours and then compared cell proliferation rate with the control group. After some tests, we discovered that 16 h long, 50 kHz bipolar square pulse could exert significant inhibitory effect on cell proliferation. As shown in Figure 21A, AC EF stimulation was applied from 1-17 h, the cell proliferation rate of control group (black line) gradually increased during the whole experiment; However, the cell proliferation rate of AC EF stimulation group (red line) declined in the first 4 h of AC EF stimulation due to cell apoptosis happened near microelectrodes, then climbed very slowly during the next 5-6 hours, after that the proliferation rate reached a plateau. Surprisingly, even after AC EF stimulation was stopped at 17 h, the plateau status remained for around 8 h and then the cell proliferation rate started to increase with a speed comparable to the control group. We speculate that

the prolonged AC EF stimulation can disrupt normal cell cycle distributions, leading to the suppression on cell proliferation. When the AC EF stimulation has been stopped, the affected cells need some time to resume their normal cell cycle distributions and start growing normally again.

After confirming the inhibitory effect of prolonged AC EF stimulation on cell proliferation, we varied the amplitude of AC EF in a physiologically relevant range and kept the other parameters fixed. In the following test, apart from the control group, 2 pairs of microelectrodes with same gap size were applied with high amplitude (3.5V) and low amplitude (2.5V) 50 kHz square pulses, respectively. When comparing the cell proliferation rate (Figure 21B), we found that the inhibitory effect from AC EF stimulation depended on amplitude, higher amplitude resulted in more obvious inhibition. Furthermore, we analyzed the cell migration during the time when AC EF was applied. According to cell trajectories in the control group and the other two EF stimulation groups (Figure 21C-E), we noticed that cell migration was more confined in AC EF stimulation groups. Then we calculated the average cell migration distance in all three groups, the control group (15.5 μm) was higher than the EF stimulation groups (12.9 μm and 12.2 μm from high and low amplitude AC EF stimulation groups), verifying that the AC EF stimulation could also suppress cell migration.

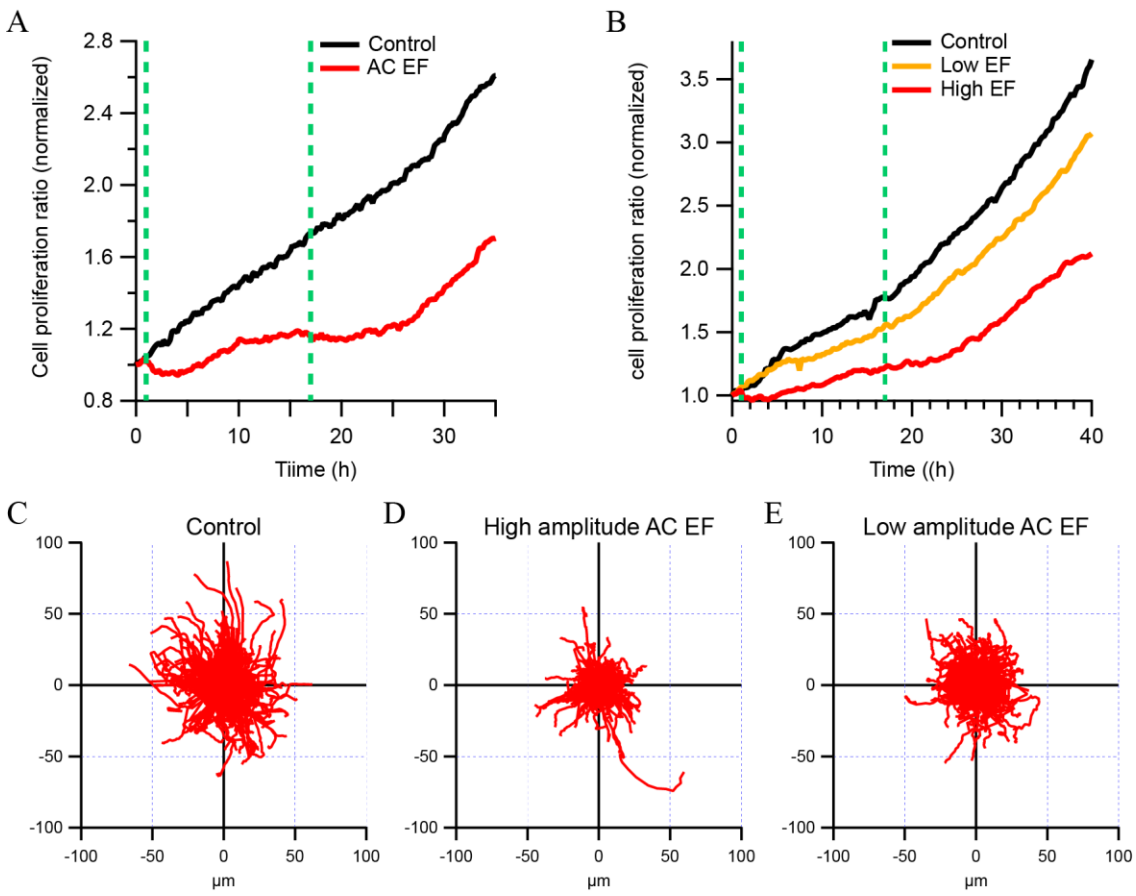

Figure 21. Cell proliferation and migration analysis with prolonged AC EF stimulation. (A) Cell proliferation rate when applied with 16 h AC EF stimulation. The control group is indicated with black line and the AC EF simulation group is indicated with red line. (B) Cell proliferation rate with different amplitude AC EF stimulations. The control group is indicated with black line, the low amplitude (2.5V) AC EF group is indicated with orange line and the high amplitude (3.5V) AC EF group is indicated with red line. AC EF on and off time are marked by two green dashed lines. (C-E) Cell migration trajectories of the control group, the high amplitude AC EF group and the low amplitude AC EF group, respectively, with starting point placed at the origin.

Apart from cell trajectories during AC EF stimulation, we also analyzed the cell speed change. From cell images, we noticed that cell migration depended heavily on cell density: closely packed cells almost stayed still for hours while cells at the cluster edge often migrated actively. Therefore, to analyze cell speed more effectively, we divided cells into 6 groups according to their real-time surrounding cell density, density 0 was the lowest and density 5 was the highest. When we checked the cell speed distribution in these 6 groups, we found that only 3 groups, density 0, 1 and 2 had enough data points for complete distributions, so we just used these three groups for cell speed analysis. Cell speed distributions with different AC EF amplitudes were summarized in Figure 22. According to the figure, the cell speed distribution shifted to the lower side as cell density increased, which was consistent with our initial observation that cell speed was dependent on cell density. From the speed distributions in three groups, the cell speed from high to low was the control, low amplitude AC EF and High amplitude AC EF. This analysis suggests that AC EF stimulation can slow down cell migration speed and this effect depends on AC EF amplitude.

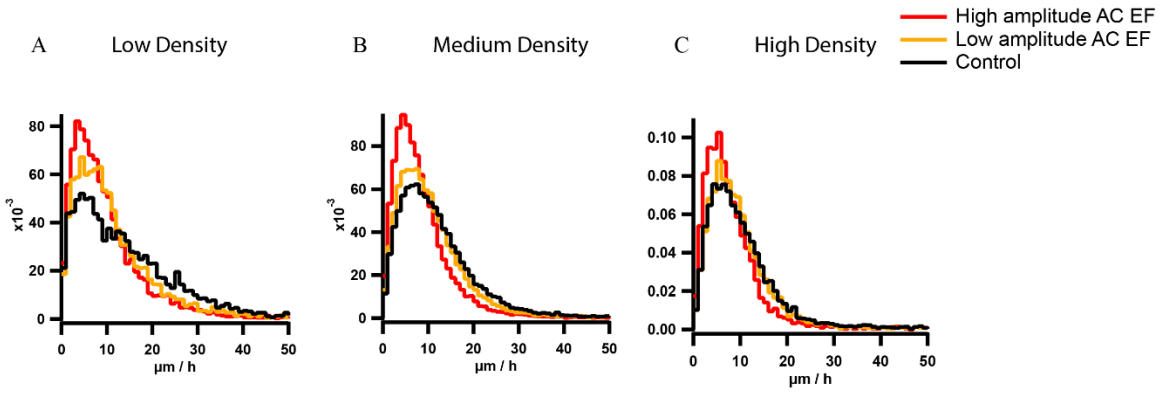

Figure 22. Cell speed distributions with different AC EF amplitudes. (A-C) Normalized cell speed distribution from low density group (A), medium density group (B), and high density group (C). The control is indicated with black line, the low amplitude (2.5V) AC EF is indicated with orange line and the high amplitude (3.5V) AC EF is indicated with red line.

Prolonged AC EF stimulation with different patterns. In the above prolonged AC EF stimulation tests, the used AC EF stimuli were always continuous during the whole 16 h. However, given the experiment results from Chapter 3, minutes of AC EF stimulation is enough to change ERK dynamics in cells. Therefore, we would like to test if repeated short-time AC EF stimulations can also alter cell physiological behaviors like continuous one. To this end, we have designed a periodic AC EF stimulation pattern (Figure 23A): in every 15 min, AC EF stimulation is only applied during the last 3 min, so through the whole AC EF application time, 80% of the time is blank. In the cell experiments, we compared this new pattern of AC EF stimulation with continuous one using MCF10A cells. The cell proliferation rates were summarized in figure 23B, to our surprise, the periodic AC EF stimulation could not only inhibit cell proliferation, but also exhibit comparable or even a little stronger (especially after AC EF stimulation was stopped) effect than the continuous one. These results may provide a new insight into the dosimetry in inhibiting cell proliferation: continuous AC EF stimulation is not necessary, repeated short-time AC EF stimulations is able to produce an enhanced effect possibly due to not waking up cell's compensation regulation. Yet these are just our speculations which need further proof with more stimulation patterns.

Regarding cell migration, as displayed in Figure 23C-E, both patterns of AC EF stimulations could suppress cell migration compared to the control group. The average cell migration distances of the control group, the continuous AC EF group and the periodic AC EF group were 21.4 μm. 14.9 μm, and 13.8 μm, respectively. In the cell speed analysis (Figure 24), the cell speed from the control group was higher than that from the continuous and the periodic AC EF groups, but there was no significant difference between these two patterns. Based on the above cell migration analysis, we can briefly conclude that continuous and periodic AC EF stimulations have comparable suppressive effect on cell migration.

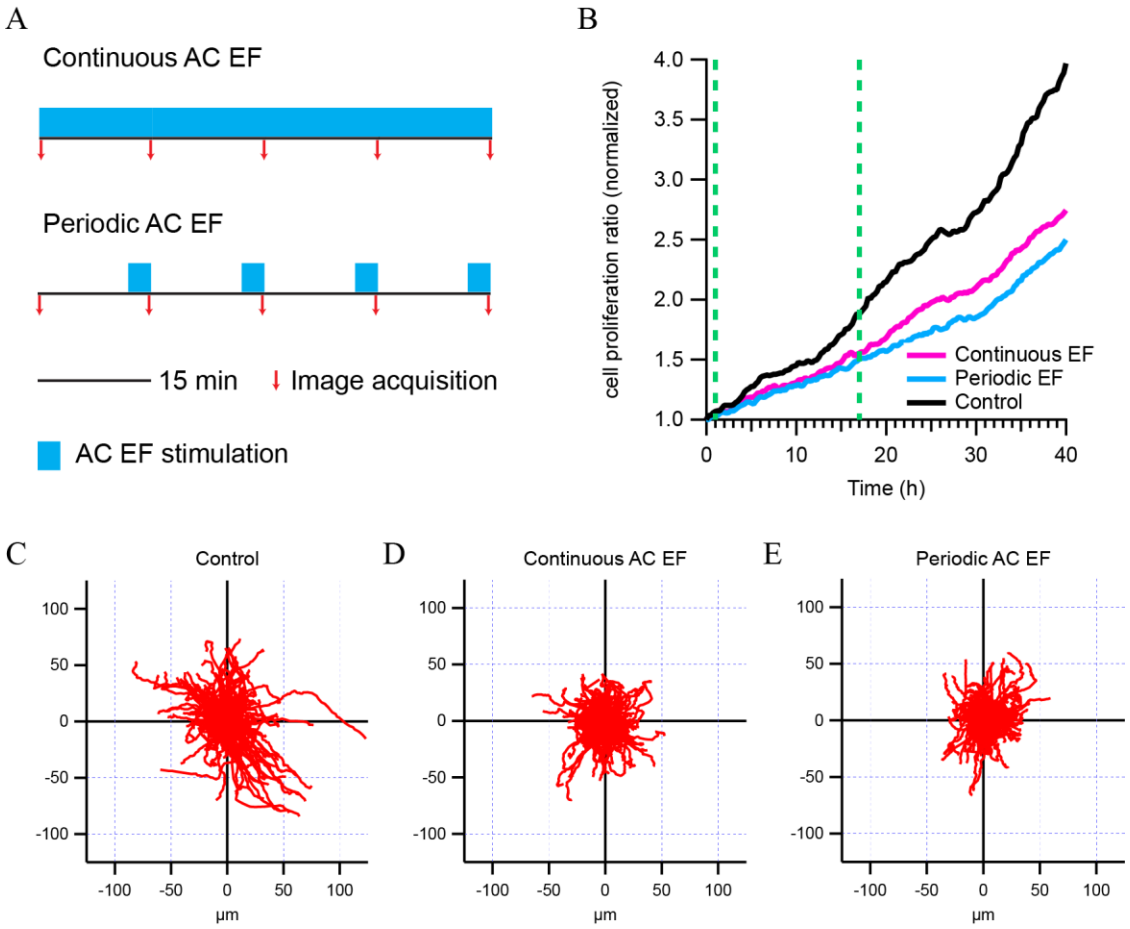

Figure 23. AC EF stimulation with different patterns. (A) Schematics of the continuous and the periodic AC EF stimulations used in tests. (B) Cell proliferation rate with different patterns of AC EF stimulations. The control group is indicated with black line, the periodic AC EF stimulation is indicated with blue line and the continuous AC EF stimulation is indicated with pink line. AC EF on and off time are marked by two green dashed lines. (C-E) Cell migration trajectories of the control group, the continuous AC EF group and the periodic AC EF group respectively, with starting point placed at the origin.

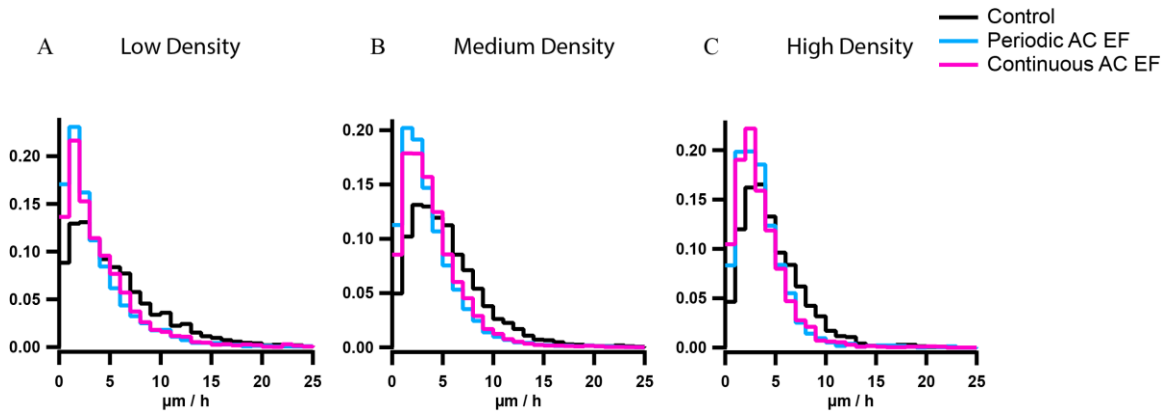

Figure 24. Cell speed distribution with different AC EF patterns. (A-C) Normalized cell speed distribution from low density group (A), medium density group (B), and high density group (C). The control is indicated with black line, the periodic AC EF is indicated with blue line and the continuous AC EF is indicated with pink line.

Prolonged AC EF stimulation with different pulse rising time. Apart from different patterns of AC EF stimulations, we also tested different pulse ramping time which was inspired by the different pulse shapes generated from different AC EF power

sources. We noticed that even though we programmed the same 50 kHz square waveform pulse, two different instruments showed different pulse shapes on the oscilloscope due to output resolution. As displayed in Figure 25A, Tektronix arbitrary function generator (AGF) has a bandwidth up to 250 MHz, much higher than the frequency of programmed pulses, so the pulse rising is almost instantaneous. On the other hand, NI-9269 module (cRIO) only has a bandwidth of 100 kHz, quite close to the frequency of programmed pulse (50 kHz), thus the pulse rising process takes several μs to complete. In the cell experiment, we used these two instruments to provide 16 h long, 50 kHz square waveform pulses to MCF10A cells and then compared cell behaviors. As shown in Figure 25B, the cell proliferation rates of both AC EF stimulation groups were lower than the control group, and the rate of fast ramping AC EF was lower than the slow ramping. This comparison suggests that fast ramping AC EF can provide augmented inhibitory effect on cell proliferation.

As for the cell migration, based on the cell trajectories (Figure 25C-E), we verified the suppressive effect on cell migration from both fast and slow ramping AC EF stimulations. After calculation, the average cell migration distances of the control group, the slow ramping AC EF group and the fast ramping AC EF group were 29.5 μm. 22.4 μm, and 20.7 μm, respectively. According to cell speed analysis (Figure 26), in all three density groups, cell speed from the control group was higher than that from the fast and the slow ramping AC EF groups, further establishing the suppression on cell migration from AC EF stimulation. However, the speed distributions from the fast and the slow ramping AC EF groups almost overlapped, demonstrating that the cell speed was not

dependent on pulse rising time. According to all the cell migration analysis, we think the pulse rising time has little effect on cell migration.

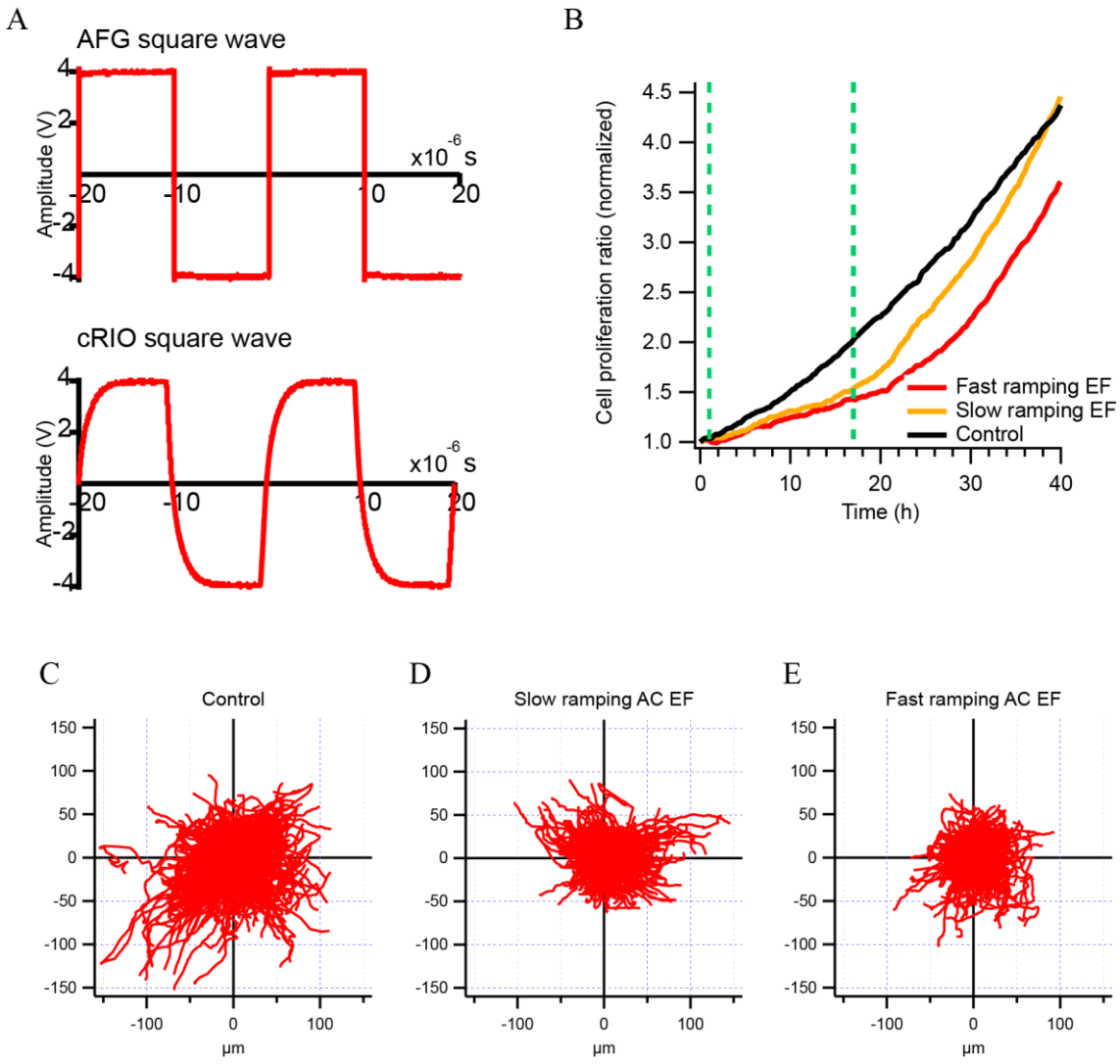

Figure 25. AC EF stimulation with different pulse rising time. (A) Recreated pulse shapes of 50 kHz square waveform pulses from Tektronix AFG and cRIO. (B) Cell proliferation rates with different pulse rising time. The control group is indicated with black line, the slow ramp AC EF stimulation is indicated with orange line and the fast ramping AC EF stimulation is indicated with red line. AC EF on and off time are marked

by two green dashed lines. (C-E) Cell migration trajectories of the control group, the slow ramping AC EF stimulation group and the fast ramping AC EF stimulation group respectively, with starting point placed at the origin.

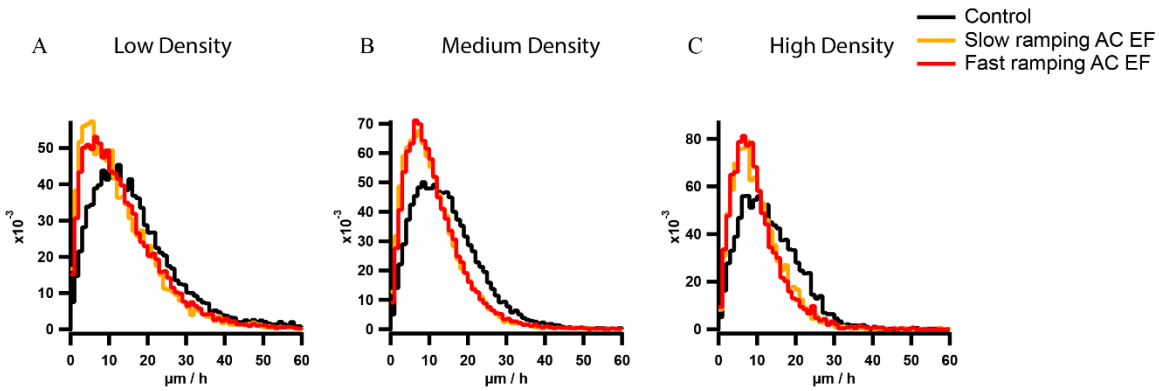

Figure 26. Cell speed distribution with different pulse rising time. (A-C) Normalized cell speed distribution from low density group (A), medium density group (B), and high density group (C). The control is indicated with black line, the slow ramp AC EF is indicated with yellow line and the fast ramp AC EF is indicated with red line.

Conclusions. In this chapter, first we have reported our collaborative research on nanotopography: the 100 nm high and spatial patterned nanoridges can provide contact guidance to cells through CEN and STEN. Then we have exploited our second-generation EF stimulation device to study how AC EF stimulation regulates cell proliferation and migration. First, we have proved that our device is fully capable of supporting long-term culture on microscope. Throughout all our experiments, no contamination has been observed. Second, we have reported that 16 h long AC EF stimulation can clearly inhibit cell proliferation in MCF10A cells. According to the cell

proliferation rate, the inhibitory effect is most obvious while AC EF stimulation is on, but in some cases, this effect can still carry on for several hours after AC EF stimulation is stopped. Additionally, we have demonstrated that the AC EF inhibition on cell proliferation shows dependence on AC EF amplitude, stimulation pattern and pulse rising time. Our findings from the cell proliferation analysis provide a new perspective in AC EF's therapeutic applications, especially the dependence on stimulation pattern and pulse rising time, which have rarely been considered as regulation parameters for clinical treatment. I think with more dose tests and mechanistic study on these two parameters, treatment via AC EF stimulation could be more precise and controllable. Last, investigation into cell migration reveals that intermediate frequency AC EF stimulation can exert suppressing effect on cell migration. So far, the suppression on cell migration has only shown sensitivity towards AC EF amplitude from the aforementioned AC EF parameters, but more qualitative and quantitative understanding of the migration process under the influence of AC EF stimulation remains to be explored in future.

CHAPTER 5

CONCLUSIONS

This dissertation is centered on cellular responses towards intermediate frequency AC EF stimulations. My research has progressed from ERK signaling pathway dynamics in individual cells to cell proliferation and migration alterations in collective cell behaviors.

In Chapter 2, I introduced the devices we used to apply AC EF stimulation to cells. Thin-film microelectrodes with HfO_2 coating were designed and fabricated to deliver capacitively coupled AC EF stimulation to cells without causing faradaic process or directional ionic flows. Based on the microelectrode chip, two generations of EF stimulation devices were developed to enable live cell culture and imaging on microelectrodes. The first-generation EF stimulation device could maintain cell culture condition for hours, so it was used to study ERK signaling pathway response to short-time AC EF stimulation; the second-generation EF stimulation device was upgraded to support long-term culture capability, and it was used to explore cell physiological changes under prolonged AC EF stimulations. Based on their applications in later AC EF stimulation experiments, both devices could fulfill their research purposes effectively.

In Chapter 3, systematic investigations into AC EF electrostatic perturbation on ERK signaling pathway were demonstrated. Due to the real-time ERK measurement with higher spatiotemporal resolution, we discovered that AC EF stimulation could trigger both ERK inhibition and activation with different thresholds and temporal characteristics. In addition, we also showed that the magnitude, frequency, and duration of ERK dynamics could be precisely synchronized and modulated by AC EF stimulation. As for

the mechanism of these ERK responses: first, their dependence on AC EF waveform and the timing of pulses suggested an electrostatic perturbation instead of electrochemical processes or chemical cues; second, according to a series of blocker tests along ERK pathway, we were able to pinpoint that ERK activation was initiated by AC EF-induced EGFR phosphorylation; last, by evaluating the Ras-GTP activity on the cell membrane, we found that the ERK inhibition was linked to the AC EF perturbation on Ras activities. However, we believe these are just part of the mechanisms behind ERK responses to AC EF stimulation, the involvements of feedback loops and interplay with other signaling pathways should not be overlooked and need further characterization. Since cell membrane is where most AC EF interactions take place, we have also been trying to find direct evidence of cell membrane fluctuations in response to AC EF stimulation. For example, we have been working on the cell membrane position analysis using Bayesian inference method, by which we hope to detect nanometer-level membrane deformation from high frame rate cell images (500-50k fps).

In Chapter 4, physical modulations of cell behaviors were demonstrated through nanotopography and EF stimulation. First, from our collaboration with the groups at University of Maryland, College Park and Johns Hopkins University, we found that parallel nanoridges of just 100 nm in height could guide cell migration by regulating CEN and STEN activities. Then preliminary studies of cell proliferation and migration alterations when applied with prolonged AC EF stimulation were demonstrated. Thanks to the cell tracking analysis pipeline based on StarDist and TrackMate, we found that 16 h long AC EF stimulation could inhibit the proliferation and migration of MCF10A cells. Furthermore, we reported that the inhibitory effect from AC EF stimulation to cell

proliferation showed sensitivity to AC EF amplitude, stimulation pattern, and pulse rising time, providing new modulation parameters in AC EF application. Although our AC EF parameters are slightly different from TTFields (Kirson et al., 2007) with lower frequency and higher intensity, our future mechanistic study can still start with their perspectives of microtubules and dielectrophoretic effects. More tests with different cell types are also needed to verify the inhibitory effect of AC EF stimulation, especially the comparison of normal and cancerous cells. Our current cell migration analysis is still quite basic, more attention should be paid to cell migration speed and differentiated analysis based on cell density.

Arkun, Y., & Yasemi, M. (2018). Dynamics and control of the ERK signaling pathway: Sensitivity, bistability, and oscillations. *PloS one, 13*(4), e0195513. doi:10.1371/journal.pone.0195513

Atkinson, S. J., Hosford, M. A., & Molitoris, B. A. (2004). Mechanism of Actin Polymerization in Cellular ATP Depletion. *Journal of Biological Chemistry, 279*(7), 5194-5199. doi:10.1074/jbc.m306973200

Bagalkot, T. R., Leblanc, N., & Craviso, G. L. (2019). Stimulation or Cancellation of Ca2+ Influx by Bipolar Nanosecond Pulsed Electric Fields in Adrenal Chromaffin Cells Can Be Achieved by Tuning Pulse Waveform. *Scientific Reports, 9*(1). doi:10.1038/s41598-019-47929-4

Banks, T., Luckman, P., Frith, J., & Cooper-White, J. (2015). Effects of electric fields on human mesenchymal stem cell behaviour and morphology using a novel multichannel device. *Integrative Biology, 7*(6), 693-712.

Barbosa, R., Acevedo, L. A., & Marmorstein, R. (2021). The MEK/ERK Network as a Therapeutic Target in Human CancerMEK/ERK Network as a Therapeutic Target. *Molecular Cancer Research, 19*(3), 361-374.

Beebe, S. J., Chen, Y.-J., Sain, N. M., Schoenbach, K. H., & Xiao, S. (2012). Transient Features in Nanosecond Pulsed Electric Fields Differentially Modulate Mitochondria and Viability. *PloS one, 7*(12), e51349. doi:10.1371/journal.pone.0051349

Bluthgen, N. (2015). Signaling output: it's all about timing and feedbacks. *Mol Syst Biol, 11*(11), 843. doi:10.15252/msb.20156642

Bodhak, S., Bose, S., Kinsel, W. C., & Bandyopadhyay, A. (2012). Investigation of in vitro bone cell adhesion and proliferation on Ti using direct current stimulation. *Materials Science and Engineering: C, 32*(8), 2163-2168.

Borgens, R., Toombs, J., Breur, G., Widmer, W., Waters, D., Harbath, A., . . . Adams, L. (1999). An imposed oscillating electrical field improves the recovery of function in neurologically complete paraplegic dogs. *Journal of neurotrauma, 16*(7), 639-657.

Cantu, J. C., Tarango, M., Beier, H. T., & Ibey, B. L. (2016). The biological response of cells to nanosecond pulsed electric fields is dependent on plasma membrane cholesterol. *Biochimica et Biophysica Acta (BBA)-Biomembranes, 1858*(11), 2636-2646.

Carnero, A., & Paramio, J. M. (2014). The PTEN/PI3K/AKT pathway in vivo, cancer mouse models. *Frontiers in oncology, 4*, 252.

Carracedo, A., & Pandolfi, P. P. (2008). The PTEN–PI3K pathway: of feedbacks and cross-talks. *Oncogene, 27*(41), 5527-5541. doi:10.1038/onc.2008.247

Chafai, D. E., Sulimenko, V., Havelka, D., Kubínová, L., Dráber, P., & Cifra, M. (2019). Reversible and Irreversible Modulation of Tubulin Self‐Assembly by Intense Nanosecond Pulsed Electric Fields. *Advanced Materials, 31*(39), 1903636. doi:10.1002/adma.201903636

Chafai, D. E., Vostárek, F., Dráberová, E., Havelka, D., Arnaud‐Cormos, D., Leveque, P., . . . Dráber, P. (2020). Microtubule Cytoskeleton Remodeling by Nanosecond Pulsed Electric Fields. *Advanced Biosystems, 4*(7), 2000070. doi:10.1002/adbi.202000070

Chang, H.-F., Lee, Y.-S., Tang, T. K., & Cheng, J.-Y. (2016). Pulsed DC Electric Field–Induced Differentiation of Cortical Neural Precursor Cells. *PloS one, 11*(6), e0158133. doi:10.1371/journal.pone.0158133

Chen, C., Ruan, S., Bai, X., Lin, C., Xie, C., & Lee, I.-S. (2019). Patterned iridium oxide film as neural electrode interface: biocompatibility and improved neurite outgrowth with electrical stimulation. *Materials Science and Engineering: C, 103*, 109865.

Cheng, N., van HOOF, H., Bockx, E., Hoogmartens, M. J., Mulier, J. C., DE DIJCKER, F. J., . . . DE LOECKER, W. (1982). The effects of electric currents on ATP generation, protein synthesis, and membrane transport in rat skin. *Clinical Orthopaedics and Related Research®, 171*, 264-272.

Cho, M. R., Thatte, H. S., Lee, R. C., & Golan, D. E. (1996). Reorganization of microfilament structure induced by ac electric fields. *The FASEB Journal, 10*(13), 1552-1558.

Cho, M. R., Thatte, H. S., Silvia, M. T., & Golan, D. E. (1999). Transmembrane calcium influx induced by ac electric fields. *The FASEB Journal, 13*(6), 677-683. doi:10.1096/fasebj.13.6.677

Cho, Y., Son, M., Jeong, H., & Shin, J. H. (2018). Electric field–induced migration and intercellular stress alignment in a collective epithelial monolayer. *Molecular Biology of the Cell, 29*(19), 2292-2302.

Choi, C. K. K., Xu, Y. J., Wang, B., Zhu, M., Zhang, L., & Bian, L. (2015). Substrate coupling strength of integrin-binding ligands modulates adhesion, spreading, and differentiation of human mesenchymal stem cells. *Nano Letters, 15*(10), 6592-6600.

Davies, A. M., Weinberg, U., & Palti, Y. (2013). Tumor treating fields: a new frontier in cancer therapy. *Annals of the New York Academy of Sciences, 1291*(1), 86-95.

Devreotes, P. N., Bhattacharya, S., Edwards, M., Iglesias, P. A., Lampert, T., & Miao, Y. (2017). Excitable Signal Transduction Networks in Directed Cell Migration. *Annual Review of Cell and Developmental Biology, 33*(1), 103-125. doi:10.1146/annurev-cellbio-100616-060739

Díaz-Vegas, A., Campos, C. A., Contreras-Ferrat, A., Casas, M., Buvinic, S., Jaimovich, E., & Espinosa, A. (2015). ROS Production via P2Y1-PKC-NOX2 Is Triggered by Extracellular ATP after Electrical Stimulation of Skeletal Muscle Cells. *PloS one, 10*(6), e0129882. doi:10.1371/journal.pone.0129882

Djamgoz, M. B. A., Mycielska, M., Madeja, Z., Fraser, S. P., & Korohoda, W. (2001). Directional movement of rat prostate cancer cells in direct-current electric field. *Journal of Cell Science, 114*(14), 2697-2705. doi:10.1242/jcs.114.14.2697

Ershov, D., Phan, M.-S., Pylvänäinen, J. W., Rigaud, S. U., Le Blanc, L., Charles-Orszag, A., . . . Tinevez, J.-Y. (2021). *Bringing TrackMate into the era of machine-learning and deep-learning*. Cold Spring Harbor Laboratory.

Fazeli, E., Roy, N. H., Follain, G., Laine, R. F., Von Chamier, L., Hänninen, P. E., . . . Jacquemet, G. (2020). Automated cell tracking using StarDist and TrackMate. *F1000Research, 9*, 1279. doi:10.12688/f1000research.27019.1

Fitzsimmons, R. J., Strong, D. D., Mohan, S., & Baylink, D. J. (1992). Low‐amplitude, low‐frequency electric field‐stimulated bone cell proliferation may in part be mediated by increased IGF‐II release. *Journal of Cellular Physiology, 150*(1), 84-89.

Forciniti, L., Ybarra III, J., Zaman, M. H., & Schmidt, C. E. (2014). Schwann cell response on polypyrrole substrates upon electrical stimulation. *Acta Biomaterialia, 10*(6), 2423-2433.

Fosbrink, M., Aye-Han, N. N., Cheong, R., Levchenko, A., & Zhang, J. (2010). Visualization of JNK activity dynamics with a genetically encoded fluorescent biosensor. *Proceedings of the National Academy of Sciences, 107*(12), 5459-5464. doi:10.1073/pnas.0909671107

Fukada, E., & Yasuda, I. (1957). On the piezoelectric effect of bone. *Journal of the physical society of Japan, 12*(10), 1158-1162.

Funk, R. H., Monsees, T., & Özkucur, N. (2009). Electromagnetic effects–From cell biology to medicine. *Progress in histochemistry and cytochemistry, 43*(4), 177-264.

Graves, M. S., Hassell, T., Beier, B. L., Albors, G. O., & Irazoqui, P. P. (2011). Electrically Mediated Neuronal Guidance with Applied Alternating Current Electric Fields. *Annals of Biomedical Engineering, 39*(6), 1759-1767. doi:10.1007/s10439-011-0259-8

Griffin, M., Iqbal, S. A., Sebastian, A., Colthurst, J., & Bayat, A. (2011). Degenerate Wave and Capacitive Coupling Increase Human MSC Invasion and Proliferation While Reducing Cytotoxicity in an In Vitro Wound Healing Model. *PloS one, 6*(8), e23404. doi:10.1371/journal.pone.0023404

Guo, A., Song, B., Reid, B., Gu, Y., Forrester, J. V., Jahoda, C. A. B., & Zhao, M. (2010). Effects of Physiological Electric Fields on Migration of Human Dermal Fibroblasts. *Journal of Investigative Dermatology, 130*(9), 2320-2327. doi:10.1038/jid.2010.96

Guo, L., Li, H., Wang, Y., Li, Z., Albeck, J., Zhao, M., & Qing, Q. (2019). Controlling ERK activation dynamics in mammary epithelial cells with alternating electric fields through microelectrodes. *Nano Letters, 19*(10), 7526-7533.

Guo, Y. J., Pan, W. W., Liu, S. B., Shen, Z. F., Xu, Y., & Hu, L. L. (2020). ERK/MAPK signalling pathway and tumorigenesis (Review). *Experimental and Therapeutic Medicine*. doi:10.3892/etm.2020.8454

Hammerick, K. E., Longaker, M. T., & Prinz, F. B. (2010). In vitro effects of direct current electric fields on adipose-derived stromal cells. *Biochemical and Biophysical Research Communications, 397*(1), 12-17. doi:10.1016/j.bbrc.2010.05.003

Hartig, M., Joos, U., & Wiesmann, H.-P. (2000). Capacitively coupled electric fields accelerate proliferation of osteoblast-like primary cells and increase bone extracellular matrix formation in vitro. *European Biophysics Journal, 29*(7), 499-506. doi:10.1007/s002490000100

Hernández-Bule, M. L., Paíno, C. L., Trillo, M. Á., & Úbeda, A. (2014). Electric Stimulation at 448 kHz Promotes Proliferation of Human Mesenchymal Stem Cells. *Cellular Physiology and Biochemistry, 34*(5), 1741-1755. doi:10.1159/000366375

Hinkle, L., McCaig, C. D., & Robinson, K. R. (1981). The direction of growth of differentiating neurones and myoblasts from frog embryos in an applied electric field. *The Journal of Physiology, 314*(1), 121-135. doi:10.1113/jphysiol.1981.sp013695

Hotary, K. B., & Robinson, K. R. (1992). Evidence of a role for endogenous electrical fields in chick embryo development. *Development, 114*(4), 985-996. doi:10.1242/dev.114.4.985

Hronik-Tupaj, M., Rice, W. L., Cronin-Golomb, M., Kaplan, D. L., & Georgakoudi, I. (2011). Osteoblastic differentiation and stress response of human mesenchymal stem cells exposed to alternating current electric fields. *BioMedical Engineering OnLine, 10*(1), 9. doi:10.1186/1475-925x-10-9

Huang, C.-W., Chen, H.-Y., Yen, M.-H., Chen, J. J. W., Young, T.-H., & Cheng, J.-Y. (2011). Gene Expression of Human Lung Cancer Cell Line CL1–5 in Response to a Direct Current Electric Field. *PloS one, 6*(10), e25928. doi:10.1371/journal.pone.0025928

Ito, M., Nagasawa, M., Omae, N., Ide, T., Akasaka, Y., & Murakami, K. (2011). Differential regulation of CIDEA and CIDEC expression by insulin via Akt1/2- and JNK2-dependent pathways in human adipocytes [S]. *Journal of lipid research, 52*(8), 1450-1460.

Jeon, T. J., Gao, R., Kim, H., Lee, A., Jeon, P., Devreotes, P. N., & Zhao, M. (2019). Cell migration directionality and speed are independently regulated by RasG and Gβ in Dictyostelium cells in electrotaxis. *Biology Open, 8*(7), bio042457.

Jing, W., Zhang, Y., Cai, Q., Chen, G., Wang, L., Yang, X., & Zhong, W. (2019). Study of Electrical Stimulation with Different Electric-Field Intensities in the Regulation of the Differentiation of PC12 Cells. *ACS Chemical Neuroscience, 10*(1), 348-357. doi:10.1021/acschemneuro.8b00286

Junge, D. (1992). *Nerve and muscle excitation*.

Kanaan, A. F., & Piedade, A. P. (2022). Electro-responsive polymer-based platforms for electrostimulation of cells. *Materials Advances, 3*(5), 2337-2353. doi:10.1039/d1ma01012c

Karabakhtsian, R., Broude, N., Shalts, N., Kochlatyia, S., Goodman, R., & Henderson, A. S. (1994). Calcium is necessary in the cell response to EM fields. *FEBS Letters, 349*(1), 1-6. doi:10.1016/0014-5793(94)00618-0

Kirson, E. D., Dbalý, V., Tovaryš, F., Vymazal, J., Soustiel, J. F., Itzhaki, A., . . . Schneiderman, R. (2007). Alternating electric fields arrest cell proliferation in animal tumor models and human brain tumors. *Proceedings of the National Academy of Sciences, 104*(24), 10152-10157.

Kirson, E. D., Gurvich, Z., Schneiderman, R., Dekel, E., Itzhaki, A., Wasserman, Y., . . . Palti, Y. (2004). Disruption of cancer cell replication by alternating electric fields. *Cancer Research, 64*(9), 3288-3295.

Kolluru, P. V., Lipner, J., Liu, W., Xia, Y., Thomopoulos, S., Genin, G. M., & Chasiotis, I. (2013). Strong and tough mineralized PLGA nanofibers for tendon-to-bone scaffolds. *Acta Biomaterialia, 9*(12), 9442-9450.

Kotnik, T., & Miklavčič, D. (2000). Theoretical evaluation of the distributed power dissipation in biological cells exposed to electric fields. *Bioelectromagnetics: Journal of the Bioelectromagnetics Society, The Society for Physical Regulation in Biology and Medicine, The European Bioelectromagnetics Association, 21*(5), 385-394.

Kotnik, T., Miklavčič, D., & Slivnik, T. (1998). Time course of transmembrane voltage induced by time-varying electric fields—a method for theoretical analysis and its application. *Bioelectrochemistry and bioenergetics, 45*(1), 3-16.

Kotnik, T., Pucihar, G., Reberšek, M., Miklavčič, D., & Mir, L. M. (2003). Role of pulse shape in cell membrane electropermeabilization. *Biochimica et Biophysica Acta (BBA) - Biomembranes, 1614*(2), 193-200. doi:10.1016/s0005-2736(03)00173-1

Kuncel, A. M., & Grill, W. M. (2004). Selection of stimulus parameters for deep brain stimulation. *Clinical neurophysiology, 115*(11), 2431-2441.

Lake, D., Corrêa, S. A., & Müller, J. (2016). Negative feedback regulation of the ERK1/2 MAPK pathway. *Cellular and Molecular Life Sciences, 73*(23), 4397-4413.

Lavoie, H., Gagnon, J., & Therrien, M. (2020). ERK signalling: a master regulator of cell behaviour, life and fate. *Nature Reviews Molecular Cell Biology, 21*(10), 607-632. doi:10.1038/s41580-020-0255-7

Leppik, L., Oliveira, K. M. C., Bhavsar, M. B., & Barker, J. H. (2020). Electrical stimulation in bone tissue engineering treatments. *European Journal of Trauma and Emergency Surgery, 46*(2), 231-244. doi:10.1007/s00068-020-01324-1

Levin, M. (2005). Left–right asymmetry in embryonic development: a comprehensive review. *Mechanisms of development, 122*(1), 3-25.

Li, F., Chen, T., Hu, S., Lin, J., Hu, R., & Feng, H. (2013). Superoxide Mediates Direct Current Electric Field-Induced Directional Migration of Glioma Cells through the Activation of AKT and ERK. *PloS one, 8*(4), e61195. doi:10.1371/journal.pone.0061195

Li, L., & Jiang, J. (2011). Stem cell niches and endogenous electric fields in tissue repair. *Frontiers of Medicine, 5*(1), 40-44. doi:10.1007/s11684-011-0108-z

Li, X., & Kolega, J. (2002). Effects of direct current electric fields on cell migration and actin filament distribution in bovine vascular endothelial cells. *Journal of vascular research, 39*(5), 391-404.

Li, X., Yang, F., & Rubinsky, B. (2021). A Correlation Between Electric Fields That Target the Cell Membrane Potential and Dividing HeLa Cancer Cell Growth Inhibition. *IEEE Transactions on Biomedical Engineering, 68*(6), 1951-1956. doi:10.1109/tbme.2020.3042650

Lin, B.-j., Tsao, S.-h., Chen, A., Hu, S.-K., Chao, L., & Chao, P.-h. G. (2017). Lipid rafts sense and direct electric field-induced migration. *Proceedings of the National Academy of Sciences, 114*(32), 8568-8573.

Lin, H., Blank, M., Rossol‐Haseroth, K., & Goodman, R. (2001). Regulating genes with electromagnetic response elements. *Journal of cellular biochemistry, 81*(1), 143-148.

Llucià-Valldeperas, A., Sanchez, B., Soler-Botija, C., Gálvez-Montón, C., Prat-Vidal, C., Roura, S., . . . Bayes-Genis, A. (2015). Electrical stimulation of cardiac adipose tissue-derived progenitor cells modulates cell phenotype and genetic machinery. *Journal of Tissue Engineering and Regenerative Medicine, 9*(11), E76-E83. doi:10.1002/term.1710

Luther, P. W., Peng, H. B., & Lin, J. J.-C. (1983). Changes in cell shape and actin distribution induced by constant electric fields. *Nature, 303*(5912), 61-64. doi:10.1038/303061a0

Martinac, B. (2004). Mechanosensitive ion channels: molecules of mechanotransduction. *Journal of Cell Science, 117*(12), 2449-2460. doi:10.1242/jcs.01232

Martinez-Ramirez, D., Hu, W., Bona, A. R., Okun, M. S., & Shukla, A. W. (2015). Update on deep brain stimulation in Parkinson's disease. *Translational Neurodegeneration, 4*(1). doi:10.1186/s40035-015-0034-0

McCaig, C. D., Rajnicek, A. M., Song, B., & Zhao, M. (2005). Controlling cell behavior electrically: current views and future potential. *Physiological reviews*.

Meng, X., Arocena, M., Penninger, J., Gage, F. H., Zhao, M., & Song, B. (2011). PI3K mediated electrotaxis of embryonic and adult neural progenitor cells in the presence of growth factors. *Experimental neurology, 227*(1), 210-217. doi:10.1016/j.expneurol.2010.11.002

Mishima, Y., & Lotz, M. (2008). Chemotaxis of human articular chondrocytes and mesenchymal stem cells. *Journal of Orthopaedic Research, 26*(10), 1407-1412. doi:10.1002/jor.20668

Morotomi-Yano, K., Akiyama, H., & Yano, K.-i. (2011). Nanosecond pulsed electric fields activate MAPK pathways in human cells. *Archives of Biochemistry and Biophysics, 515*(1-2), 99-106.

Morotomi-Yano, K., Uemura, Y., Katsuki, S., Akiyama, H., & Yano, K.-i. (2011). Activation of the JNK pathway by nanosecond pulsed electric fields. *Biochemical and Biophysical Research Communications, 408*(3), 471-476.

Nie, K., & Henderson, A. (2003). MAP kinase activation in cells exposed to a 60 Hz electromagnetic field. *Journal of cellular biochemistry, 90*(6), 1197-1206. doi:10.1002/jcb.10704

Onuma, E. K., & Hui, S. W. (1988). Electric field-directed cell shape changes, displacement, and cytoskeletal reorganization are calcium dependent. *Journal of Cell Biology, 106*(6), 2067-2075. doi:10.1083/jcb.106.6.2067

Pai, V. P., Willocq, V., Pitcairn, E. J., Lemire, J. M., Paré, J.-F., Shi, N.-Q., . . . Levin, M. (2017). HCN4 ion channel function is required for early events that regulate anatomical left-right patterning in a Nodal- and Lefty asymmetric gene expression-independent manner. *Biology Open, 6*(10), 1445-1457. doi:10.1242/bio.025957

Pal, D. S., Li, X., Banerjee, T., Miao, Y., & Devreotes, P. N. (2019). The excitable signal transduction networks: movers and shapers of eukaryotic cell migration. *The International Journal of Developmental Biology, 63*(8-9-10), 407-416. doi:10.1387/ijdb.190265pd

Perike, S., Özkucur, N., Sharma, P., Staroske, W., Bläsche, R., Barth, K., & Funk, R. H. (2014). Phospho-NHE3 forms membrane patches and interacts with beta-actin to sense and maintain constant direction during cell migration. *Experimental cell research, 324*(1), 13-29.

Pettersen, E., Anderson, J., & Ortiz-Catalan, M. (2022). Electrical stimulation to promote osseointegration of bone anchoring implants: a topical review. *Journal of NeuroEngineering and Rehabilitation, 19*(1). doi:10.1186/s12984-022-01005-7

Pilla, A. A. (2007). Mechanisms and therapeutic applications of time-varying and static magnetic fields. *Biological and medical aspects of electromagnetic fields, 3*.

Qin, S., Zhou, W., Liu, S., Chen, P., & Wu, H. (2015). Icariin stimulates the proliferation of rat bone mesenchymal stem cells via ERK and p38 MAPK signaling. *International Journal of Clinical and Experimental Medicine, 8*(5), 7125.

Radisic, M., Park, H., Shing, H., Consi, T., Schoen, F. J., Langer, R., . . . Vunjak-Novakovic, G. (2004). Functional assembly of engineered myocardium by electrical stimulation of cardiac myocytes cultured on scaffolds. *Proceedings of the National Academy of Sciences, 101*(52), 18129-18134. doi:10.1073/pnas.0407817101

Regot, S., Jacob, Bryce, Carrasco, S., & Markus. (2014). High-Sensitivity Measurements of Multiple Kinase Activities in Live Single Cells. *Cell, 157*(7), 1724-1734. doi:10.1016/j.cell.2014.04.039

Ross, C. L., Siriwardane, M., Almeida-Porada, G., Porada, C. D., Brink, P., Christ, G. J., & Harrison, B. S. (2015). The effect of low-frequency electromagnetic field on human bone marrow stem/progenitor cell differentiation. *Stem cell research, 15*(1), 96-108.

Roussos, E. T., Condeelis, J. S., & Patsialou, A. (2011). Chemotaxis in cancer. *Nature Reviews Cancer, 11*(8), 573-587. doi:10.1038/nrc3078

Ruprecht, V., Monzo, P., Ravasio, A., Yue, Z., Makhija, E., Strale, P. O., . . . Viasnoff, V. (2016). How cells respond to environmental cues – insights from bio-functionalized substrates. *Journal of Cell Science, 130*(1), 51-61. doi:10.1242/jcs.196162

Ryan, C. N., Doulgkeroglou, M. N., & Zeugolis, D. I. (2021). Electric field stimulation for tissue engineering applications. *BMC Biomedical Engineering, 3*(1), 1-9.

Ryu, H., Chung, M., Dobrzynski, M., Fey, D., Blum, Y., Lee, S. S., . . . Pertz, O. (2015). Frequency modulation of ERK activation dynamics rewires cell fate. *Mol Syst Biol, 11*(11), 838. doi:10.15252/msb.20156458

Ryu, H., Chung, M., Dobrzyński, M., Fey, D., Blum, Y., Lee, S. S., . . . Pertz, O. (2015). Frequency modulation of ERK activation dynamics rewires cell fate. *Molecular Systems Biology, 11*(11), 838. doi:10.15252/msb.20156458

Safa, A., Abak, A., Shoorei, H., Taheri, M., & Ghafouri-Fard, S. (2020). MicroRNAs as regulators of ERK/MAPK pathway: a comprehensive review. *Biomedicine & Pharmacotherapy, 132*, 110853.

Schmidt, U., Weigert, M., Broaddus, C., & Myers, G. (2018). Cell Detection with Star-Convex Polygons. In (pp. 265-273): Springer International Publishing.

Sheikh, A. Q., Taghian, T., Hemingway, B., Cho, H., Kogan, A. B., & Narmoneva, D. A. (2013). Regulation of endothelial MAPK/ERK signalling and capillary morphogenesis by low-amplitude electric field. *Journal of The Royal Society Interface, 10*(78), 20120548. doi:10.1098/rsif.2012.0548

Shin, S.-Y., Rath, O., Choo, S.-M., Fee, F., McFerran, B., Kolch, W., & Cho, K.-H. (2009). Positive- and negative-feedback regulations coordinate the dynamic behavior of the Ras-Raf-MEK-ERK signal transduction pathway. *Journal of Cell Science, 122*(3), 425-435. doi:10.1242/jcs.036319

Sparta, B., Pargett, M., Minguet, M., Distor, K., Bell, G., & Albeck, J. G. (2015). Receptor Level Mechanisms Are Required for Epidermal Growth Factor (EGF)-stimulated Extracellular Signal-regulated Kinase (ERK) Activity Pulses. *Journal of Biological Chemistry, 290*(41), 24784-24792. doi:10.1074/jbc.m115.662247

Stupp, R., Taillibert, S., Kanner, A., Kesari, S., Toms, S. A., Barnett, G. H., . . . Zhu, J.-J. (2015). Tumor treating fields (TTFields): A novel treatment modality added to standard chemo-and radiotherapy in newly diagnosed glioblastoma—First report of the full dataset of the EF14 randomized phase III trial. In: American Society of Clinical Oncology.

Stupp, R., Taillibert, S., Kanner, A., Read, W., Steinberg, D. M., Lhermitte, B., . . . Ram, Z. (2017). Effect of Tumor-Treating Fields Plus Maintenance Temozolomide vs Maintenance Temozolomide Alone on Survival in Patients With Glioblastoma. *JAMA, 318*(23), 2306. doi:10.1001/jama.2017.18718

Sun, S., Liu, Y., Lipsky, S., & Cho†, M. (2007). Physical manipulation of calcium oscillations facilitates osteodifferentiation of human mesenchymal stem cells. *The FASEB Journal, 21*(7), 1472-1480. doi:10.1096/fj.06-7153com

Sun, S., Titushkin, I., & Cho, M. (2006). Regulation of mesenchymal stem cell adhesion and orientation in 3D collagen scaffold by electrical stimulus. *Bioelectrochemistry, 69*(2), 133-141.

Sun, Y. H., Sun, Y., Zhu, K., Reid, B., Gao, X., Draper, B. W., . . . Mogilner, A. (2018). Electric fields accelerate cell polarization and bypass myosin action in motility initiation. *Journal of Cellular Physiology, 233*(3), 2378-2385.

Taghian, T., Narmoneva, D. A., & Kogan, A. B. (2015). Modulation of cell function by electric field: a high-resolution analysis. *Journal of The Royal Society Interface, 12*(107), 20150153. doi:10.1098/rsif.2015.0153

Tan, A. R., Alegre-Aguarón, E., O'Connell, G. D., Vandenberg, C. D., Aaron, R. K., Vunjak-Novakovic, G., . . . Hung, C. T. (2015). Passage-dependent relationship between mesenchymal stem cell mobilization and chondrogenic potential. *Osteoarthritis and Cartilage, 23*(2), 319-327. doi:10.1016/j.joca.2014.10.001

Tao, Q., & Henderson, A. (1999). EMF induces differentiation in HL‐60 cells. *Journal of cellular biochemistry, 73*(2), 212-217.

Teissie, J., Knox, B. E., Tsong, T. Y., & Wehrle, J. (1981). Synthesis of adenosine triphosphate in respiration-inhibited submitochondrial particles induced by microsecond electric pulses. *Proceedings of the National Academy of Sciences, 78*(12), 7473-7477. doi:10.1073/pnas.78.12.7473

Thrivikraman, G., Boda, S. K., & Basu, B. (2018). Unraveling the mechanistic effects of electric field stimulation towards directing stem cell fate and function: A tissue engineering perspective. *Biomaterials, 150*, 60-86.

Tinevez, J.-Y., Perry, N., Schindelin, J., Hoopes, G. M., Reynolds, G. D., Laplantine, E., . . . Eliceiri, K. W. (2017). TrackMate: An open and extensible platform for single-particle tracking. *Methods, 115*, 80-90.

Titushkin, I., & Cho, M. (2009). Regulation of Cell Cytoskeleton and Membrane Mechanics by Electric Field: Role of Linker Proteins. *Biophysical journal, 96*(2), 717-728. doi:10.1016/j.bpj.2008.09.035

Tonelli, F. M. P., Santos, A. K., Gomes, D. A., Da Silva, S. L., Gomes, K. N., Ladeira, L. O., & Resende, R. R. (2012). Stem Cells and Calcium Signaling. In (pp. 891-916): Springer Netherlands.

Tsai, C.-H., Lin, B.-J., & Chao, P.-H. G. (2013). α2β1 integrin and RhoA mediates electric field-induced ligament fibroblast migration directionality. *Journal of Orthopaedic Research, 31*(2), 322-327. doi:10.1002/jor.22215

Tsong, T. Y. (1989). Deciphering the language of cells. *Trends in Biochemical Sciences, 14*(3), 89-92.

Tsong, T. Y., & Gross, C. J. (2012). Membrane Enzymes: Cellular Transduction of High- and Low-Level Periodic Signals. *Biological Effects of Electric and Magnetic Fields: Sources and Mechanisms*, 143.

Varani, K., Vincenzi, F., Pasquini, S., Blo, I., Salati, S., Cadossi, M., & De Mattei, M. (2021). Pulsed Electromagnetic Field Stimulation in Osteogenesis and Chondrogenesis: Signaling Pathways and Therapeutic Implications. *International Journal of Molecular Sciences, 22*(2), 809. doi:10.3390/ijms22020809

Von Chamier, L., Laine, R. F., Jukkala, J., Spahn, C., Krentzel, D., Nehme, E., . . . Henriques, R. (2021). Democratising deep learning for microscopy with ZeroCostDL4Mic. *Nature Communications, 12*(1). doi:10.1038/s41467-021-22518-0

Weaver, J. C. (2003). Electroporation of biological membranes from multicellular to nano scales. *IEEE Transactions on Dielectrics and Electrical Insulation, 10*(5), 754-768. doi:10.1109/tdei.2003.1237325

Weaver, J. C., & Astumian, R. D. (1990). The response of living cells to very weak electric fields: the thermal noise limit. *Science, 247*(4941), 459-462.

Wenger, C., Miranda, P. C., Salvador, R., Thielscher, A., Bomzon, Z., Giladi, M., . . . Korshoej, A. R. (2018). A Review on Tumor-Treating Fields (TTFields): Clinical Implications Inferred From Computational Modeling. *IEEE Reviews in Biomedical Engineering, 11*, 195-207. doi:10.1109/rbme.2017.2765282

Wolf-Goldberg, T., Barbul, A., Ben-Dov, N., & Korenstein, R. (2013). Low electric fields induce ligand-independent activation of EGF receptor and ERK via electrochemical elevation of H+ and ROS concentrations. *Biochimica et Biophysica Acta (BBA)-Molecular Cell Research, 1833*(6), 1396-1408.

Xie, T. D., & Tsong, T. Y. (1990). Study of mechanisms of electric field-induced DNA transfection. II. Transfection by low-amplitude, low-frequency alternating electric fields. *Biophysical journal, 58*(4), 897-903. doi:10.1016/s0006-3495(90)82434-6

Xing, F., Li, L., Zhou, C., Long, C., Wu, L., Lei, H., . . . Zhang, X. (2019). Regulation and directing stem cell fate by tissue engineering functional microenvironments: scaffold physical and chemical cues. *Stem cells international, 2019*.

Xu, H., Zhang, J., Lei, Y., Han, Z., Rong, D., Yu, Q., . . . Tian, J. (2016). Low frequency pulsed electromagnetic field promotes C2C12 myoblasts proliferation via activation of MAPK/ERK pathway. *Biochemical and Biophysical Research Communications, 479*(1), 97-102.

Yang, Q., Miao, Y., Banerjee, P., Hourwitz, M. J., Hu, M., Qing, Q., . . . Losert, W. (2022). Nanotopography modulates intracellular excitable systems through cytoskeleton actuation. *bioRxiv*, 2022.2006. 2009.495528.

Yao, J., Liu, B., & Qin, F. (2009). Rapid Temperature Jump by Infrared Diode Laser Irradiation for Patch-Clamp Studies. *Biophysical journal, 96*(9), 3611-3619. doi:10.1016/j.bpj.2009.02.016

Yao, L., Li, Y., Knapp, J., & Smith, P. (2015). Exploration of molecular pathways mediating electric field-directed schwann cell migration by RNA-seq. *Journal of Cellular Physiology, 230*(7), 1515-1524. doi:10.1002/jcp.24897

Yao, L., Pandit, A., Yao, S., & McCaig, C. D. (2011). Electric field-guided neuron migration: a novel approach in neurogenesis. *Tissue Engineering Part B: Reviews, 17*(3), 143-153.

Zhan, H., Bhattacharya, S., Cai, H., Iglesias, P. A., Huang, C.-H., & Devreotes, P. N. (2020). An Excitable Ras/PI3K/ERK Signaling Network Controls Migration and Oncogenic Transformation in Epithelial Cells. *Developmental Cell, 54*(5), 608-623.e605. doi:10.1016/j.devcel.2020.08.001

Zhang, H. L., & Peng, H. B. (2011). Mechanism of acetylcholine receptor cluster formation induced by DC electric field. *PloS one, 6*(10), e26805.

Zhang, J., Calafiore, M., Zeng, Q., Zhang, X., Huang, Y., Li, R. A., . . . Zhao, M. (2011). Electrically Guiding Migration of Human Induced Pluripotent Stem Cells. *Stem Cell Reviews and Reports, 7*(4), 987-996. doi:10.1007/s12015-011-9247-5

Zhao, H., Steiger, A., Nohner, M., & Ye, H. (2015). Specific Intensity Direct Current (DC) Electric Field Improves Neural Stem Cell Migration and Enhances Differentiation towards βIII-Tubulin+ Neurons. *PloS one, 10*(6), e0129625. doi:10.1371/journal.pone.0129625

Zhao, M. (2009). *Electrical fields in wound healing—an overriding signal that directs cell migration.* Paper presented at the Seminars in cell & developmental biology.

Zhao, M., Agius-Fernandez, A., Forrester, J. V., & McCaig, C. D. (1996). Directed migration of corneal epithelial sheets in physiological electric fields. *Investigative ophthalmology & visual science, 37*(13), 2548-2558.

Zhao, M., Dick, A., Forrester, J. V., & McCaig, C. D. (1999). Electric Field–directed Cell Motility Involves Up-regulated Expression and Asymmetric Redistribution of the Epidermal Growth Factor Receptors and Is Enhanced by Fibronectin and Laminin. *Molecular Biology of the Cell, 10*(4), 1259-1276. doi:10.1091/mbc.10.4.1259

Zhao, M., Pu, J., Forrester, J. V., & McCaig, C. D. (2002). Membrane lipids, EGF receptors, and intracellular signals colocalize and are polarized in epithelial cells moving directionally in a physiological electric field. *The FASEB Journal, 16*(8), 857-859. doi:10.1096/fj.01-0811fje

Zhao, M., Song, B., Pu, J., Wada, T., Reid, B., Tai, G., . . . Penninger, J. M. (2006). Electrical signals control wound healing through phosphatidylinositol-3-OH kinase-γ and PTEN. *Nature, 442*(7101), 457-460. doi:10.1038/nature04925

Zhao, S., Mehta, A. S., & Zhao, M. (2020). Biomedical applications of electrical stimulation. *Cellular and Molecular Life Sciences, 77*(14), 2681-2699. doi:10.1007/s00018-019-03446-1

Zhu, R., Sun, Z., Li, C., Ramakrishna, S., Chiu, K., & He, L. (2019). Electrical stimulation affects neural stem cell fate and function in vitro. *Experimental neurology, 319*, 112963.

Zrimec, A., Jerman, I., & Lahajnar, G. (2002). Alternating electric fields stimulate ATP synthesis in Escherichia coli. *Cellular and Molecular Biology Letters, 7*(1), 172-175.